TECHNICAL REPORT SL-89-6

(2)

THERMAL STRESS ANALYSIS OF LOCK WALL DASHIELDS LOCKS, OHIO RIVER

by

Michael F. Hammons, Sharon B. Garner, Donald M. Smith

Structures Laboratory

DEPARTMENT OF THE ARMY
Waterways Experiment Station, Corps of Engineers
PO Box 631, Vicksburg, Mississippi 39181-0631

June 1989
Final Report

Prepared for US Army Engineer District, Pittsburgh
Pittsburgh, Pennsylvania 52222-4186

US Army Corps of Engineers

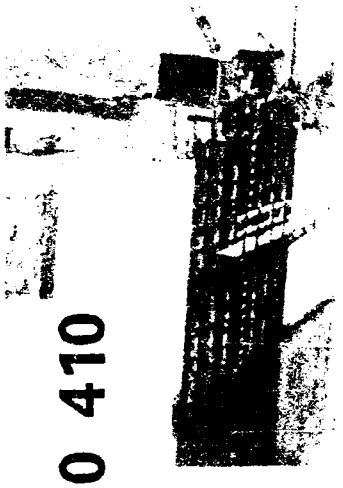

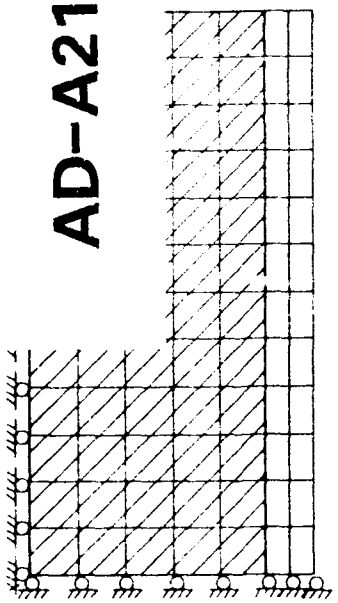

STRUCTURES LABORATORY

Destroy this report when no longer needed. Do not return it to the originator.

The findings in this report are not to be construed as an official Department of the Army position unless so designated by other authorized documents.

The contents of this report are not to be used for advertising, publication, or promotional purposes. Citation of trade names does not constitute an official endorsement or approval of the use of such commercial products.

Unclassified

SECURITY CLASSIFICATION OF THIS PAGE

REPORT DOCUMENTATION PAGE

Form Approved OMB No. 0704-0188

1a. REPORT SECURITY CLASSIFICATION Unclassified	1b. RESTRICTIVE MARKINGS
2a. SECURITY CLASSIFICATION AUTHORITY	3. DISTRIBUTION/AVAILABILITY OF REPORT Approved for public release; distribution unlimited.
2b. DECLASSIFICATION/DOWNGRADING SCHEDULE	
4. PERFORMING ORGANIZATION REPORT NUMBER(S) Technical Report SL-89-6	5. MONITORING ORGANIZATION REPORT NUMBER(S)
6a. NAME OF PERFORMING ORGANIZATION USAEWES Structures Laboratory 6b. OFFICE SYMBOL (If applicable) CEWES-SC-CE	7a. NAME OF MONITORING ORGANIZATION
6c. ADDRESS (City, State, and ZIP Code) PO Box 631 Vicksburg, MS 39180-0631	7b. ADDRESS (City, State, and ZIP Code)
8a. NAME OF FUNDING/SPONSORING ORGANIZATION US Army Engineer District, Pittsburgh 8b. OFFICE SYMBOL (If applicable) CEORP-ED	9. PROCUREMENT INSTRUMENT IDENTIFICATION NUMBER CEORP-ED-88-35
8c. ADDRESS (City, State, and ZIP Code) 1000 Liberty Avenue Federal Building Pittsburgh, PA 52222-4186	10. SOURCE OF FUNDING NUMBERS PROGRAM ELEMENT NO. / PROJECT NO. / TASK NO. / WORK UNIT ACCESSION NO.
11. TITLE (Include Security Classification) Thermal Stress Analysis of Lock Wall, Dashields Locks, Ohio River	
12. PERSONAL AUTHOR(S) Hammons, Michael I.; Garner, Sharon B.; Smith, Donald M.	
13a. TYPE OF REPORT Final report 13b. TIME COVERED FROM _____ TO _____ 14. DATE OF REPORT (Year, Month, Day) June 1989 15. PAGE COUNT 76	
16. SUPPLEMENTARY NOTATION Available from National Technical Information Service, 5285 Port Royal Road, Springfield, VA 22161.	

17. COSATI CODES			18. SUBJECT TERMS (Continue on reverse if necessary and identify by block number)		
FIELD	GROUP	SUB-GROUP	Aging material	Lock walls	Repair
			Creep	Navigation locks	Shrinkage
			Finite element method	Overlays	Thermal stress

19. ABSTRACT (Continue on reverse if necessary and identify by block number)

A recently developed thermal stress analysis procedure was used to study the effects of a variety of parameters on cracking in concrete overlays for the Dashields Locks, Ohio River, Pennsylvania. The objective of the research was to develop improved designs and construction procedures to substantially reduce or inhibit cracking in the concrete overlay sections. Thermal stress analyses included the effects of placement temperature, ambient temperature, thermal properties of overlay, shrinkage, creep, reinforcing steel, and restraint at the interface between the overlay and existing concrete. These analyses indicated that shrinkage was the predominant factor in overlay cracking for the particular mixture to be used on the project. It was recommended that shrinkage be reduced by adopting one or more of the following modifications: decreasing the cement content of the mixture, decreasing the water-cement ratio of the mixture, using a larger maximum size aggregate, or limiting drying shrinkage by using wet curing. It was also demonstrated that an effective bond breaker at the interface would eliminate cracking.

20. DISTRIBUTION/AVAILABILITY OF ABSTRACT ☐ UNCLASSIFIED/UNLIMITED ☒ SAME AS RPT ☐ DTIC USERS	21. ABSTRACT SECURITY CLASSIFICATION Unclassified
22a. NAME OF RESPONSIBLE INDIVIDUAL	22b. TELEPHONE (Include Area Code) / 22c. OFFICE SYMBOL

DD Form 1473, JUN 86 *Previous editions are obsolete.*

SECURITY CLASSIFICATION OF THIS PAGE

Unclassified

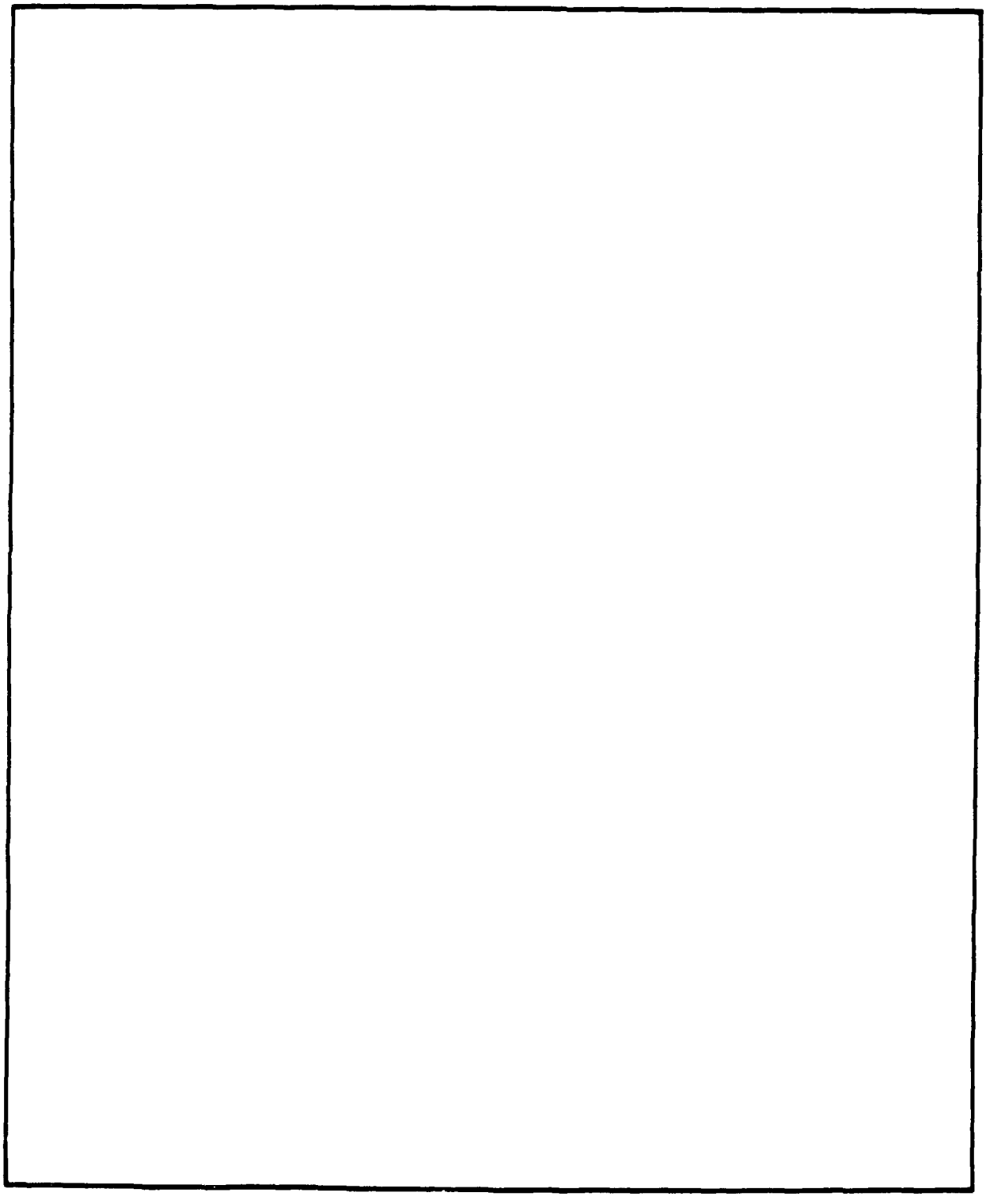

PREFACE

The investigation described in this report was conducted for the US Army Engineer District, Pittsburgh. Authorization was given by DA Form 2544, CEORP-ED-88-35, dated 17 Dec 1987.

The mixture proportioning, specimen preparation, and testing were performed at the US Army Engineer Waterways Experiment Station (WES) by personnel of the Structures Laboratory, under the general supervision of Messrs. Bryant Mather, Chief, J. T. Ballard, Assistant Chief, and K. L. Saucier, Chief, Concrete Technology Division (CTD). Direct supervision and technical guidance was provided by Mr. C. Dean Norman, Chief, Evaluation and Monitoring Unit, CTD. This report was prepared by Mr. Michael I. Hammons, Ms. Sharon B. Garner, and Mr. Donald M. Smith of the Evaluation and Monitoring Unit, CTD. The authors acknowledge Messrs. Dan Wilson, Andy Shirley, and Brent Lamb and Ms. Linda Mayfield of the Evaluation and Monitoring Unit, CTD, for their help during this investigation. This report was prepared for publication by Mmes. Gilda Miller and Chris Habeeb, Editor and Editorial Assistant, respectively, Information Products Division, Information Technology Laboratory, WES.

Acting Commander and Director of WES during preparation of this report was LTC Jack R. Stephens, EN. Technical Director was Dr. Robert W. Whalin.

CONTENTS

	Page
PREFACE	1
CONVERSION FACTORS, NON-SI TO SI (METRIC) UNITS OF MEASUREMENT	3
PART I: INTRODUCTION	4
Background	4
Objective	5
Scope	5
PART II: ANALYSIS PROCEDURE	6
Finite Element Code	6
Concrete Mixture	7
Material Properties Tests	8
Aging Material Model Calibration and Verification	9
PART III: THERMAL STRESS ANALYSES	11
Factors Affecting Cracking of Overlay Sections	11
Finite Element Discretization	11
Finite Element Analyses	12
PART IV: CONCLUSIONS AND RECOMMENDATIONS	17
Conclusions	17
Recommendations	17
REFERENCES	19
FIGURES 1-53	

CONVERSION FACTORS, NON-SI TO SI (METRIC) UNITS OF MEASUREMENT

Non-SI units of measurement used in this report can be converted to SI (metric) units as follows:

Multiply	By	To Obtain
cubic yards	0.02831685	cubic metres
Fahrenheit degrees	5/9	Celsius degrees or kelvins*
feet	0.3048	metres
inches	25.4	millimetres
miles (US statute)	1.609347	metres
ounces (US fluid)	0.02957353	litres
pounds (force) per square inch	0.006894757	megapascals
pounds (mass)	0.4535924	kilograms
pounds (mass) per cubic foot	16.01846	kilograms per cubic metre

* To obtain Celsius (C) temperature readings from Fahrenheit (F) readings, use the following formula: $C = (5/9)(F - 32)$. To obtain kelvin (K) readings, use: $K = (5/9)(F - 32) + 273.15$.

THERMAL STRESS ANALYSIS OF LOCK WALL DASHIELDS LOCKS, OHIO RIVER

PART I: INTRODUCTION

Background

1. The Dashields Locks and Dam were constructed in 1927-1928 on the Ohio River 13.3 miles* downstream of the confluence of the Allegheny and Monongahela Rivers at Pittsburgh, PA. The locks consist of two chambers: a landward chamber with dimensions 110 by 600 ft and a riverward chamber 56 by 360 ft. The lift of the lock is 10 ft. The main lock walls are concrete gravity structures founded on rock. The guide and guard walls are concrete gravity parapet walls spanning individual piers founded on rock.

2. A condition survey of the Dashields Locks conducted by the US Army Engineer Waterways Experiment Station (WES) revealed the presence of significant damage to the concrete on both horizontal and vertical lock wall surfaces (Wong and Stowe 1985). The depth of the damaged concrete ranged from a minimum of 0.1 ft to a maximum of 2 ft. This damage was primarily attributed to freezing and thawing action.

3. The US Army Engineer District, Pittsburgh (ORP), has rehabilitated a number of similarly damaged locks on the upper Ohio River and its tributaries. The basic lock wall repair procedure has been to remove the damaged concrete to its full depth and then overlay the sound concrete with a layer of high-quality, air-entrained concrete. This repair method has resulted in significant cracking in the overlay concrete in ORP as well as in a number of other Corps districts using similar repair procedures (McDonald 1987). Cracking of this type can result in decreased durability and increased maintenance costs for the repaired lock walls.

4. ORP began a similar lock wall repair to the Dashields Locks in 1988. In December 1987, the district requested the Concrete Technology Division, Structures Laboratory, WES, to use a recently developed thermal stress analysis procedure to study the effects of a variety of parameters on cracking in

---

* A table of factors for converting non-SI units of measurement to SI (metric) units is presented on page 3.

concrete overlays for the Dashields Locks. This report presents the results of material properties tests conducted in support of the analyses, the results of the analyses, and conclusions and recommendations from the analyses.

Objective

5. The objective of this research was to develop improved design and construction procedures for concrete overlay sections at Dashields Locks so that cracking can be substantially reduced or inhibited.

Scope

6. A recently developed thermal stress analysis procedure was used to study the effects of a variety of parameters on cracking in concrete overlays. These parameters include mechanical and thermal properties, shrinkage, reinforcing steel, restraint at the old concrete/new concrete interface, placement temperature, and ambient temperature. Previous construction techniques as well as plans for construction procedures for Dashields Locks were reviewed. Critical material properties tests were conducted in support of the calibration of an aging material model for concrete used in the analyses. Thermal stress analyses for typical overlay sections were conducted to examine the effects of various parameters on the potential for cracking of the overlay concrete. The results of the analyses were evaluated to select optimum construction procedures.

PART II: ANALYSIS PROCEDURE

Finite Element Code

7. A general-purpose finite element code (ABAQUS) with a user-defined, aging material model (UMAT) was used for the heat transfer and structural analysis of the lock wall resurfacing problem. This analysis procedure was developed at WES and was reported in some detail by Norman, Campbell, and Garner (1988). Some of the features of the code and material model are discussed in the following paragraphs.

8. Transient heat transfer analyses can be conducted using ABAQUS with heat transfer elements from the ABAQUS library of elements. The adiabatic temperature rise of the concrete is used as the forcing function for the analysis. Boundary conditions for the heat transfer analysis can be easily varied. Forms or other insulating materials can be simulated with film coefficients applied to the exterior faces of the element. Ambient temperature conditions as well as placement temperatures of the new concrete and equilibrium temperature of the old concrete can be modeled. The results of the heat transfer analysis are temperature-time histories at each node or integration point of the model.

9. The temperature-time history obtained in the heat transfer analysis is used as the loading for a structural analysis. This analysis can be conducted using plane stress or plane strain elements from the ABAQUS element library. Significant changes in strength, modulus, creep, shrinkage, etc. must be accounted for in a consistent and numerically efficient manner in the finite element solution procedure. This is accomplished using a user-defined, two-dimensional aging material model with cracking capabilities in the ABAQUS-UMAT subroutine format. This model includes the effects of aging on the elastic modulus and cracking strength and the effects of changing temperatures on the creep compliance, the elastic modulus, and the ultimate/cracking strength. These properties as a function of time and temperature are included in a separate subroutine which can be easily modified by the user for a specific material. The model assumes cracking to occur when an interactive cracking criterion is satisfied.

10. The material model incorporated in ABAQUS uses a smeared crack approach to model the cracked regions of the structure. This approach is

based upon the assumptions that cracks form in an element when the interactive cracking criteria are exceeded. The cracks are straight and perpendicular to the direction of maximum principal stress or strain. The cracked region is modeled as an anisotropic continuum effectively "smearing" the cracks in a continuous manner throughout the element (Norman and Anderson 1985). These assumptions allow the stress in the tensile direction to drop suddenly while retaining shear stress transfer across rough cracks or aggregate interlock. Thus, the overall structural response can be modeled quite adequately without regard to completely realistic crack patterns and local stresses (Chen 1982).

11. The finite element model allows the user to study the effects of construction parameters readily. Reinforcement and dowel bars can be added to an element. The effects of bond-breaking materials to reduce the restraint at the old concrete/new concrete interface can be simulated with interface elements from the ABAQUS element library. Incremental construction procedures can be simulated effectively through the "model change" option. This option allows the user to remove or include previously defined elements from the analysis in a specified solution step.

Concrete Mixture

12. The mixture proportions for the overlay concrete were furnished to WES by ORP with quantities of materials sufficient to cast specimens for a limited series of material properties tests. WES was instructed by ORP not to modify the mixture proportions or change materials used in the mixture.

13. The mixture had a nominal unconfined compressive strength of 4,000 psi at 28 days. The water-cement ratio was 0.45. Batch weights for 1 yd^3 of concrete were as follows:

Material	Weight
Cement	600 lb
Fine aggregate	1,330 lb
Coarse aggregate	1,725 lb
Water	270 lb
Water-reducing admixture	18 oz
Air-entraining admixture	Adjustable

All aggregate weights are saturated-surface-dry weights.

14. The cement was Type II, Low Alkali, produced by SME/Bessemer, Inc. of Bessemer, PA. A cement mill test report, as furnished to WES by ORP, is shown in Figure 1. The fine aggregate was classified by the Pennsylvania Department of Transportation as a Type A (American Society for Testing and Materials (ASTM) C 33 (ASTM 1988a)) concrete sand supplied by Dravo Corporation of Pittsburgh, PA, from their Pike Island Dredge on the Ohio River. The coarse aggregate was 0.75-in. maximum size limestone supplied by SME Carbon Stone of Hillsville, PA. The water-reducing admixture and air-entraining admixture were WRDA (with Hycol) and Daravair, respectively, both manufactured by W. R. Grace of Boston, MA.

15. A 7.5-ft^3 batch was prepared in the laboratory at WES and specimens were made from it according to ASTM C 192 (ASTM 1988f) from the materials supplied by ORP. Tests were conducted on the fresh concrete to determine such parameters as slump, unit weight, air content, and time of final setting (TOFS). The ASTM methods used for conducting these tests and the test results are presented below:

Test	Method	Result
Slump	ASTM C 143 (ASTM 1988d)	1.75 in.
Unit weight	ASTM C 138 (ASTM 1988c)	146.4 lb/ft^3
Air content	ASTM C 231 (ASTM 1988g)	5%
Time of final setting	ASTM C 403 (ASTM 1988h)	5.5 hr

Material Properties Tests

16. A series of early-time material properties tests were conducted on hardened concrete specimens at six ages of loading to provide data necessary for the calibration of the aging material model used in ABAQUS. The series of tests conducted are presented in the test matrix shown in the following tabulation:

Age at Loading*	Type of Test	Specimens
7 hr	Unconfined compression	2
(TOFS + 1.5 hr)	Creep of concrete	2

* Batching of the concrete mixture is zero time event for determining age of loading.

Age at Loading	Type of Test	Specimens
15 hr	Unconfined compression	2
(TOFS + 9.5 hr)	Creep of concrete	2
24 hr	Unconfined compression	2
	Creep of concrete	2
48 hr	Unconfined compression	2
	Creep of concrete	2
72 hr	Unconfined compression	2
	Creep of concrete	2
8 days	Unconfined compression	2
	Creep of concrete	2

17. Unconfined compression tests were conducted in accordance with ASTM C 39 (ASTM 1988b) at the ages shown in paragraph 16 to provide data on strength as a function of time. The properties of specific creep, shrinkage, and elastic modulus (as functions of time) were calculated from the compressive creep tests on the overlay concrete mixture. The creep tests were conducted according to ASTM C 512 (ASTM 1988i) modified to include early ages of loading, modulus calculation, and continuous data acquisition by computer. The elastic modulus of the concrete was calculated from the initial loading phase of the creep tests. The shrinkage data were obtained from the sealed creep test control specimens.

18. The results of these tests are shown in Figures 2 through 4. Figures 2 and 3 show the strength and modulus gain, respectively, of the mixture for the first 8 days after casting. Using the modulus of elasticity, specific creep strains were calculated from the raw creep test data. The specific creep strains at each age of loading are shown in Figure 4.

Aging Material Model Calibration and Verification

19. The UMAT in ABAQUS was calibrated for the Dashields concrete mixture. The information needed for calibration included the adiabatic temperature rise, creep compliance, shrinkage, and modulus of elasticity as a function of time. These are discussed in the following paragraphs.

20. An adiabatic temperature rise curve for the overlay mixture was estimated from adiabatic temperature rise data obtained on a laboratory mixture containing a chemically comparable cement. The laboratory mixture, however, had a cement content of 282 lb/yd^3, while the Dashields overlay concrete

mixture had a cement content of 600 lb/yd^3. Thus, the test temperatures were multiplied by a factor of 600/282 to adjust for the variation in cement content. The resulting adiabatic temperature rise curve is shown in Figure 5.

21. A creep compliance curve was calculated from creep test data performed at WES on the Dashields concrete mixture. The relationship between creep compliance, C(t), total compliance, J(t), and elastic specific strain, 1/E(t) is shown in Figure 6. These data were fit with an exponential curve for input into the aging material model.

22. The sealed volume change for the mixture was estimated from tests of similar concretes conducted by the University of Michigan under contract to WES (Tjiptobroto and Hansen 1988).

23. The elastic modulus as a function of time for the Dashields overlay mixture was determined from mechanical properties tests conducted at WES. These data were fit with an exponential curve for input into the aging material model.

24. The material model was verified with respect to total strain observed in a creep test by comparing the observed elastic and creep strains with an axial pressure of 1,250 psi at an age of 3 days. The calculated strains were obtained by conducting a finite element analysis on a single element subjected to the same loading and environmental conditions as the 3-day creep test specimen. The results of the comparison are shown in Figure 7. Clearly the material model accurately models the observed elastic and creep strains.

PART III: THERMAL STRESS ANALYSES

Factors Affecting Cracking of Overlay Sections

25. Previous research at WES has shown that a number of factors can affect the cracking of overlay sections of lock walls (Norman, Campbell, and Garner 1988). These factors include the following:

a. Amount of volume change (both sealed volume change and drying shrinkage).

b. Temperature gradient through the concrete.

c. Thickness of the overlay section.

d. Bond between the overlay section and the existing concrete.

e. Ambient temperature.

f. Extent of insulation during cold weather.

Finite element calculations were made varying some of these parameters to determine the critical combination for cracking and methods for reducing that cracking.

Finite Element Discretization

26. The finite element calculations for both horizontal and vertical overlays were conducted using the grid shown in Figure 8. The grid consists of a 12- by 5-ft section of existing concrete with a 12-in.-thick overlay of new concrete placed directly on the old concrete. The 5-ft depth was chosen based on thermal calculations showing 5 ft as the depth below which the temperature of the existing concrete is no longer affected by the heat generated during hydration of the cement in the overlay section. The boundary conditions for thermal calculations for a 12-in.-thick overlay are shown in Figures 9 and 10 for horizontal and vertical overlays, respectively. The major difference in the calculations for horizontal and vertical overlays was the placing of the forms in the finite element thermal calculations.

27. The boundary conditions assumed for stress calculations are shown in Figure 11. Identical boundary conditions were assumed for both horizontal and vertical overlays.

Finite Element Analyses

Horizontal overlay

28. In the analysis of the horizontal overlay, a plane strain element was used. For this type of analysis, cracking occurs in the out-of-plane direction. A thermal analysis (Run 8) was conducted of a 12-in.-thick overlay with boundary conditions as follows: 0.75-in.-thick forms removed at 1 day, 75° F ambient temperature, and 75° F placement temperature of overlay concrete.

29. Key node point locations in the overlay were selected for plots of temperature-time histories. These locations are shown in Figure 12. Figures 13, 14, and 15 show the temperature-time histories at the selected nodes for Run 8.

30. Using the temperatures from the thermal analysis, stress analyses were conducted to determine the effects of thermal stresses of both sealed volume change and drying shrinkage. The amount of volume change is input into the code by varying the shrinkage factor, defined as the ratio of total volume change (sealed volume change plus drying shrinkage) to sealed volume change alone. Two stress analyses were conducted: Run 10 (shrinkage factor = 1) and Pun 11 (shrinkage factor = 2).

31. For plotting the output of stress analyses, certain critical Gauss (integration) points were selected in key elements of the overlay. These points are located as shown in Figure 16. For the above stress analyses, out-of-plane stress-time histories are plotted in Figures 17 and 18. It should be noted that the algebraic sign of compressive stresses and strains is positive in this report.

32. In the stress-time history plots, cracking is characterized by an instantaneous drop in tensile stresses. The analysis shows that cracking will occur first at the center line in approximately 10 days and spread to the end of the overlay by the twelfth day. Because the cracking does not occur during the first few days after placement (when the maximum thermal gradient exists (Figures 13 and 14)), it can be concluded that temperature differential alone should not cause cracking during the initial construction period. Also, a shrinkage factor of 1 (no drying shrinkage) indicates that cracking will occur due to sealed volume change alone. However, some drying shrinkage will occur; thus a shrinkage factor of 1 is not realistic.

33. In Run 11 a shrinkage factor of 2 was used to investigate the influence of drying shrinkage. Cracking in Run 11 started at the outer corner (elements 143 and 144) at 4.5 days after time of final set and spread quickly throughout the overlay (Figures 19 and 20). Thus, it appears that any drying shrinkage which may occur will only hasten the onset of cracking. Field observations have indicated that cracking typically begins about 2 to 3 days after casting. These analyses are indicating the onset of cracking at a later time (4.5 to 10 days after final set) indicating that shrinkage under field conditions is likely much greater than assumed in the analyses.

34. The analyses indicate that the onset of cracking occurs in the upper element (element 133) at the center line of the overlay. We do not believe this to be an accurate representation of the cracking phenomenon in overlay slabs with continuous base restraint. Cracking should originate at the point of maximum restraint, i.e., near the center line of the overlay at the old concrete/overlay interface. The analyses are predicting the initiation of cracking in the upper element for one or both of the following reasons: (a) the finite element mesh may be too coarse, or (b) the imposed boundary conditions at the center line have given rise to spurious results in the immediate vicinity of the boundary. However, these items do not invalidate the analysis of the overall cracking phenomenon in the overlays.

Vertical overlay

35. To better model the out-of-plane cracking in the vertical overlay, a plane stress analysis of a section through the length of the structure was used. The overlay thickness for the vertical overlays was limited to 12 in.

36. The following thermal calculations were made for vertical overlays:

Run No.	Description	Figures
18	Heat transfer analysis of vertical overlay with 1.5-in. forms removed at 1 day, 75° F ambient and placement temperatures of overlay concrete	21, 22, 23
18L	Heat transfer analysis with 1.5-in. forms removed at 3 days and 75° F ambient and placement temperatures of overlay concrete	24, 25, 26

Run No.	Description	Figures
18H	Heat transfer analysis with 1.5-in. forms removed at 1 day, 90° F ambient and 85° F placement temperatures of overlay concrete	27, 28
18Ha	Heat transfer analysis with 1.5-in. forms removed at 1 day, 90° F ambient and 75° F placement temperatures of overlay concrete	29, 30, 31
18C	Heat transfer analysis with 1.5-in. forms removed at 1 day, 40° F ambient and 50° F placement temperatures and insulation with a thermal resistance (R-value) of 4	32, 33

37. Runs 18 and 18L are characteristic of moderate weather conditions, while Runs 18H and 18Ha are representative of extreme summer conditions. Run 18C is typical of winter conditions with the addition of insulation.

38. The following stress analyses were loaded by temperatures from Run 18:

Run No.	Description	Figures
20S	Shrinkage factor = 1, no reinforcing bars	34, 35
21S	Shrinkage factor = 2, no reinforcing bars	36, 37
22R	Shrinkage factor = 2, No. 5 reinforcing bars at 12-in. spacing (on center) located 4 in. from overlay/old concrete interface	38, 39
23R	Shrinkage factor = 2, No. 5 reinforcing bars at 12-in. spacing (on center) located 4 in. from top face of overlay	40, 41
24S	Shrinkage factor = 2, bond breaker (100%)	42, 43
26S	Shrinkage factor = 2, partial bond breaker	44, 45

39. The following stress analyses were loaded with the temperature data from Runs 18L, 18H, 18Ha, and 18C:

Run No.	Description	Figures
21L	Stress analysis loaded by temperatures from Run 18L, shrinkage factor = 2, no reinforcing bars	46, 47

Run No.	Description	Figures
21H	Stress analysis loaded by temperatures from Run 18H, shrinkage factor = 2, no reinforcing bars	48, 49
21Ha	Stress analysis loaded by temperatures from Run 18Ha, shrinkage factor = 2, no reinforcing bars	50, 51
21C	Stress analysis loaded by temperatures from Run 18C, shrinkage factor = 2, no reinforcing bars	52, 53

40. In all analyses where cracking occurred, cracking began at the center of the overlay and spread along the interface. As observed in the horizontal overlays, the onset of cracking occurs at later times than field observations indicate. Again, this shows that total volume change in the field is more severe than assumed in the analyses. Cracking in Run 20S occurred at the center only. This run represented an overlay with sealed volume change only (i.e., no volume change due to shrinkage). Results of Runs 21S, 22R, and 23R, with a shrinkage factor of 2, showed much more extensive cracking. Cracking was initiated at the center at approximately 6 days and spread along the interface and upward until only the top end elements remained uncracked at 12 days. Very little difference in stress or strain was observed between reinforced and unreinforced overlays. Runs 21S, 22S, and 23S did not show cracking in the quarter-point top element (element 138). Runs 24S and 26S showed no cracking. An interface element was used in each case to allow bond strength to vary. Run 24S simulated zero bond strength, while bond was simulated in Run 26S by applying a gradually increasing normal force (from 0 to 100 psi) and a constant friction factor.

41. The cracked elements and sequence of cracking for Run 21L was identical to Run 21S. In Run 21H, cracking occurred at the center line at 6 days, but extended along the interface more slowly, reaching the outer elements at 14 days and extending only through upper elements near the center. Cracking was similar but occurred slightly later in Run 21C. In Run 21Ha, the cracking patterns were similar, but, in addition, cracking occurred at midpoint top element (element 138).

42. From these analyses it is obvious that shrinkage is the most influential factor in overlay cracking. Since the restraint against shrinkage is similar throughout a thin overlay, stresses are high throughout. The additional stress due to the thermal gradient is relatively small but is enough to influence the location and propagation of cracks. All effective solutions to the problem must concentrate on limiting shrinkage and stresses due to the restraint of shrinkage.

PART IV: CONCLUSIONS AND RECOMMENDATIONS

Conclusions

43. Finite element analyses made with ABAQUS incorporating the UMAT calibrated for the Dashields overlay concrete show that shrinkage is the primary factor in overlay cracking. Because the overlays are relatively thin, thermal stress gradients are small. The major influence of the thermal stresses is to control the location and propagation of cracking in the overlay.

44. The concrete mixture supplied to WES by ORP had a cement content of 600 lb/yd^3, a water-cement ratio of 0.45, and a maximum aggregate size of 0.75 in. This combination of parameters yields a mixture inherently susceptible to shrinkage problems. In addition, no curing procedures other than applying a membrane-forming curing compound are used. The potential for shrinkage may be greater than if curing procedures involving added water were used; however, in field practice better moisture retention is normally achieved when curing compounds are used, since added water procedures are rarely employed other than intermittently.

45. The analyses have shown that an effective bond breaker will eliminate the cracking problem completely. However, there is a legitimate concern about the field applicability of a bond breaker. This concern should be addressed by field personnel and further research.

46. The analyses have also shown that reinforcing steel has little effect on the tendency for cracking to occur in the overlay. It will, however, control the spacing and size of the cracks throughout the overlay.

Recommendations

47. We recommend that concrete mixture proportions should be selected to limit shrinkage. Shrinkage increases with increasing water content and decreases with increasing aggregate size. Also, additional steps (other than applying a curing compound) should be taken in curing to limit drying shrinkage such as adopting moist curing procedures, etc.

48. A bond breaker can be used to limit stresses at an interface. However, the use of a bond breaker would require careful preparation of the

existing concrete surface to reduce roughness which tends to form a mechanical interlock between existing and overlay concrete. More research into bond breaking techniques and their effectiveness may be required prior to field application.

49. A very thick overlay surface (probably 3 ft or more) would provide less restraint at the surface and possibly prevent cracking from extending to the surface.

REFERENCES

American Society for Testing and Materials. 1988. 1988 Annual Book of ASTM Standards, Philadelphia, PA.

a. Designation C 33-86. "Standard Specification of Concrete Aggregates."

b. Designation C 39-86. "Standard Test Method for Compressive Strength of Cylindrical Concrete Specimens."

c. Designation C 138-81. "Standard Test Method for Unit Weight, Yield, and Air Content (Gravimetric) of Concrete."

d. Designation C 143-78. "Standard Test Method for Slump of Portland Cement Concrete."

e. Designation C 150-86. "Standard Specification for Portland Cement."

f. Designation C 192-88. "Standard Method of Making and Curing Concrete Test Specimens in the Laboratory."

g. Designation C 231-82. "Standard Test Method for Air Content of Freshly Mixed Concrete by the Pressure Method."

h. Designation C 403-88. "Standard Test Method for Time of Setting of Concrete Mixtures for Penetration Resistance."

i. Designation C 512-87. "Standard Test Method for Creep of Concrete in Compression."

Chen, W. F. 1982. Plasticity in Reinforced Concrete, McGraw-Hill, New York.

McDonald, James E. 1987 (Dec). "Rehabilitation of Navigation Lock Walls: Case Histories," Technical Report REMR-CS-13, US Army Engineer Waterways Experiment Station, Vicksburg, MS.

Norman, C. Dean, and Anderson, Fred A. 1985. "Reanalysis of Cracking in Large Concrete Dams in the US Army Corps of Engineers," Commission Internationale Des Grande Barrages, Quinzième Congrès Des Grande Barrages, Lausanne, Switzerland.

Norman, C. Dean, Campbell, Roy L., Sr., and Garner, Sharon. 1988 (Jun). "Analysis of Concrete Cracking in Lock Wall Resurfacing," Technical Report REMR-CS-15, US Army Engineer Waterways Experiment Station, Vicksburg, MS.

Tjiptobroto, W., and Hansen, W. 1988 (Mar). "Autogenous Shrinkage in Mass Concrete," Letter Report to US Army Engineer Waterways Experiment Station, Vicksburg, MS, from University of Michigan, Ann Arbor, MI.

Wong, G. S., and Stowe, R. L. 1985. "Condition Survey of Dashields Locks, Ohio River," Manuscript report with letter of transmittal to US Army Engineer District, Vicksburg, Vicksburg, MS, from US Army Engineer Waterways Experiment Station, Vicksburg, MS.

SME BESSEMER CEMENT COMPANY

MILL TEST REPORT

TO: Beaver Concrete & Gravel
P. O. Box 62
Rochester, Pa. 15074

DATE: 2 2 88

PORTLAND & BLOCK

Type I — Type III
Type I-A — Block
Type II - LOW ALKALI

MASONRY

Type N — Type M
Type S — Color

SHIPPED FROM: SME Bessemer
TRUCK/CAR NO: 240
TONS: 24.23

CHEMICAL

SiO_2	21.7
Al_2O_3	4.4
Fe_2O_3	5.4
CaO	63.2
MgO	1.2
SO_3	2.8
Loss On Ignition	0.43
Insoluble Residue	0.19
C_3A 4.2 C_3S 47.8	
Total Alkalies, as Na_2O	0.49

PHYSICAL

Gillmore Initial Min.	165
Time of Set Final, Min.	270
Fineness, Blaine, cm2/gm	3526
Autoclave Expansion %	0.07
Air Content %	9.8
Compressive Strength, psi	
1-Day	
3-Day	2110
7-Day	3435
28-Day	5615
Water Rentention %	

These Test Data are Average of Silo or Lot from which cement was shipped and meet the latest revision of ASTM Specification C 150

Harry Irwin
Harry Irwin
Chief Chemist

Figure 1. Cement Mill Test Report

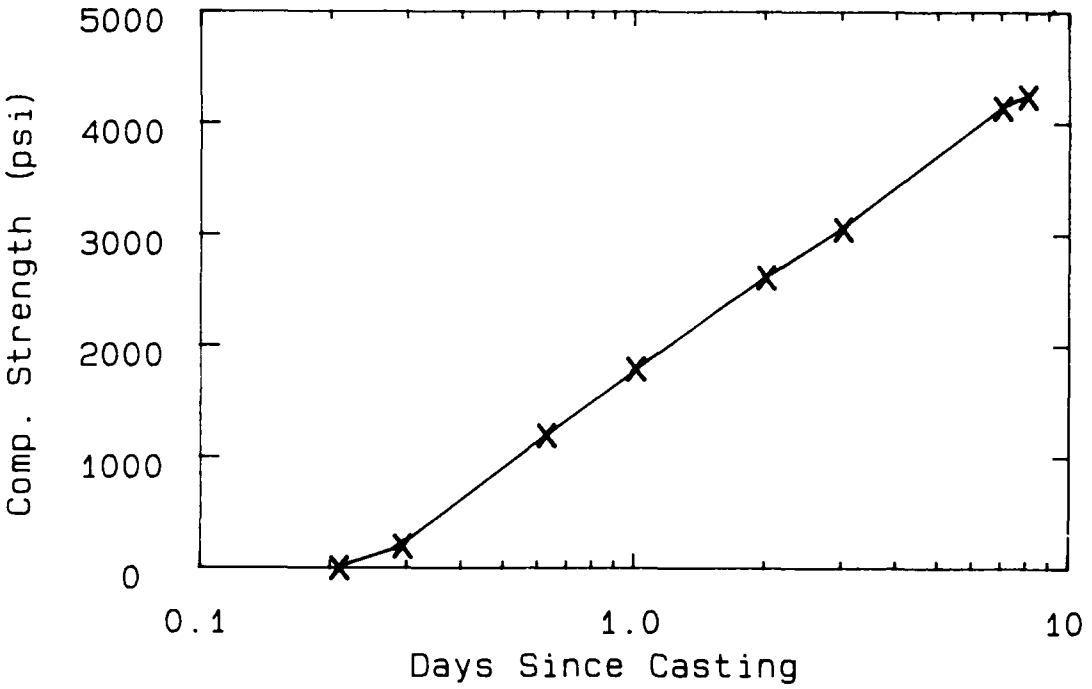

Figure 2. Compressive strength development

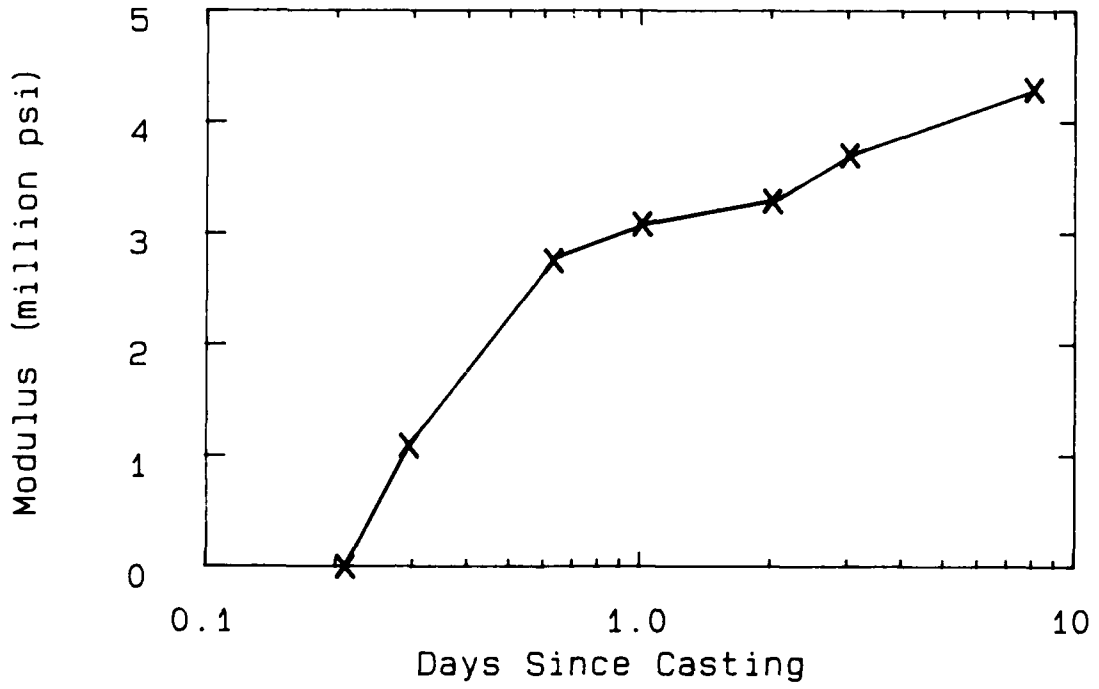

Figure 3. Elastic modulus development

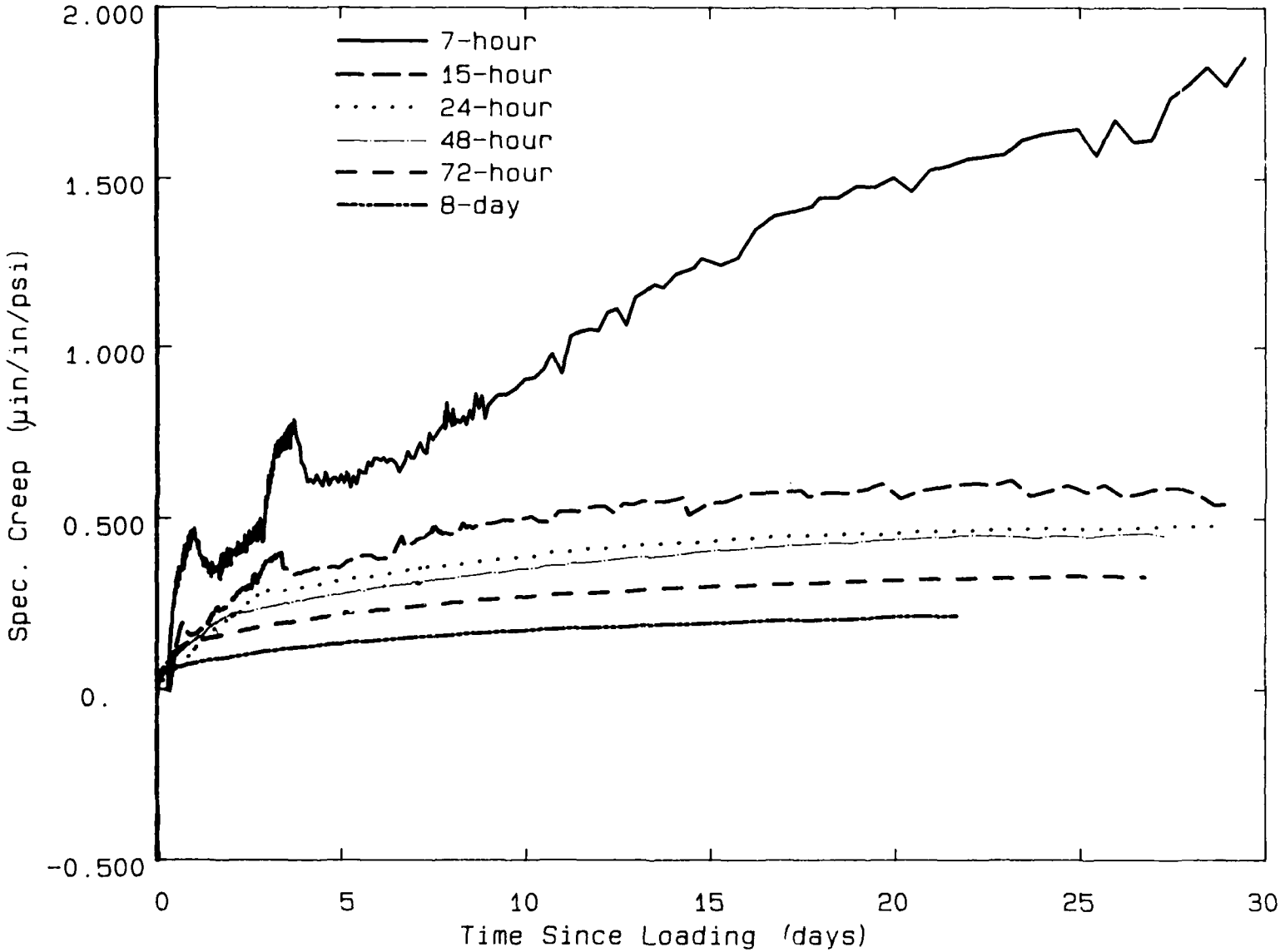

Figure 4. Family of specific creep curves

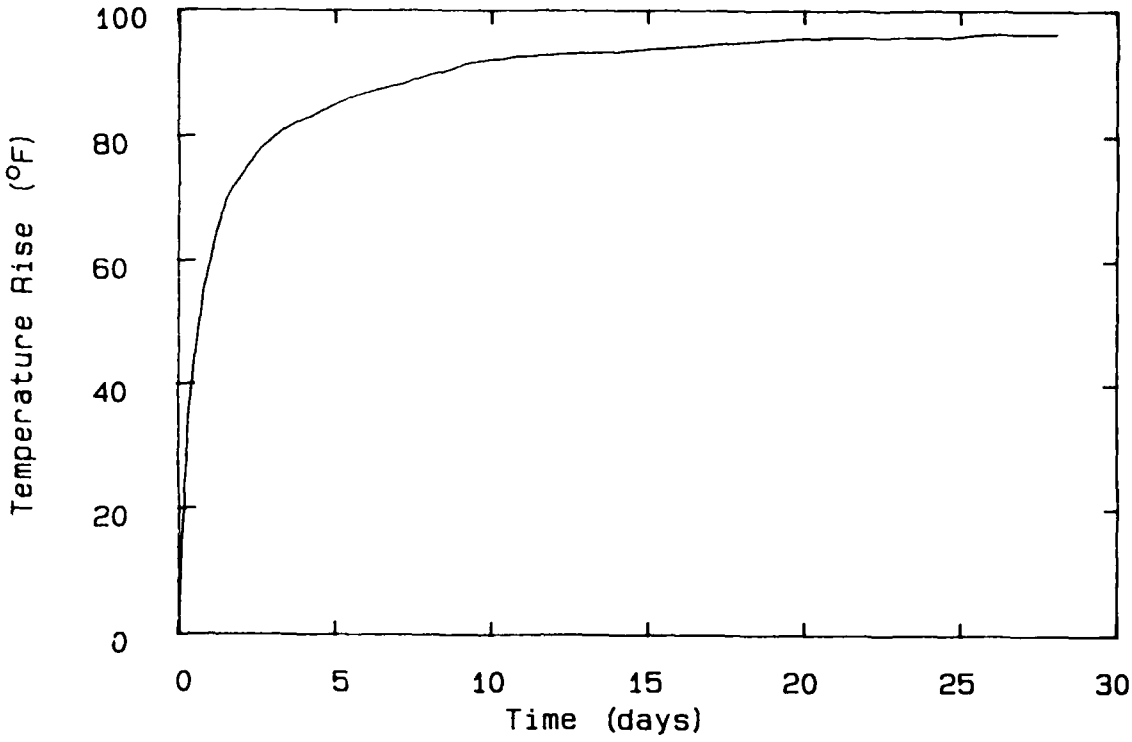

Figure 5. Adiabatic temperature rise curve used in thermal analyses

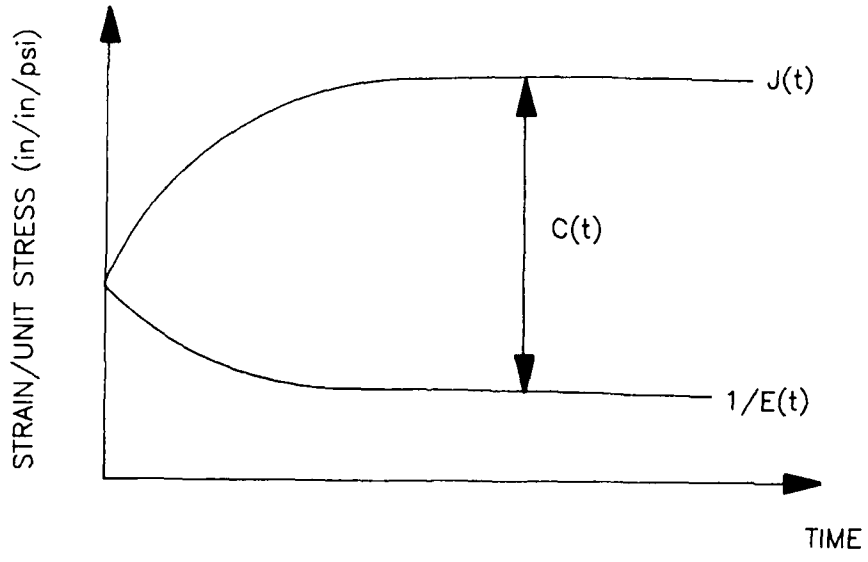

$$J(t) = C(t) + 1/E(t)$$

J(t) = Total strain/unit stress
C(t) = Specific creep
E(t) = Modulus of elasticity

Figure 6. Idealized curve showing parameters used in data reduction

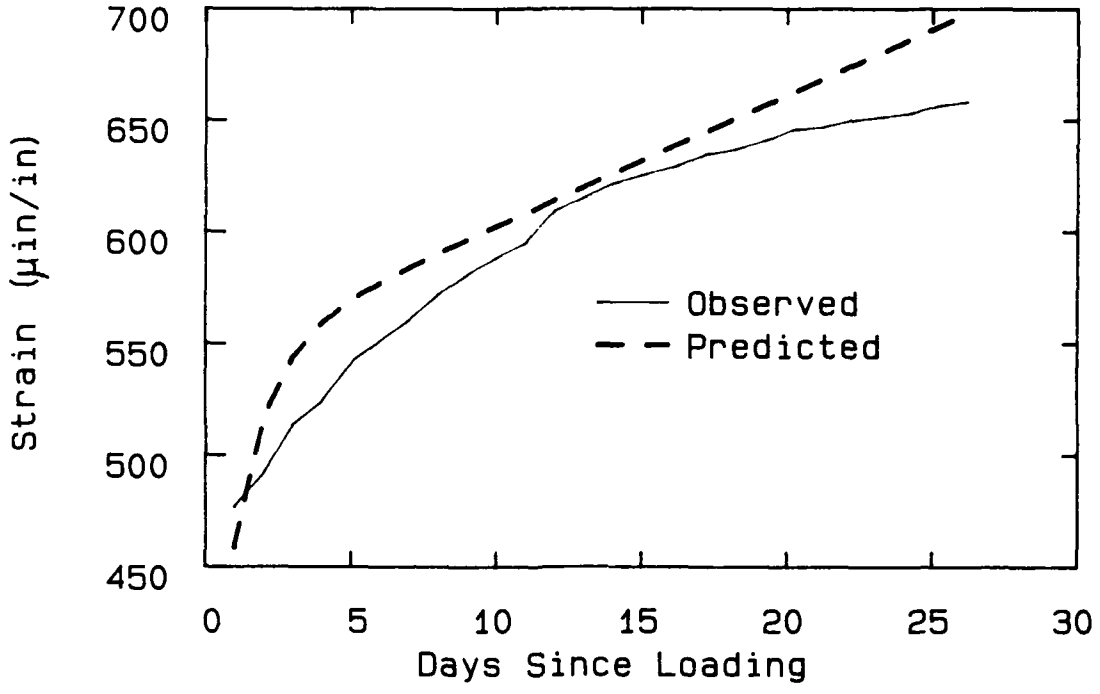

Figure 7. Comparison of ABAQUS model with 3-day creep test

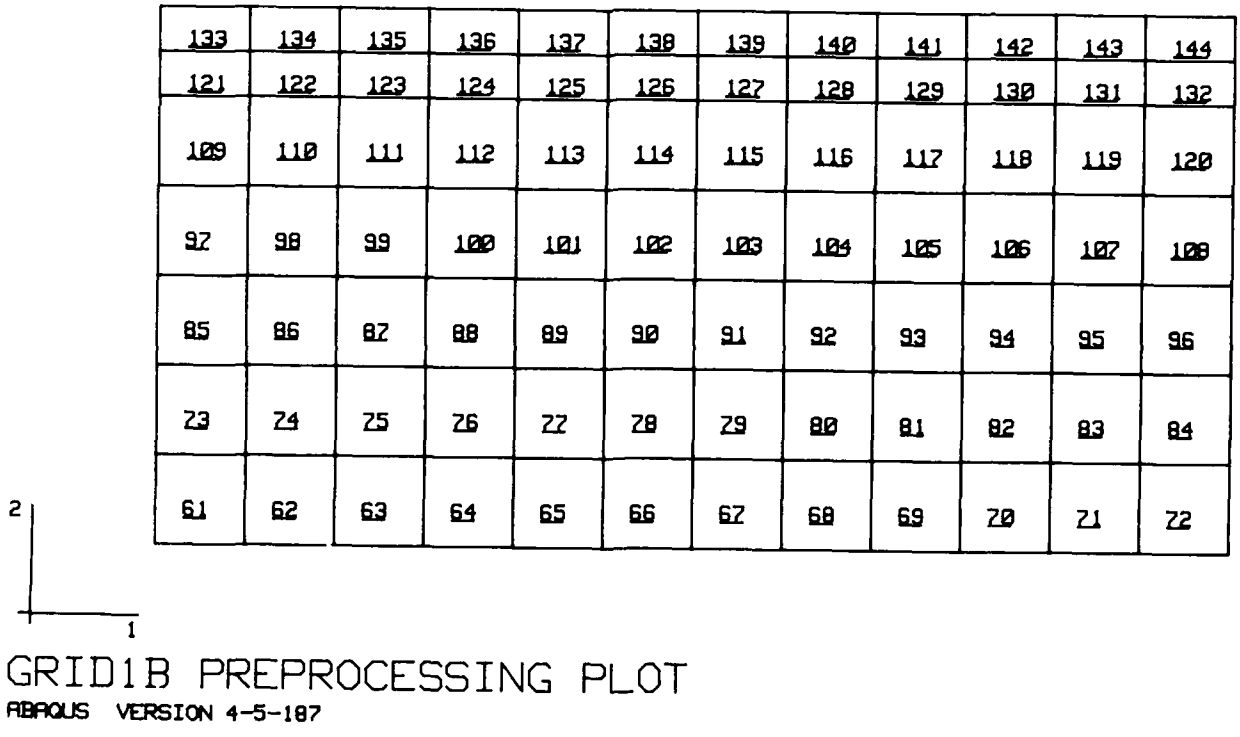

Figure 8. Finite element grid showing element numbers

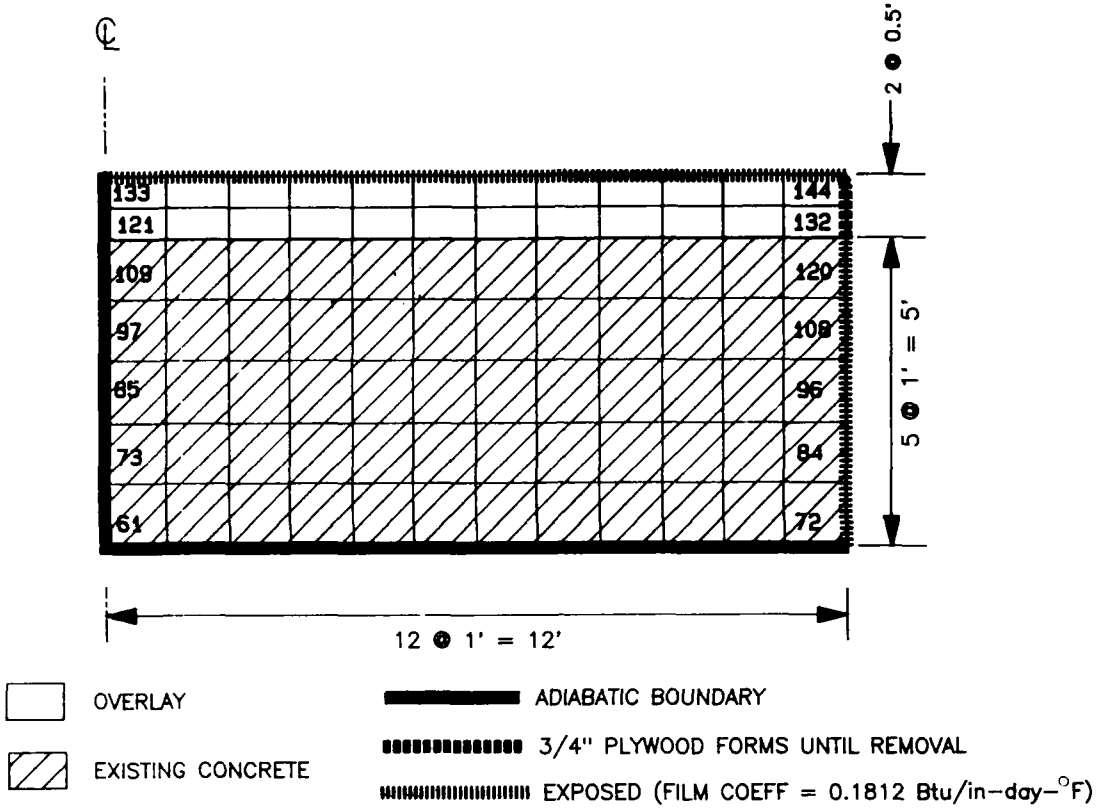

Figure 9. Finite element grid showing boundary conditions for thermal analyses on horizontal overlays

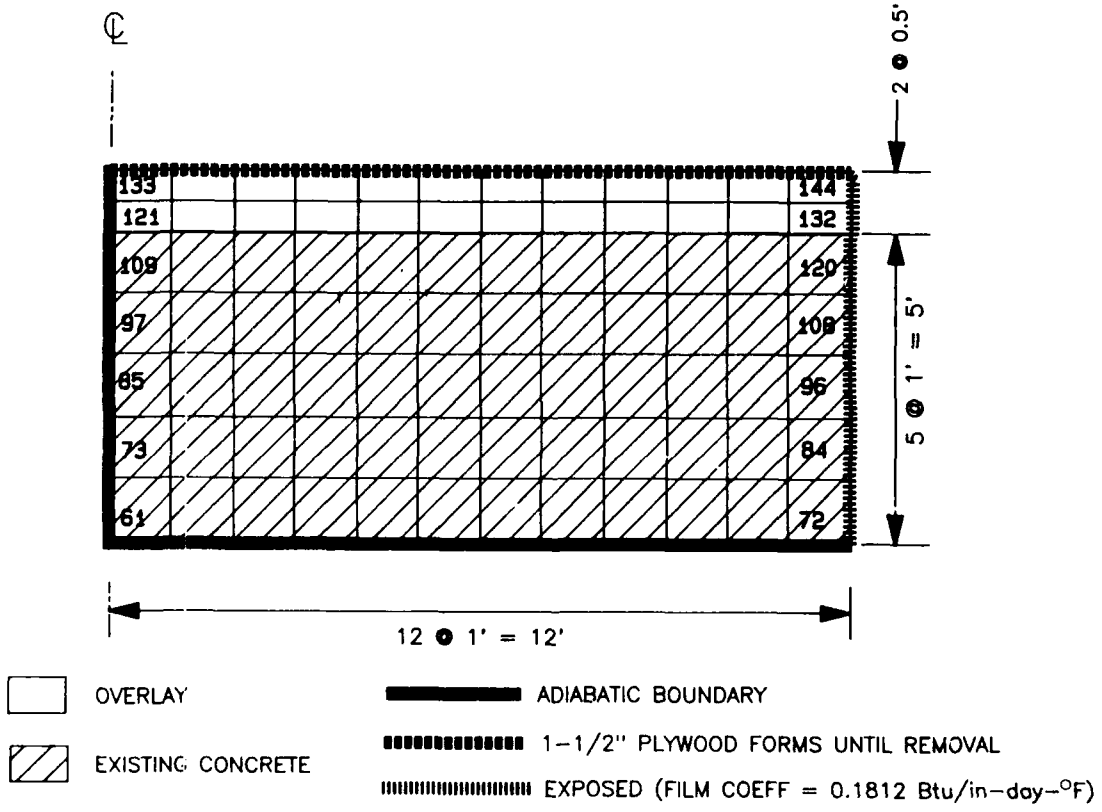

Figure 10. Finite element grid showing boundary conditions for thermal analyses on vertical overlays

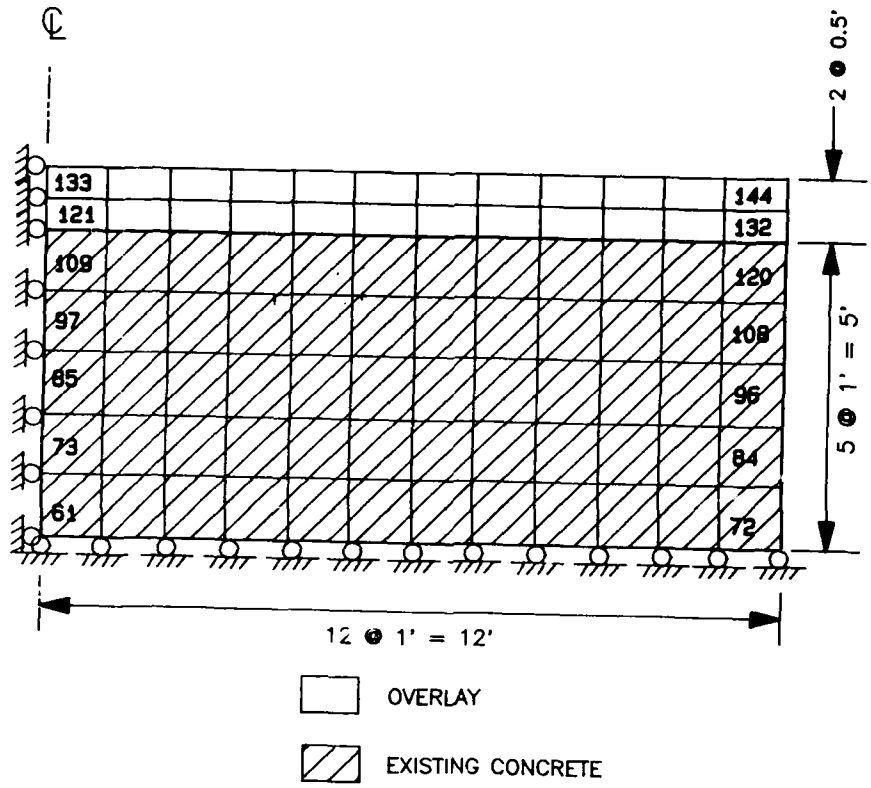

Figure 11. Finite element grid showing boundary conditions for stress analyses

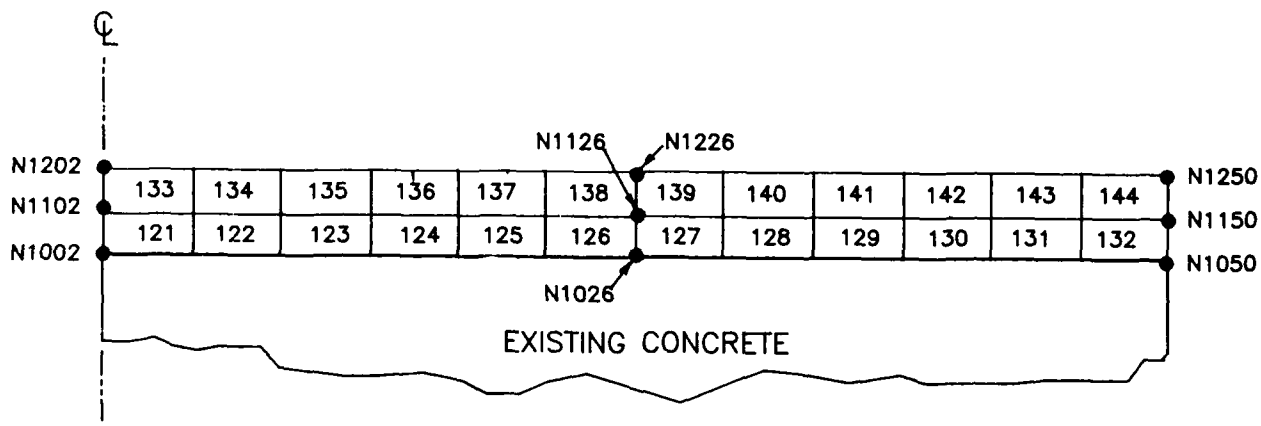

Figure 12. Finite element grid of overlay section showing node numbers chosen for data plots

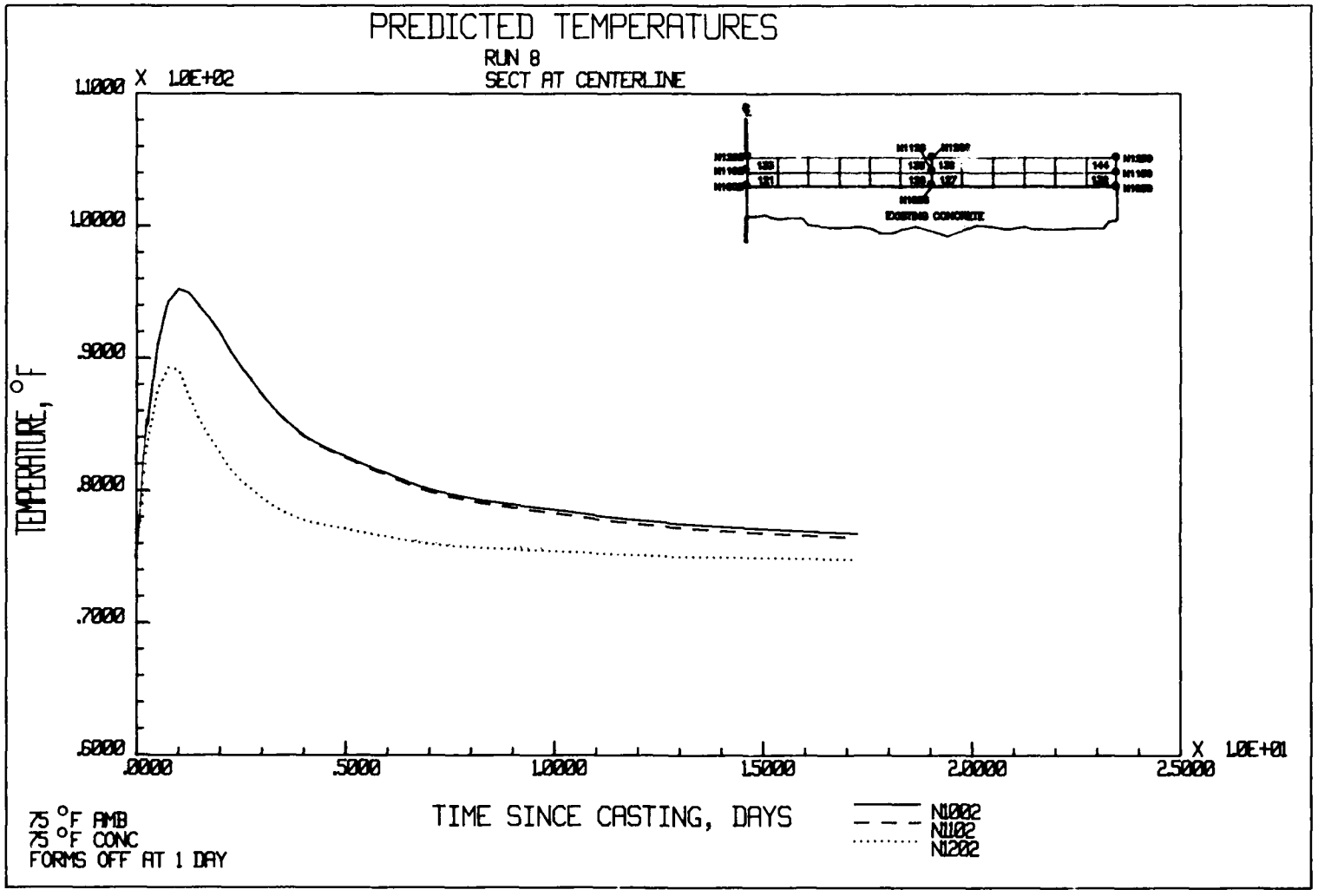

Figure 13. Predicted temperatures, Run 8, nodes 1002, 1102, and 1202

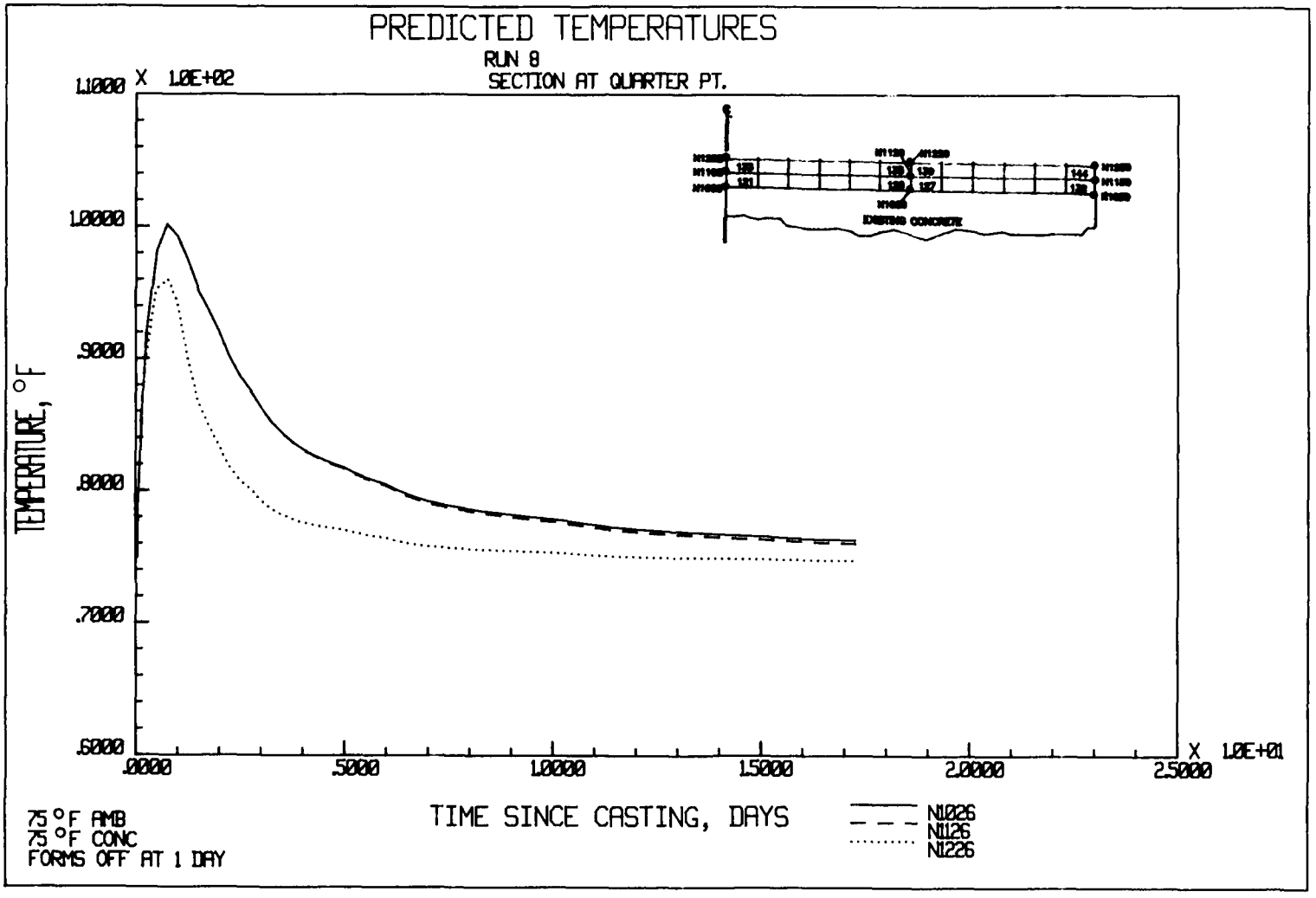

Figure 14. Predicted temperatures, Run 8, nodes 1026, 1126, and 1226

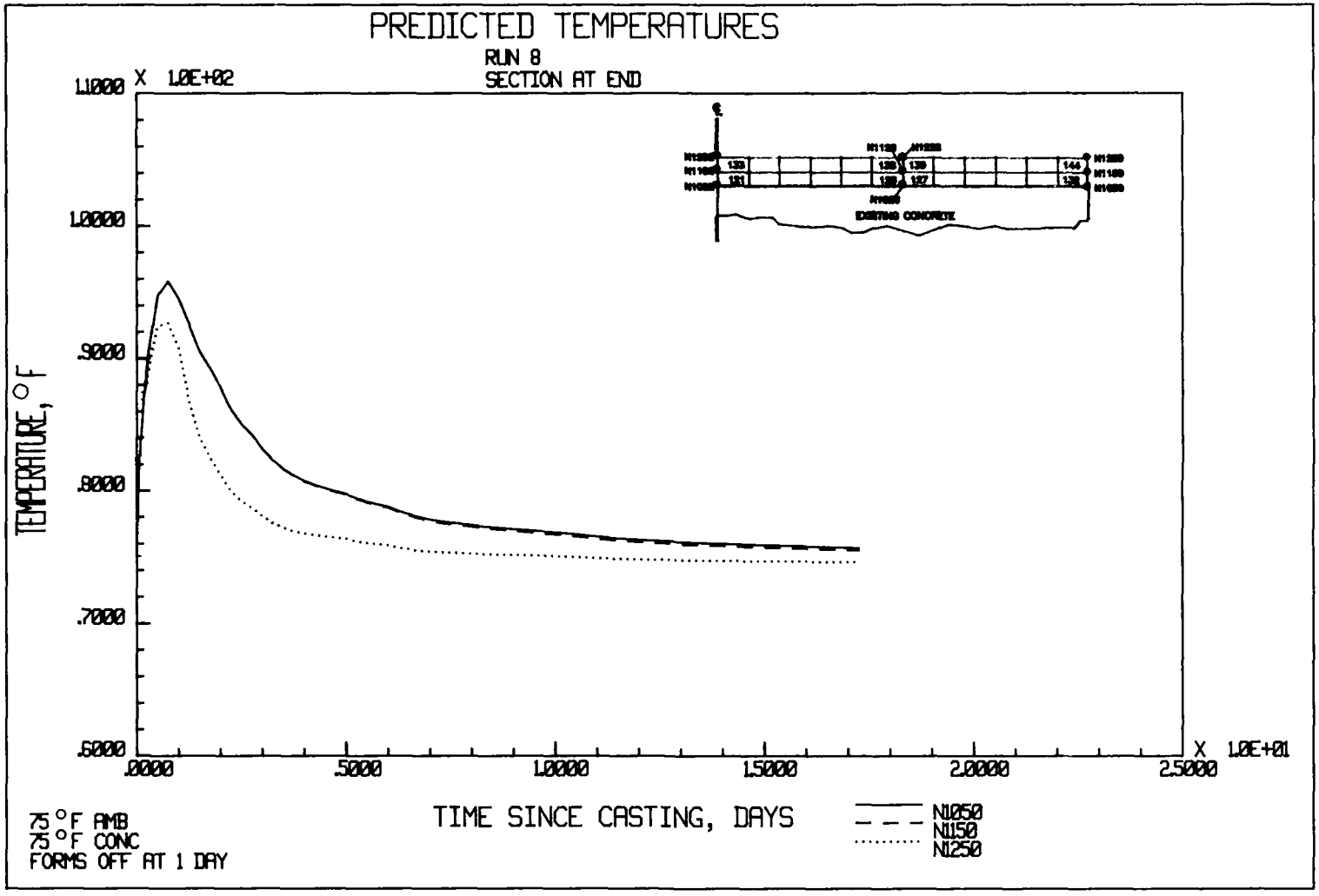

Figure 15. Predicted temperatures, Run 8, nodes 1050, 1150, and 1250

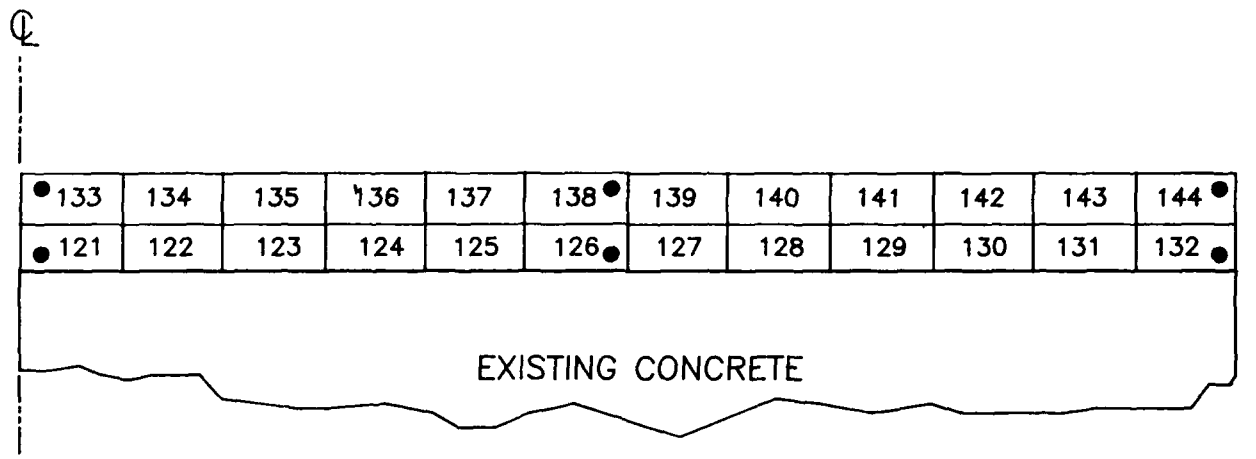

Figure 16. Finite element grid of overlay section showing Gauss points selected for data plots

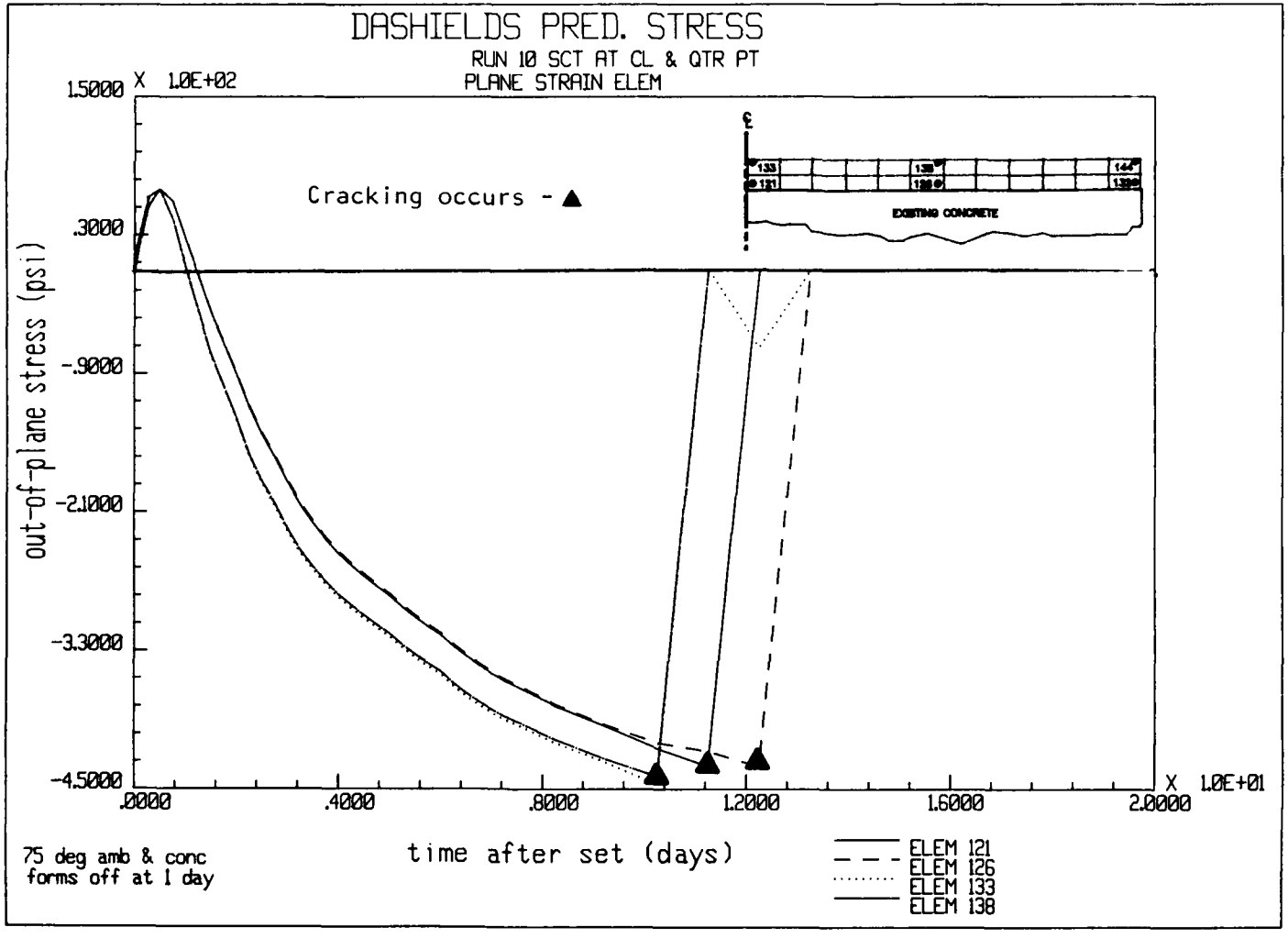

Figure 17. Predicted stress, Run 10, elements 121, 126, 133, and 138

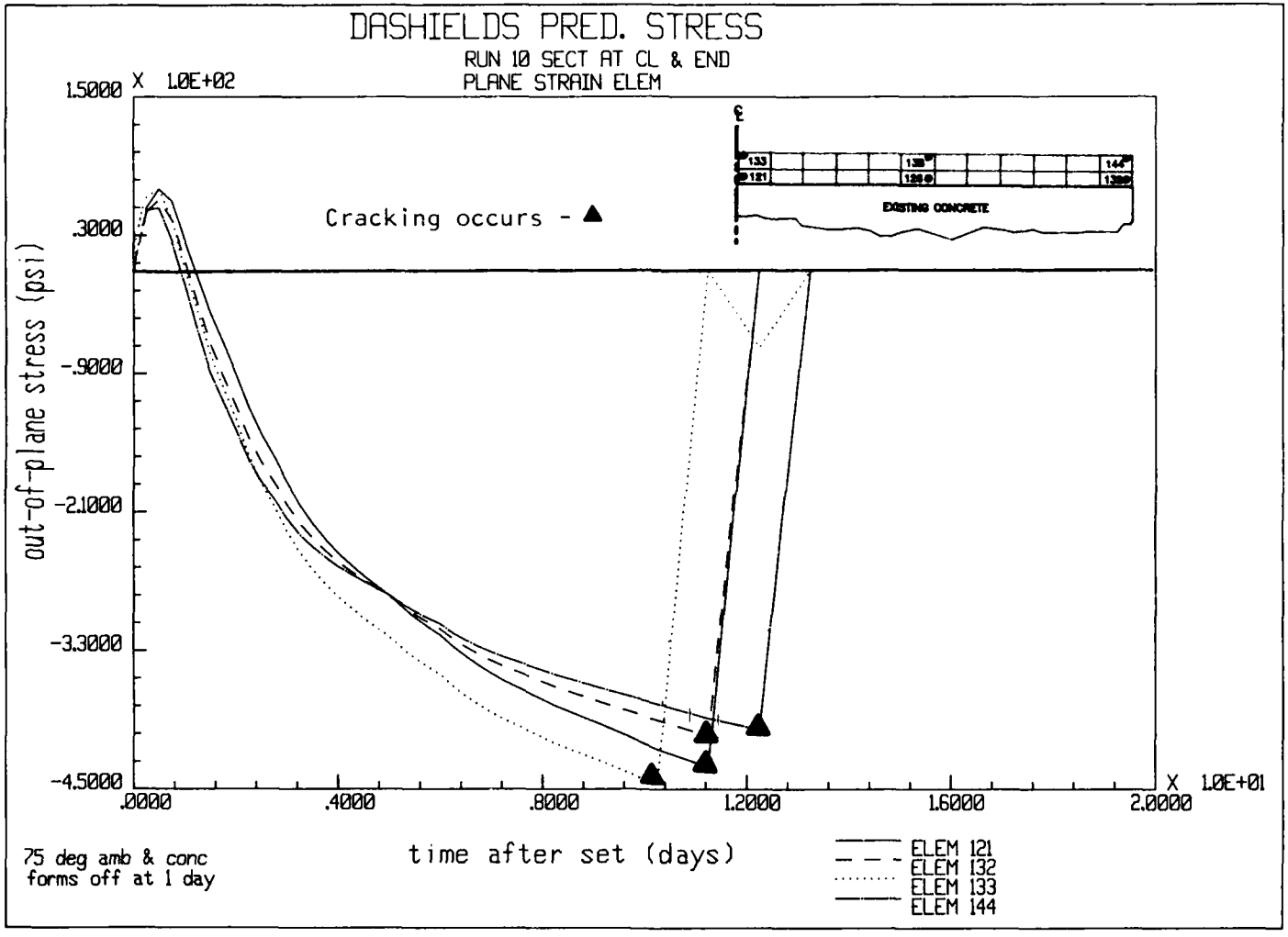

Figure 18. Predicted stress, Run 10, elements 121, 132, 133, and 144

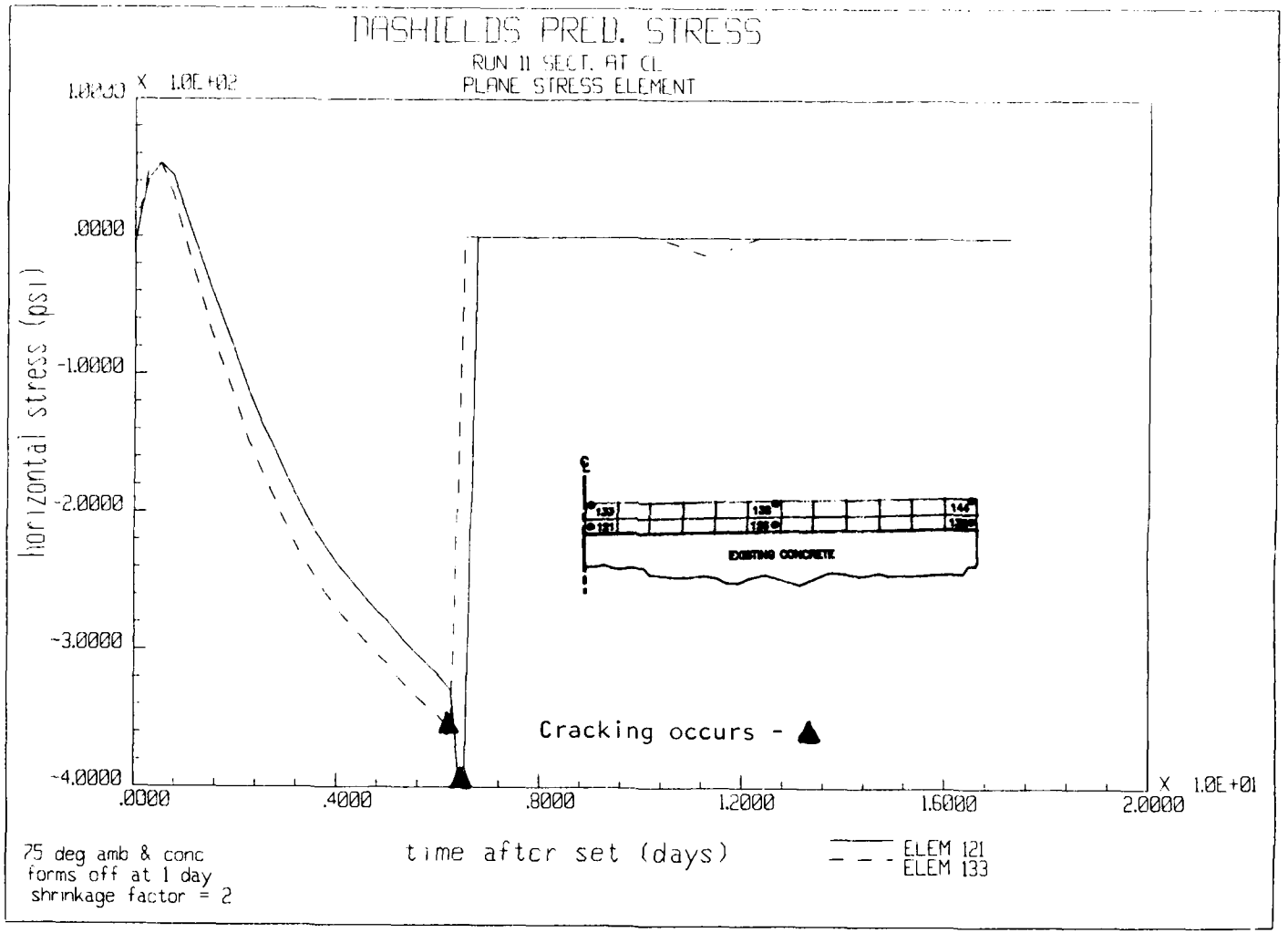

Figure 19. Predicted stress, Run 11, elements 121 and 133

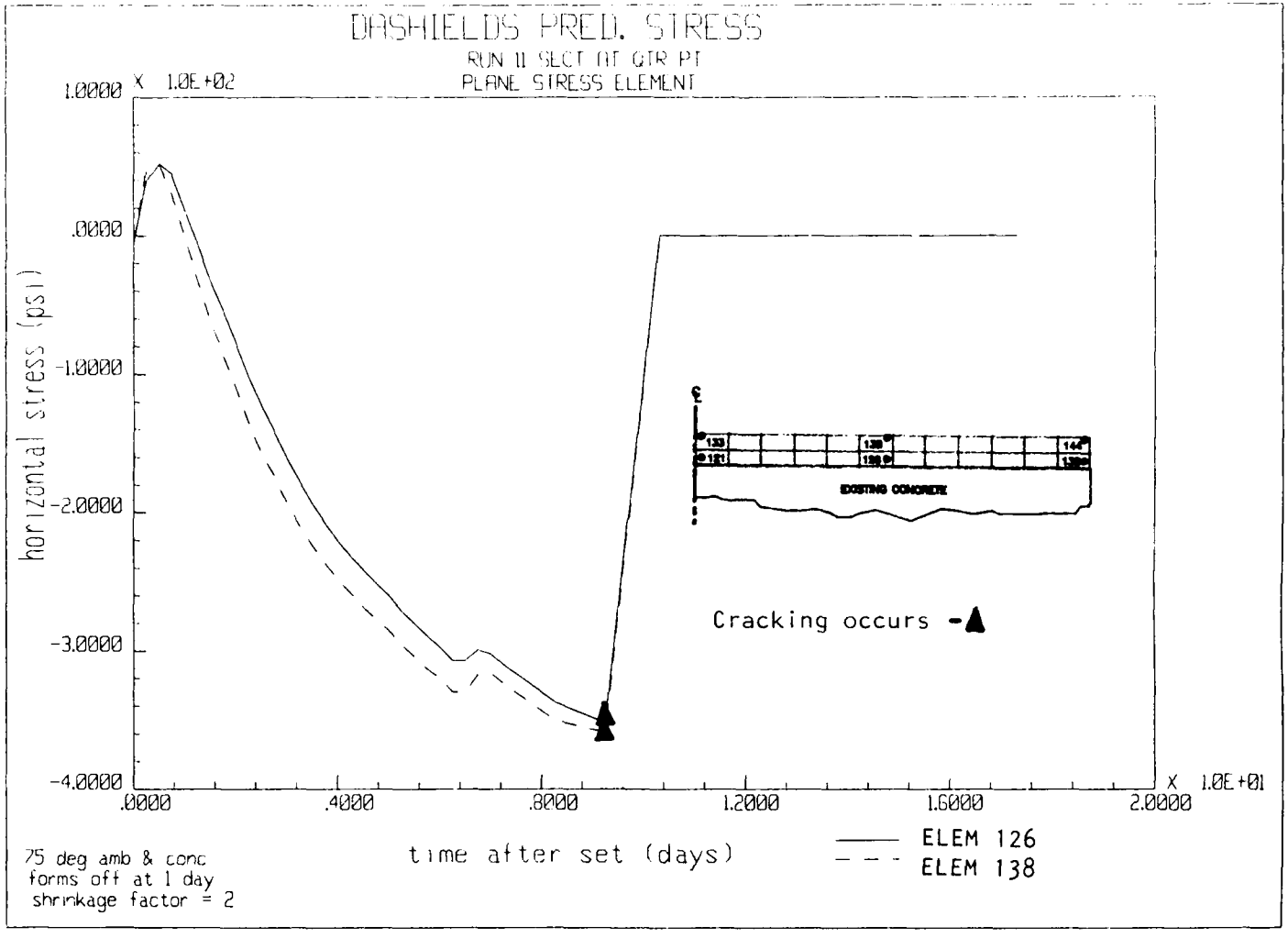

Figure 20. Predicted stress, Run 11, elements 126 and 138

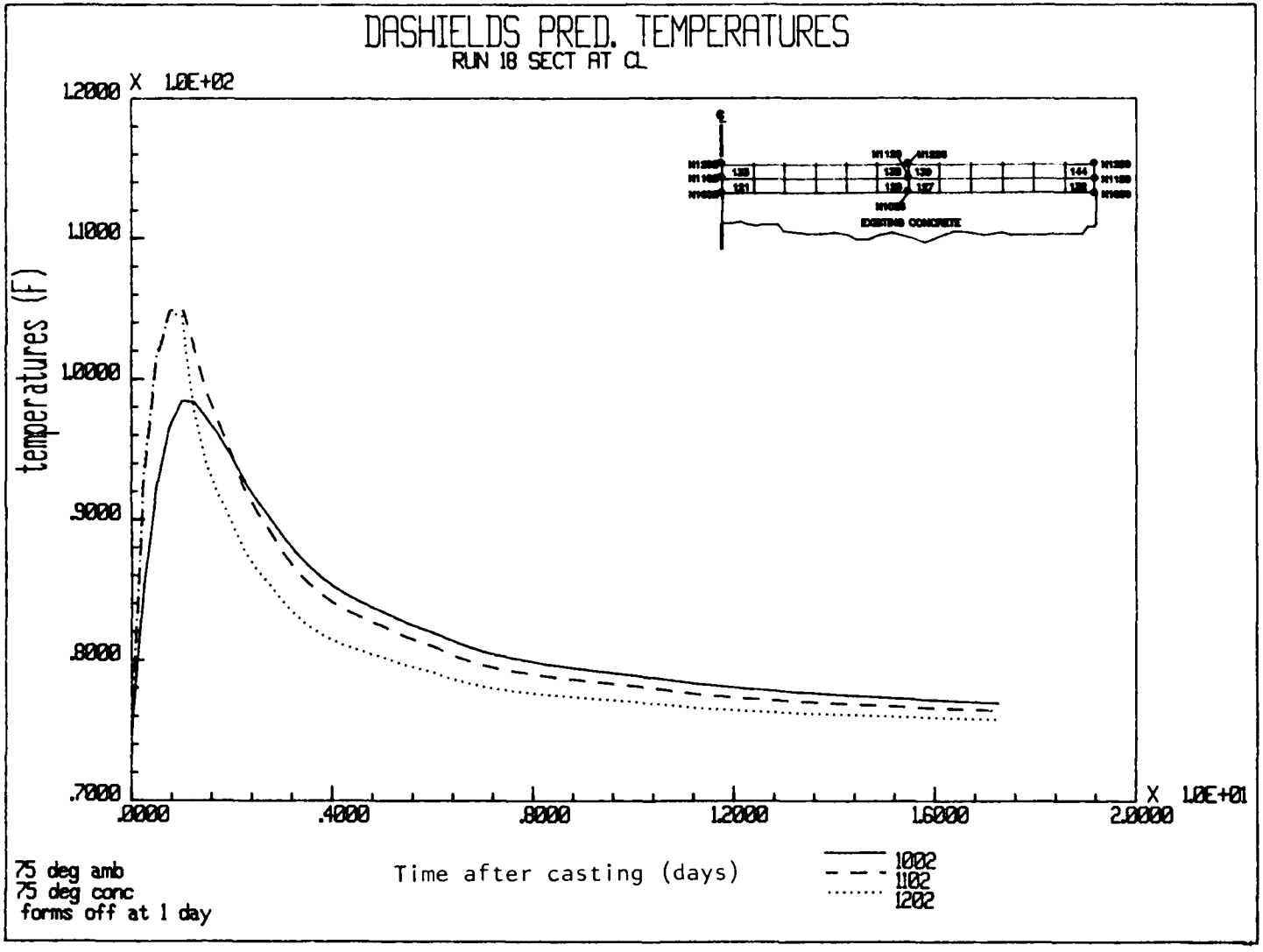

Figure 21. Predicted temperatures, Run 18, nodes 1002, 1102, and 1202

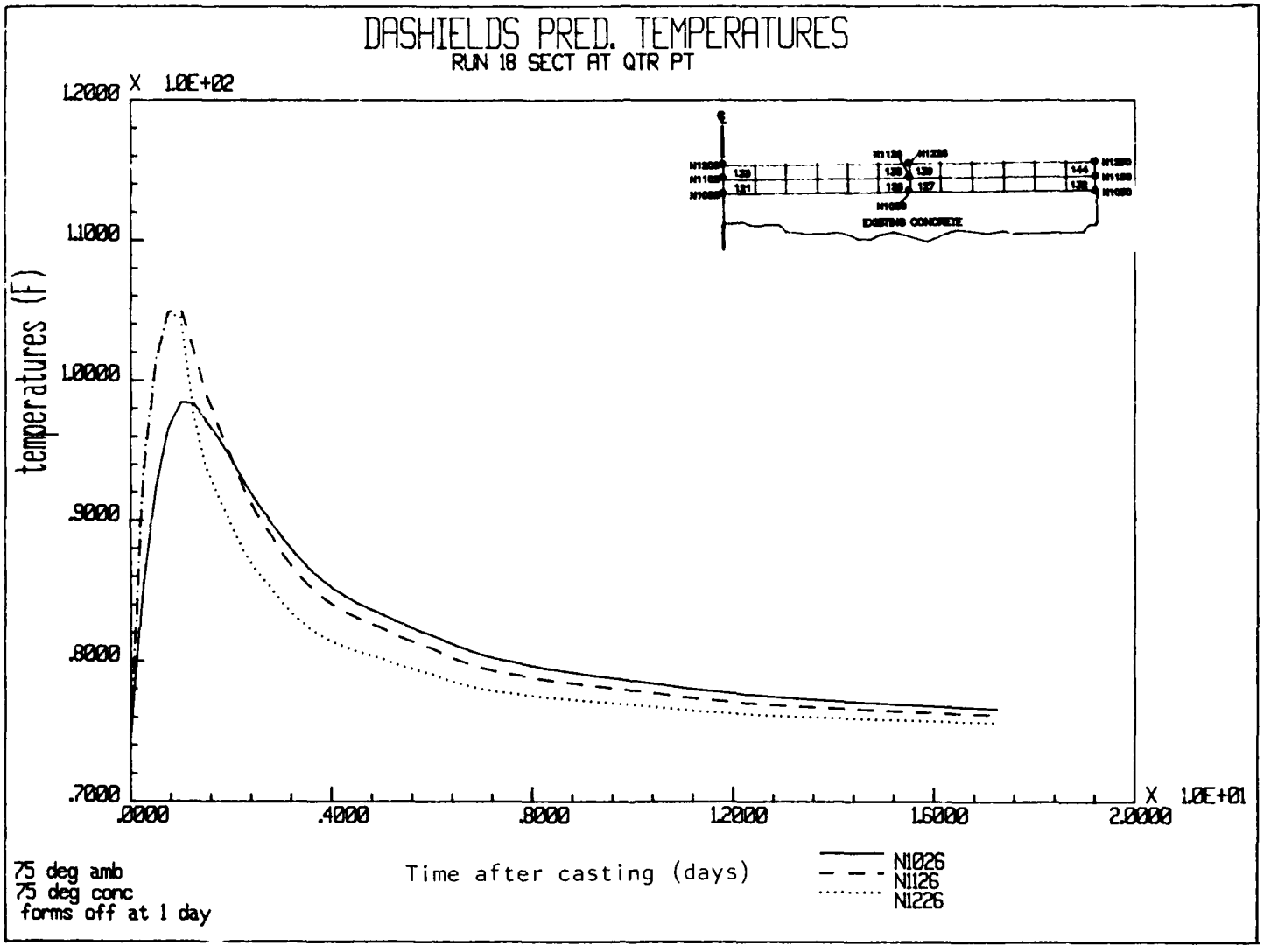

Figure 22. Predicted temperatures, Run 18, nodes 1026, 1126, and 1226

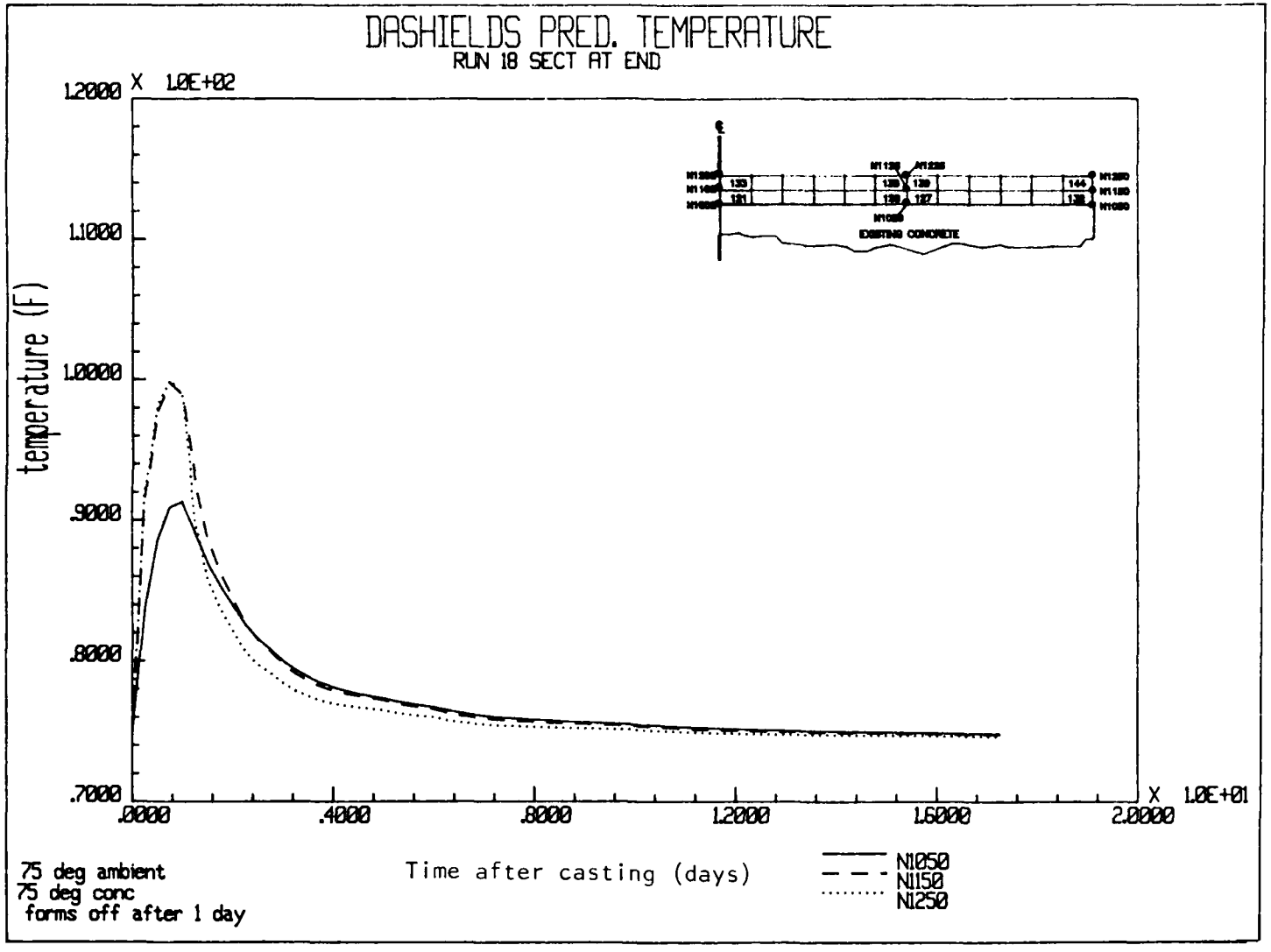

Figure 23. Predicted temperatures, Run 18, nodes 1050, 1140, and 1250

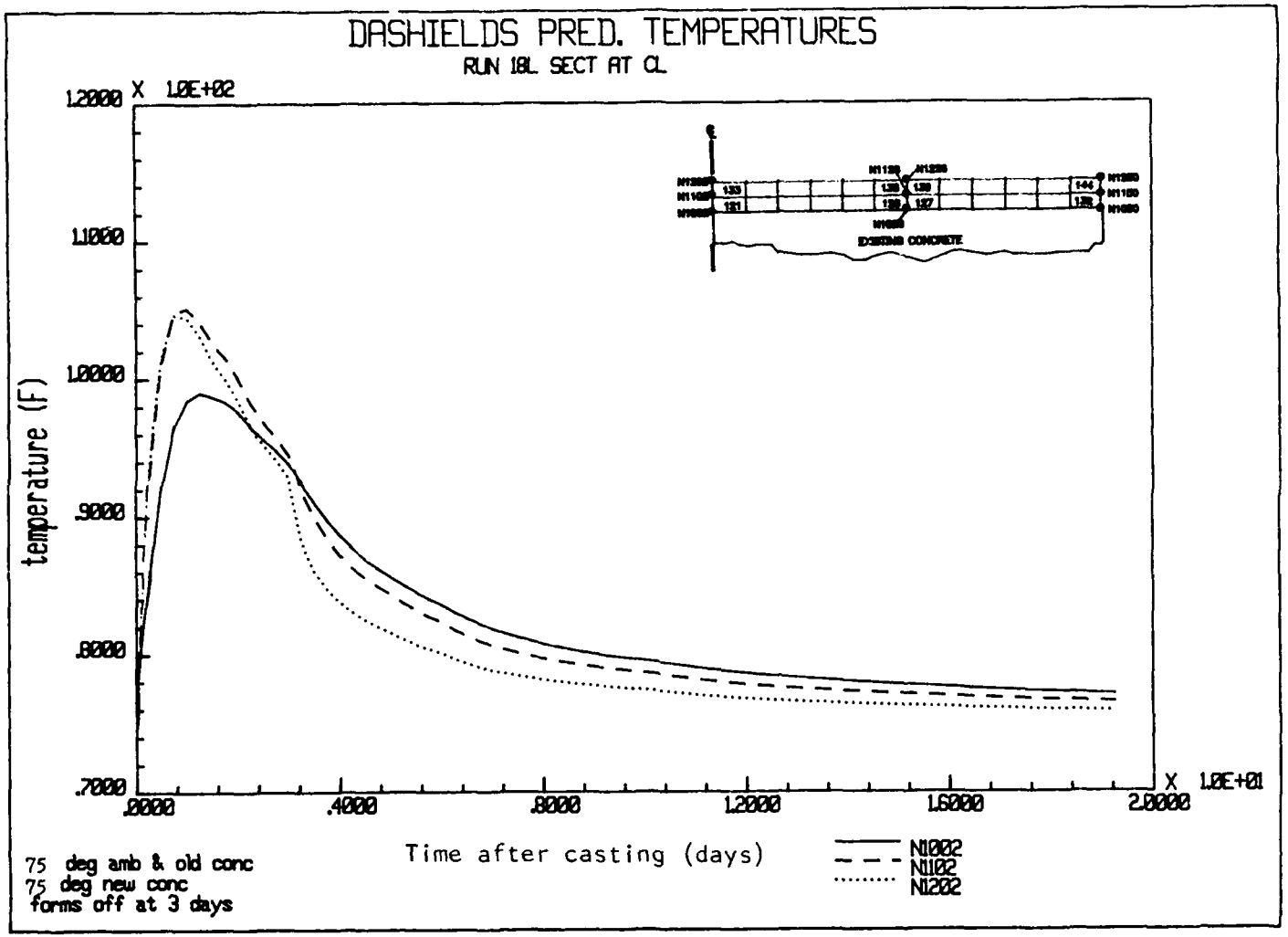

Figure 24. Predicted temperatures, Run 18L, nodes 1002, 1102, and 1202

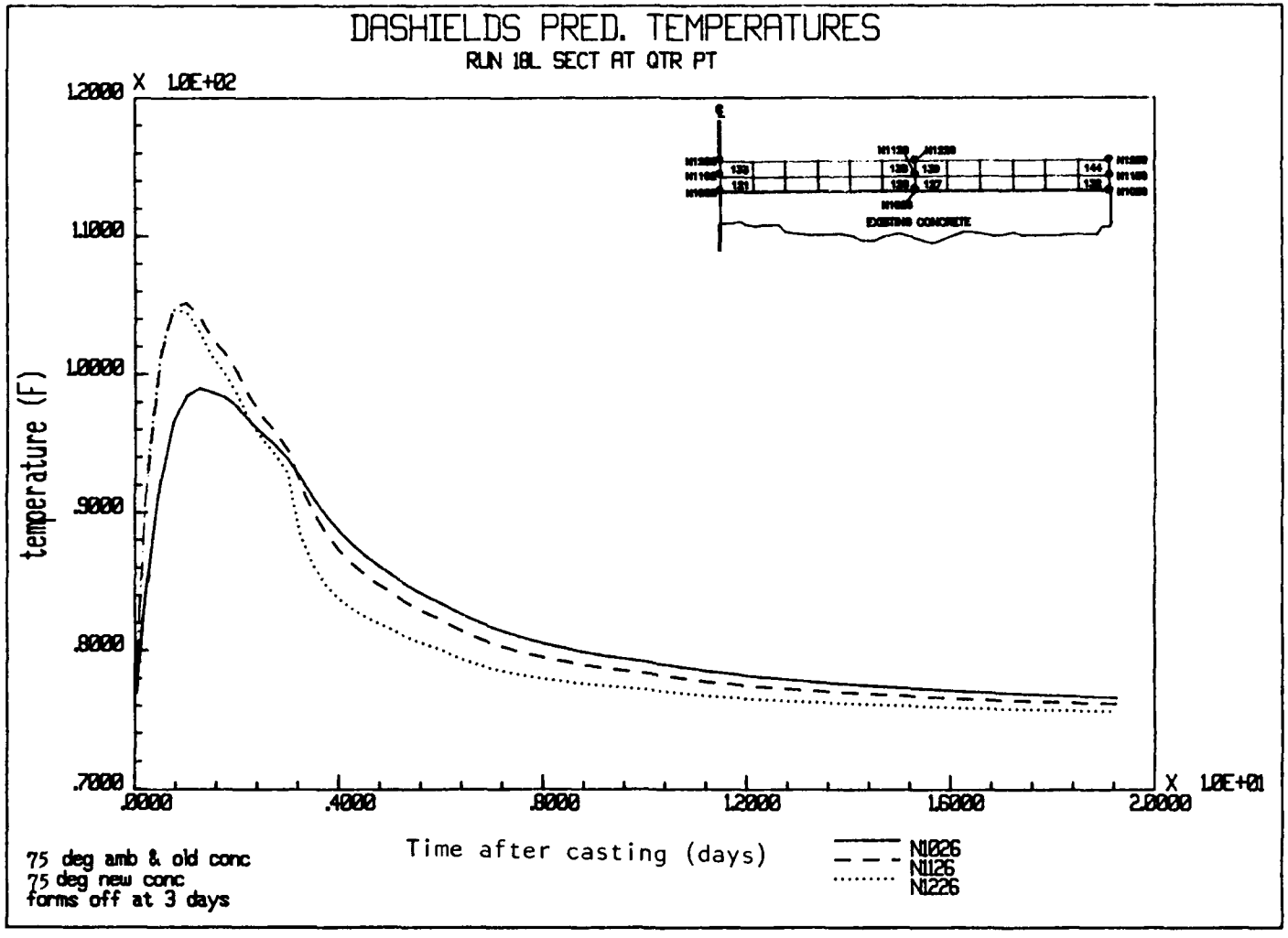

Figure 25. Predicted temperatures, Run 18L, nodes 1026, 1126, and 1226

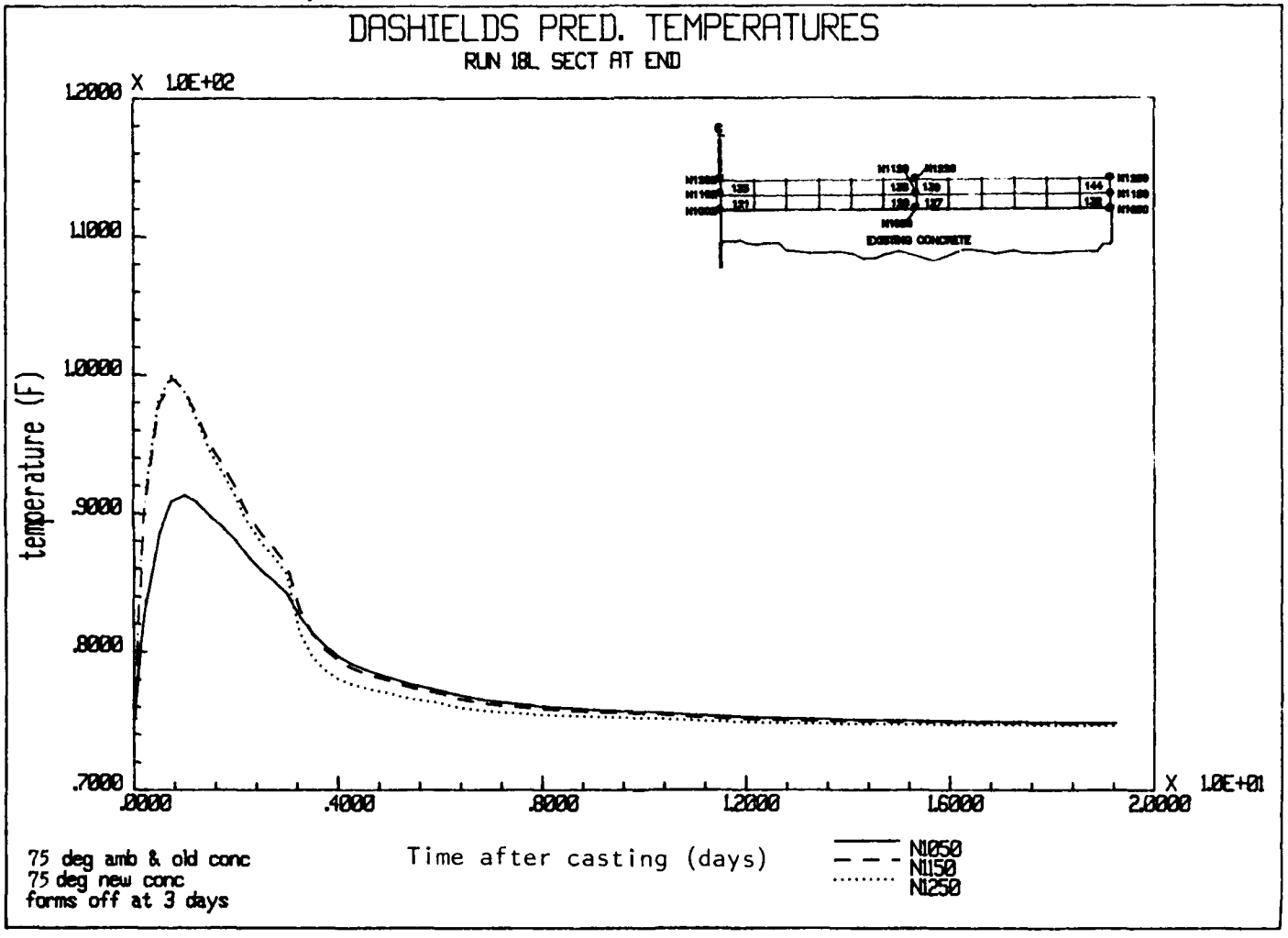

Figure 26. Predicted temperatures, Run 18L, nodes 1050, 1150, and 1250

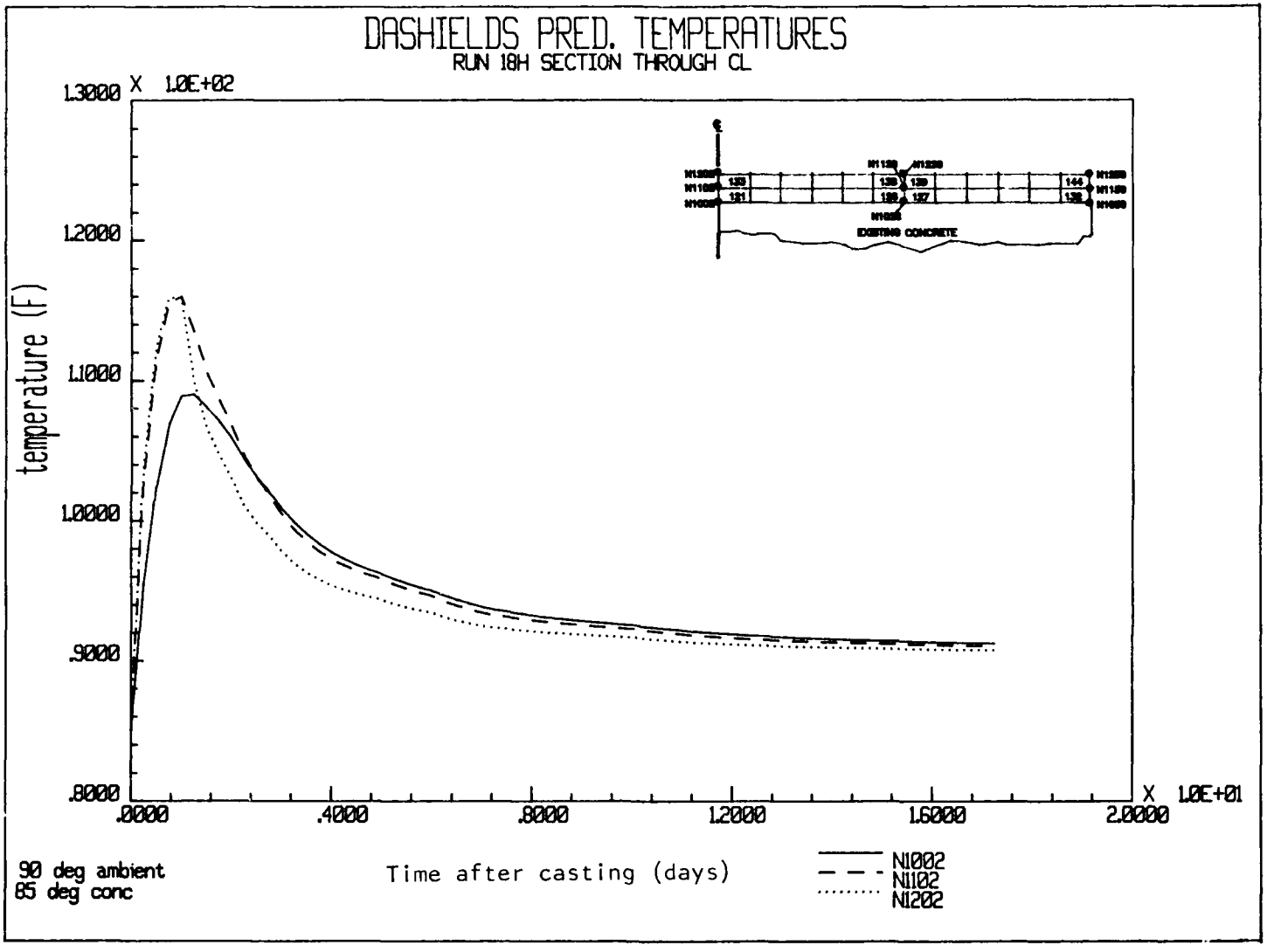

Figure 27. Predicted temperatures, Run 18H, nodes 1002, 1102, and 1202

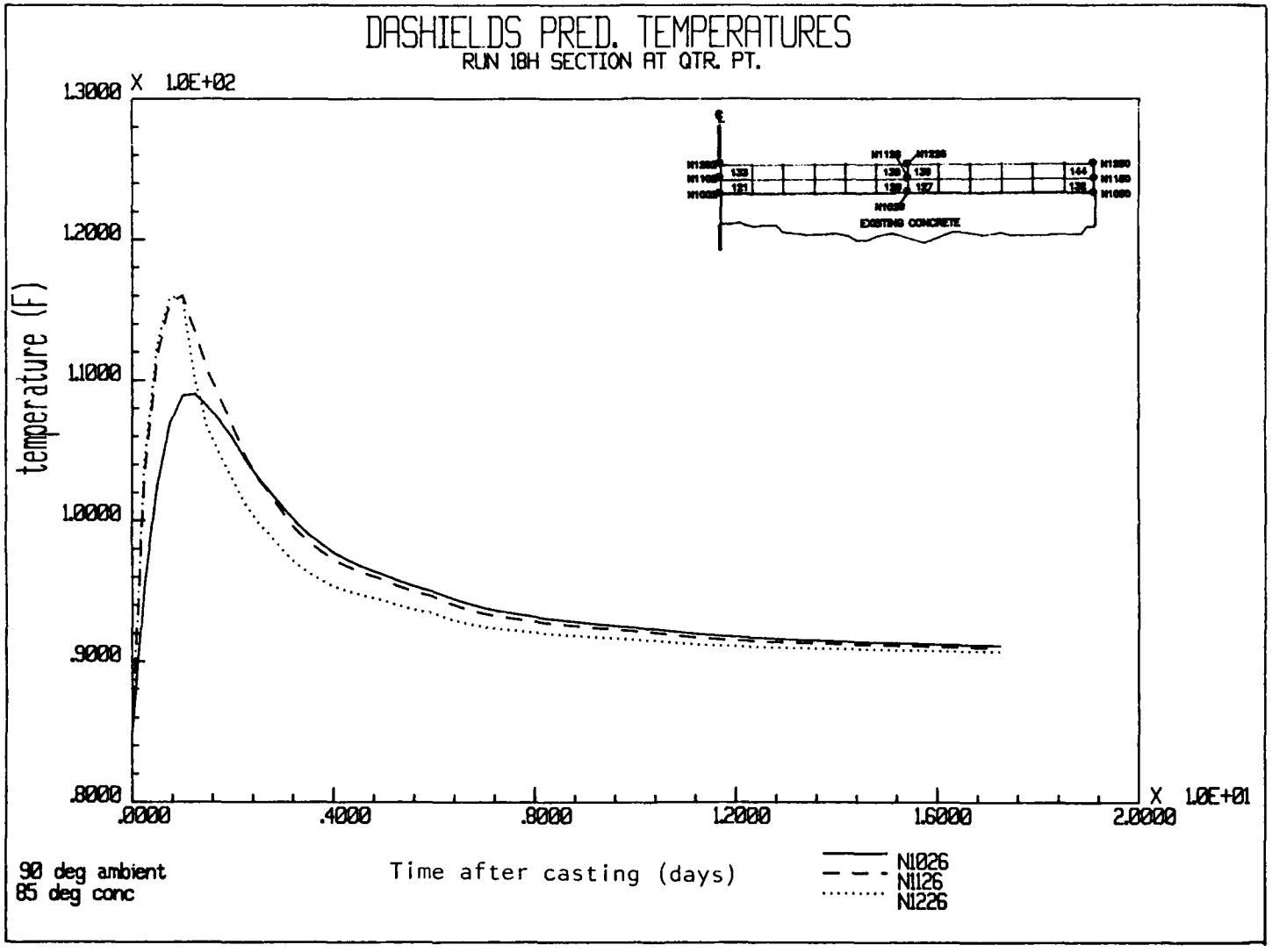

Figure 28. Predicted temperatures, Run 18H, nodes 1026, 1126, and 1226

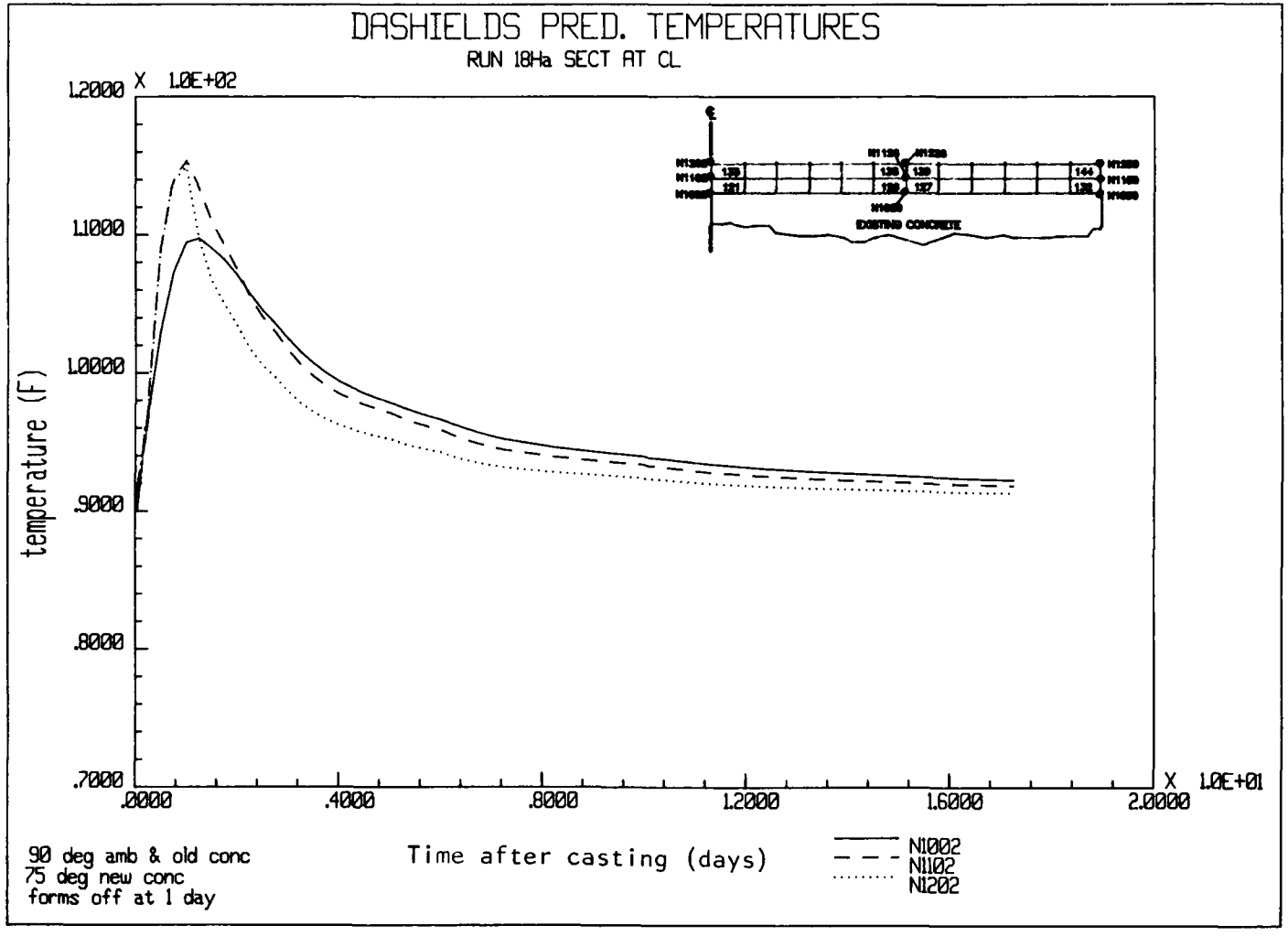

Figure 29. Predicted temperatures, Run 18Ha, nodes 1002, 1102, and 1202

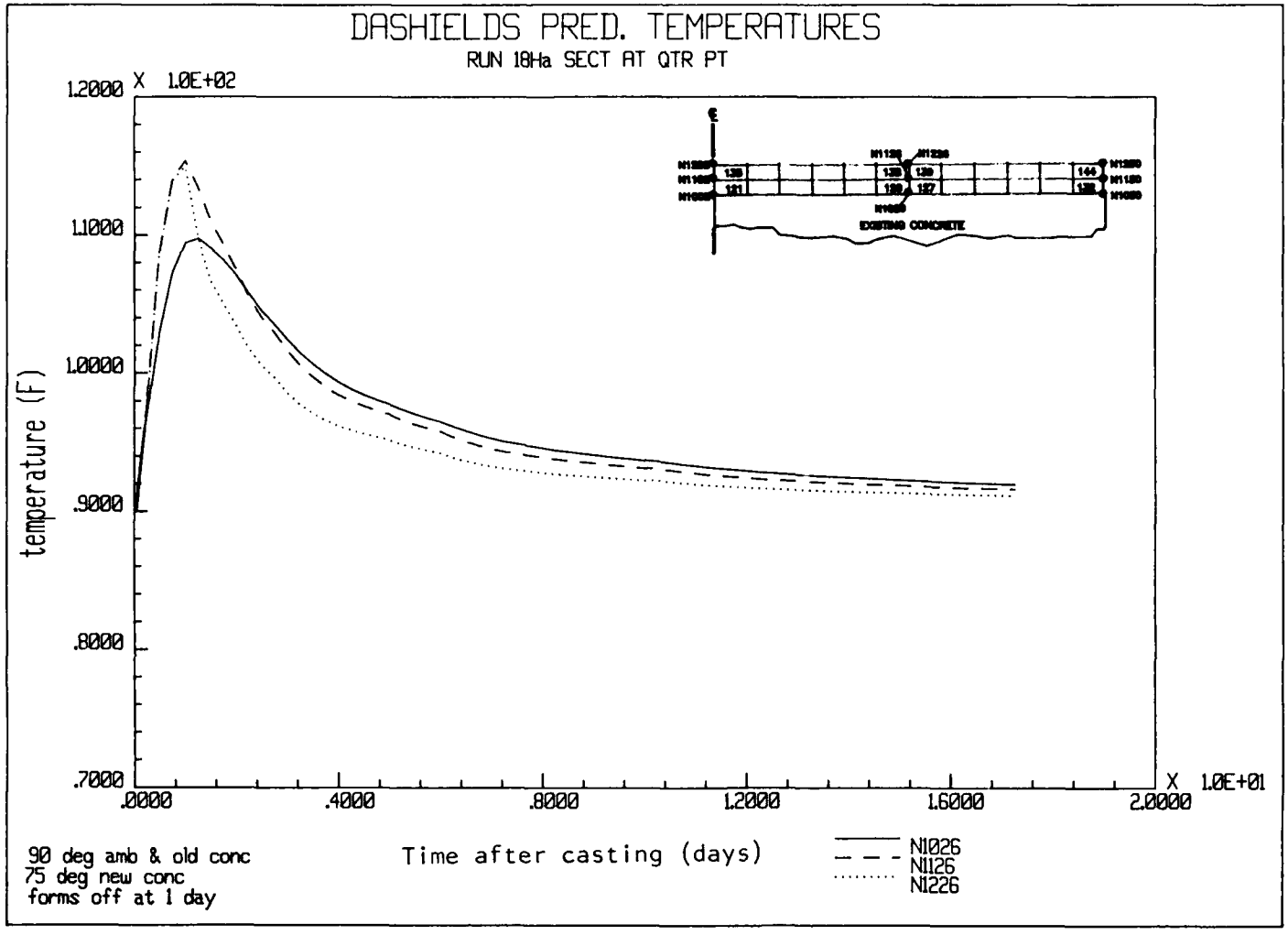

Figure 30. Predicted temperatures, Run 18Ha, nodes 1026, 1126, and 1226

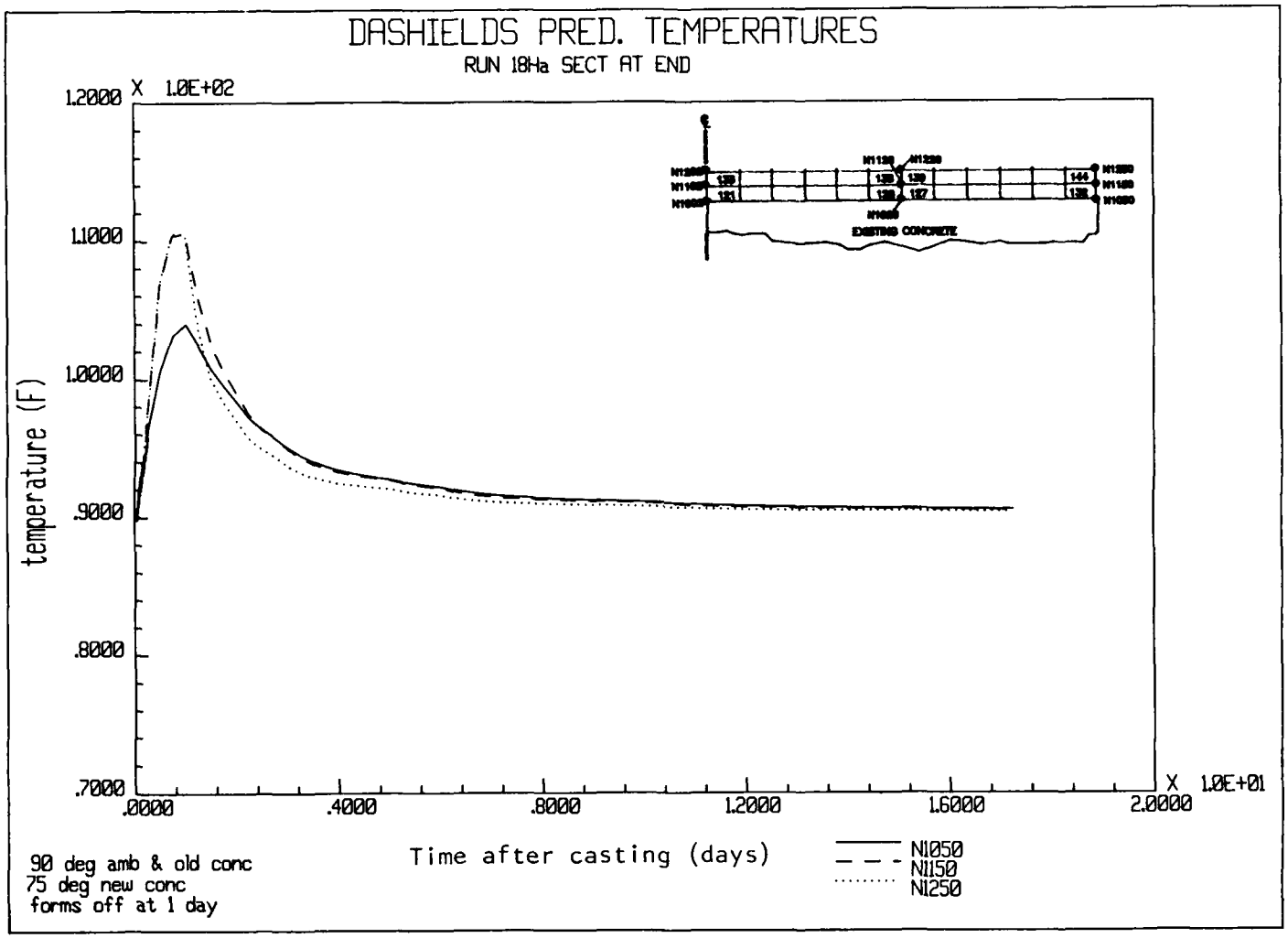

Figure 31. Predicted temperatures, Run 18Ha, nodes 1050, 1150, and 1250

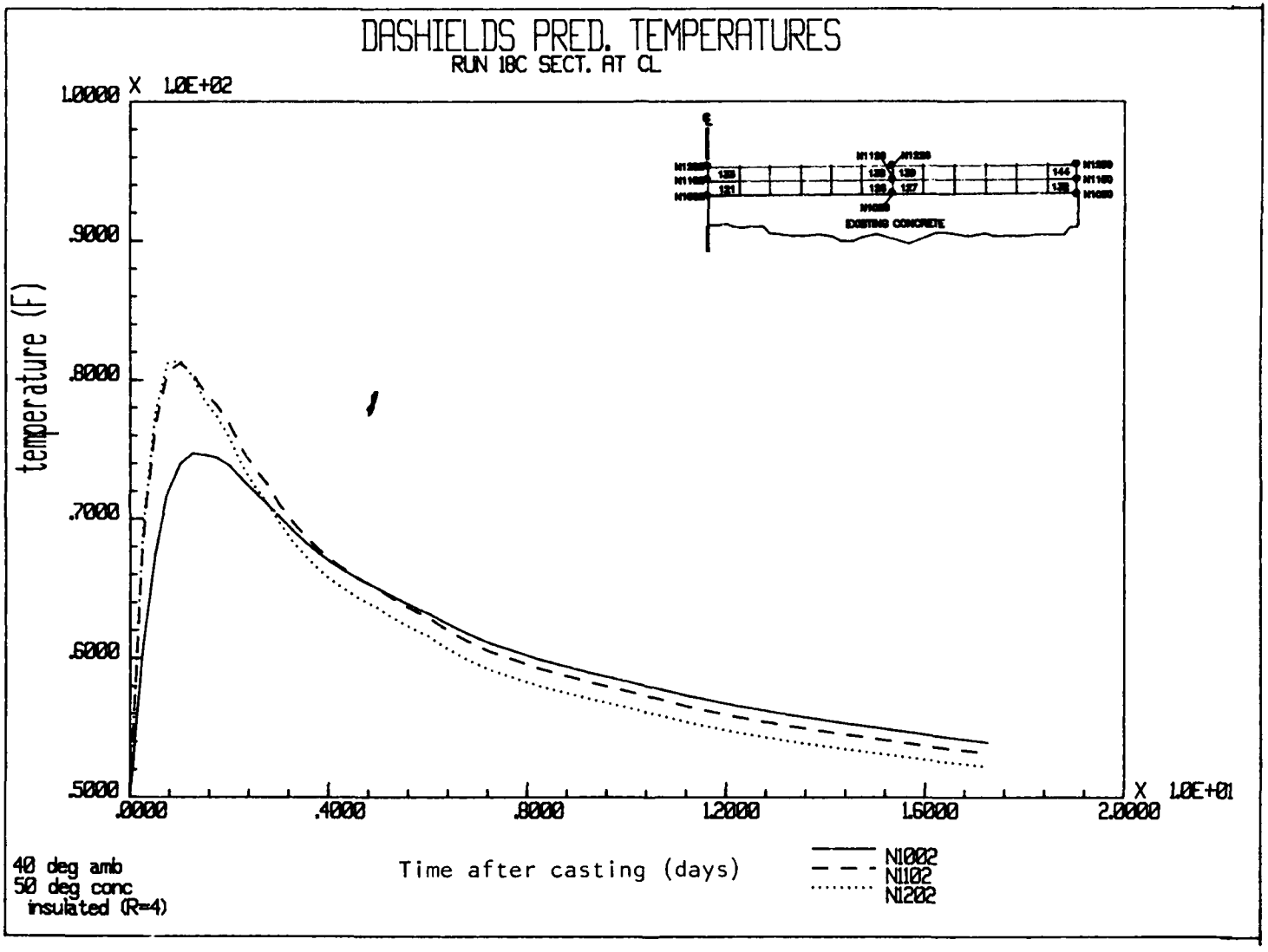

Figure 32. Predicted temperatures, Run 18C, nodes 1002, 1102, and 1202

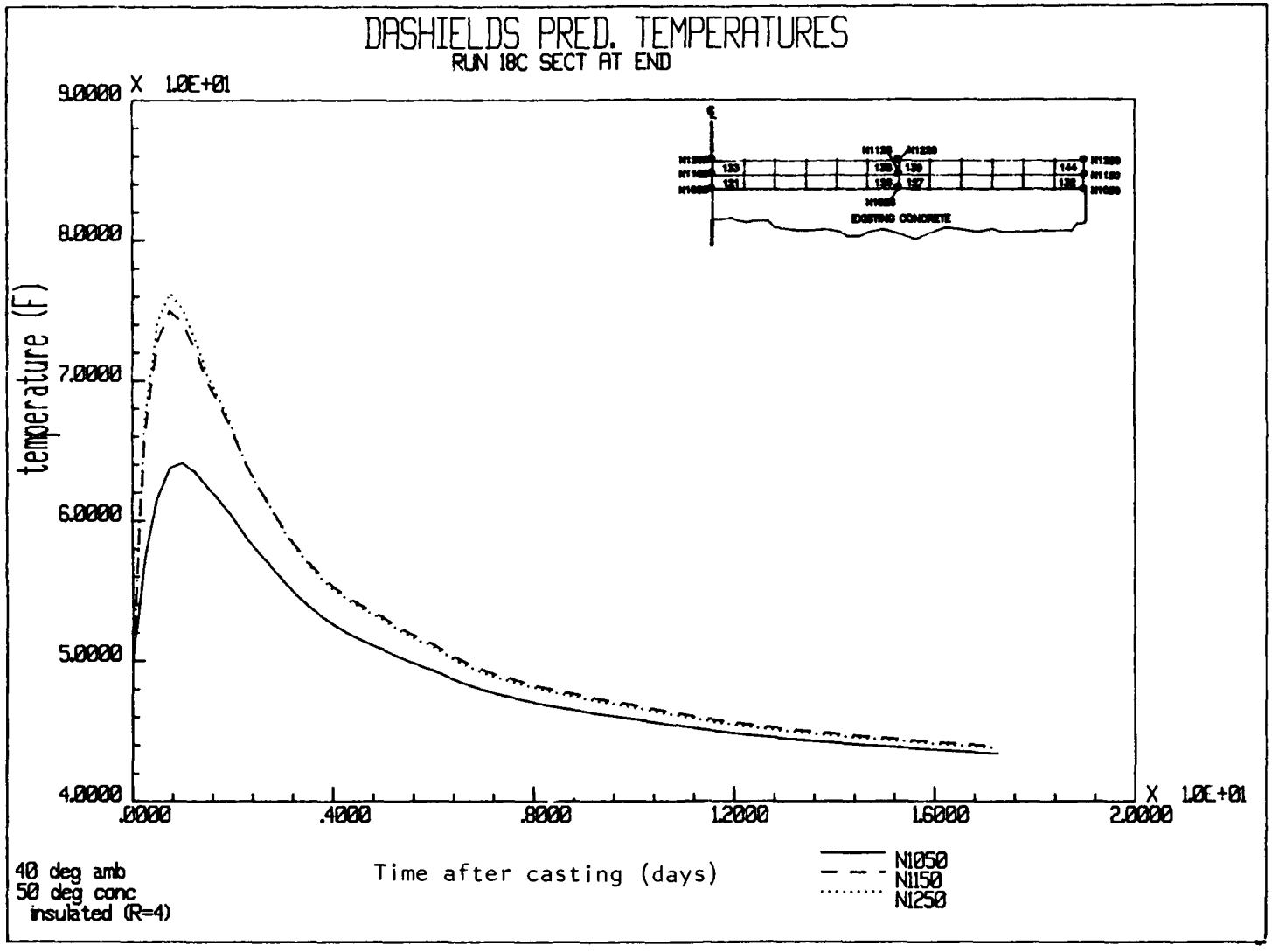

Figure 33. Predicted temperatures, Run 18C, nodes 1050, 1150, and 1250

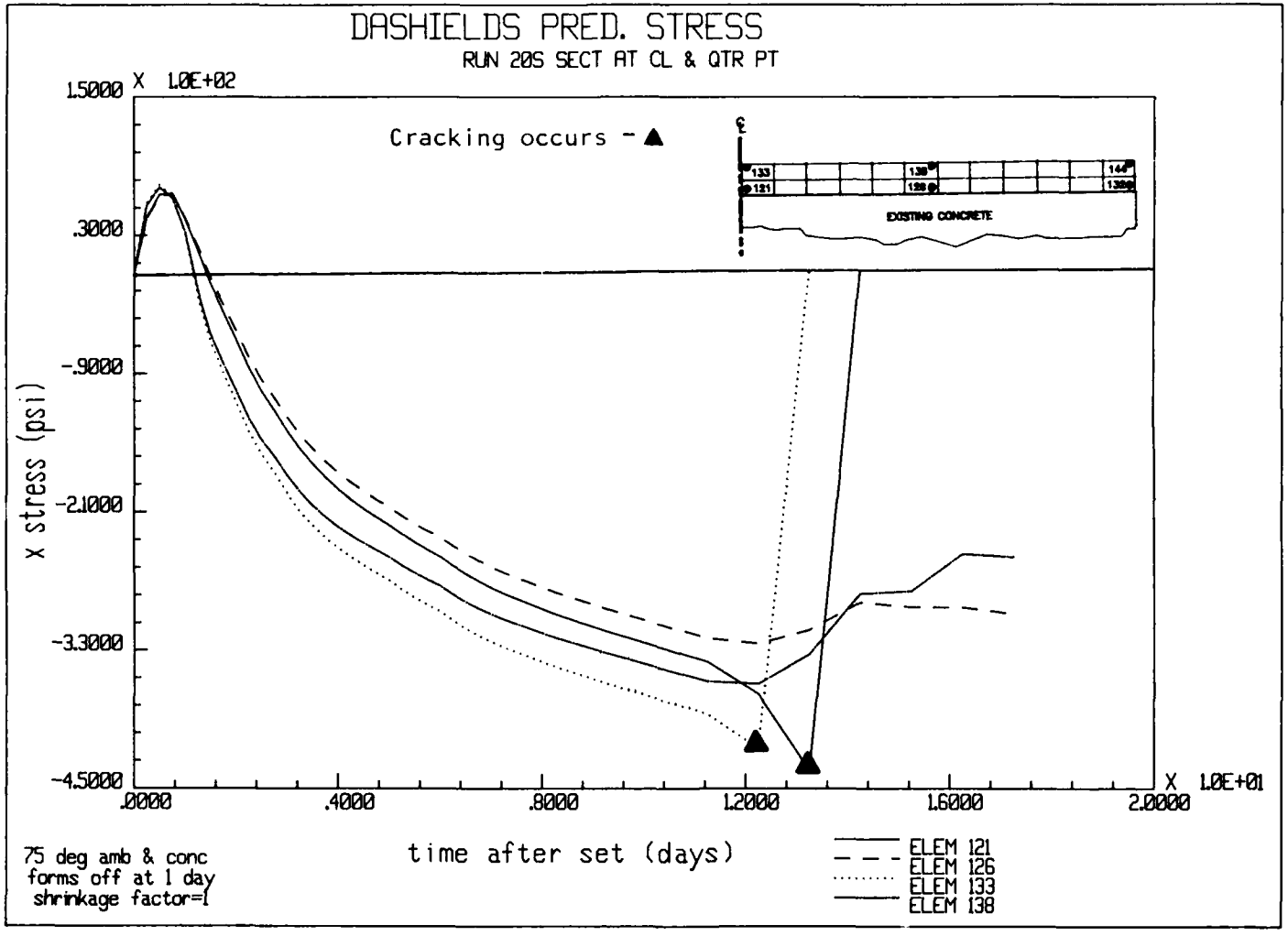

Figure 34. Predicted stresses, Run 20S, elements 121, 126, 133, and 138

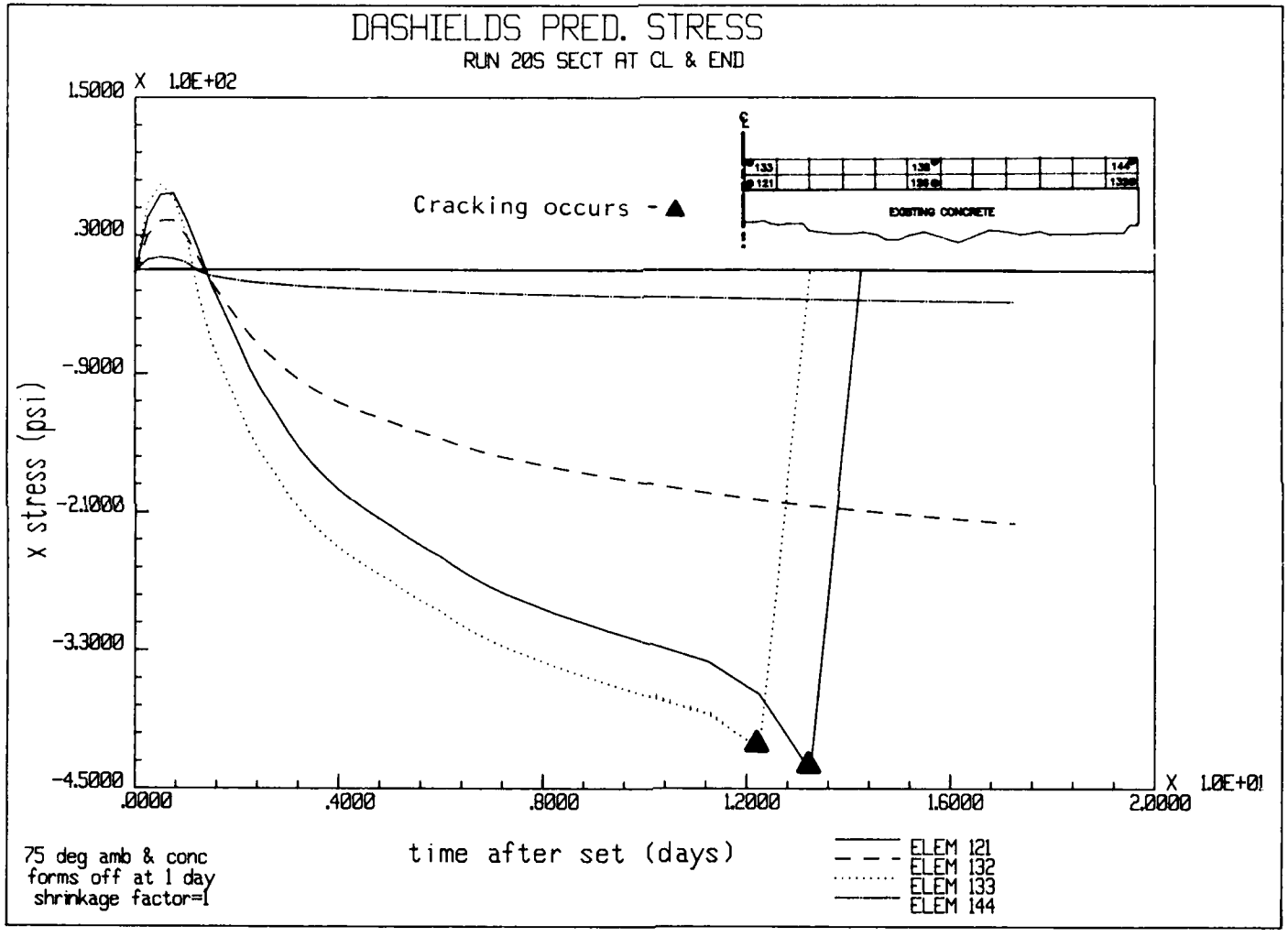

Figure 35. Predicted stresses, Run 20S, elements 121, 132, 133, and 144

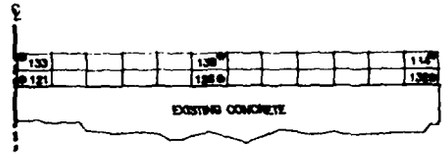

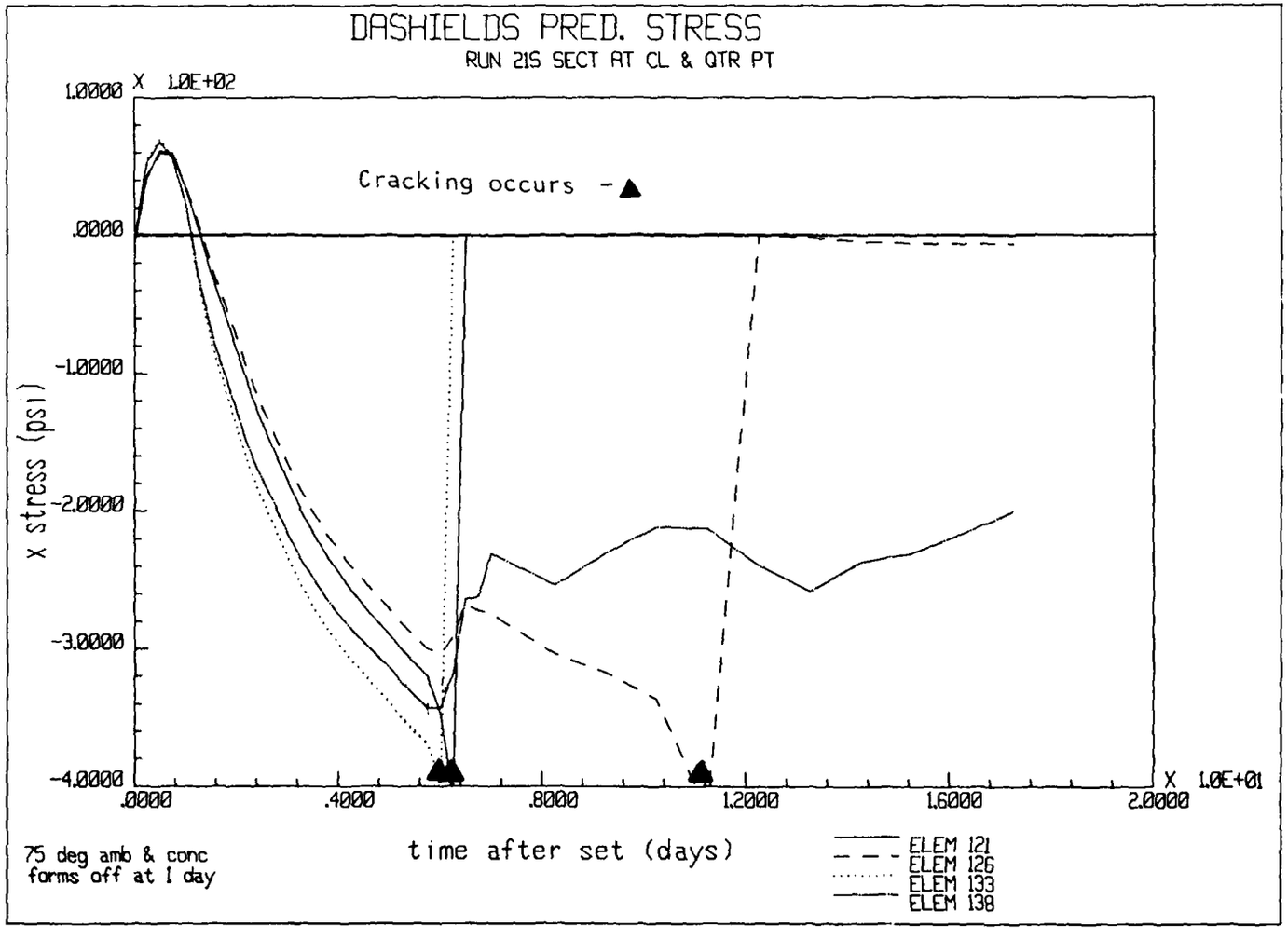

Figure 36. Predicted stresses, Run 215, elements 121, 126, 133, and 138

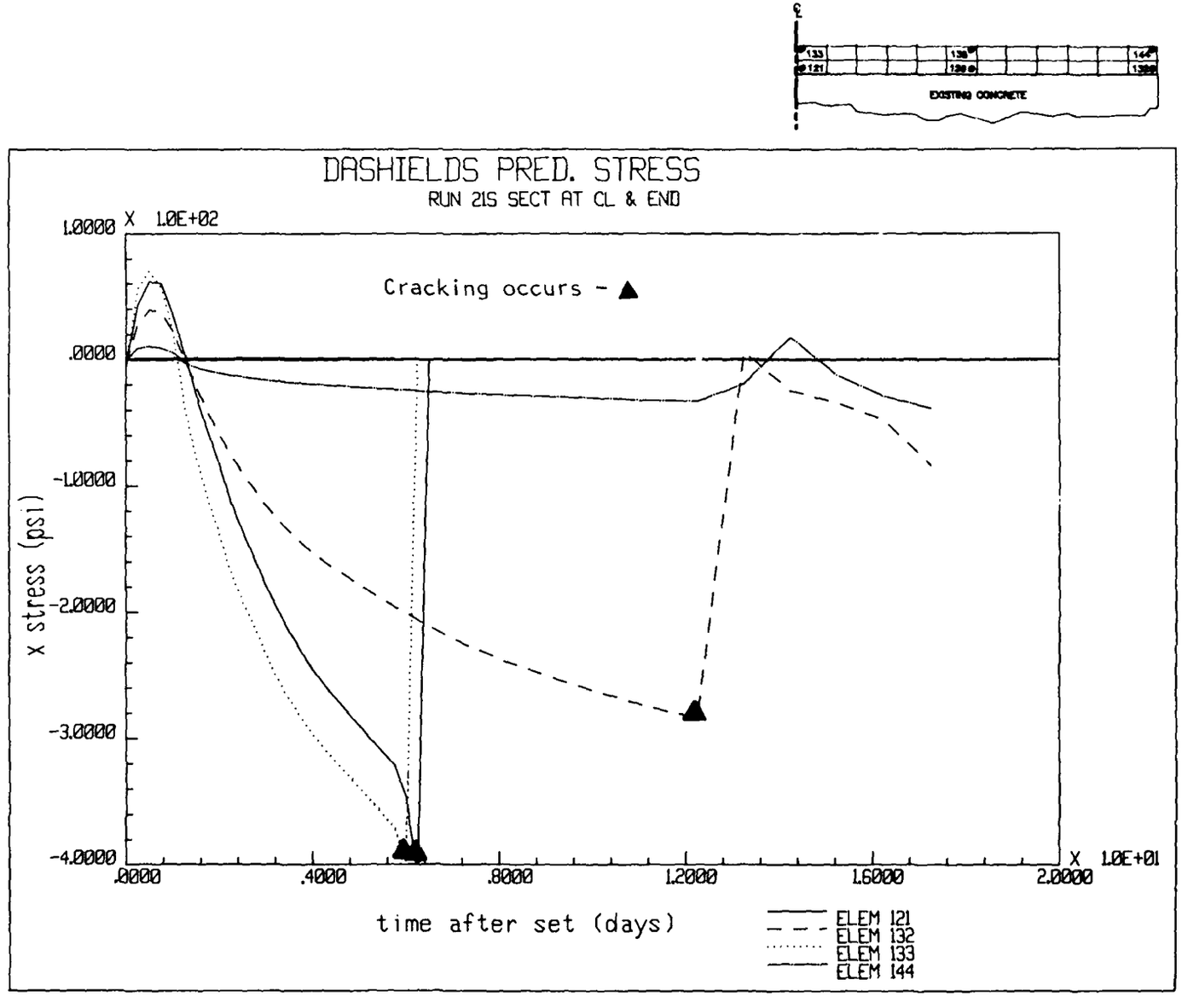

Figure 37. Predicted stresses, Run 21S, elements 121, 132, 133, and 144

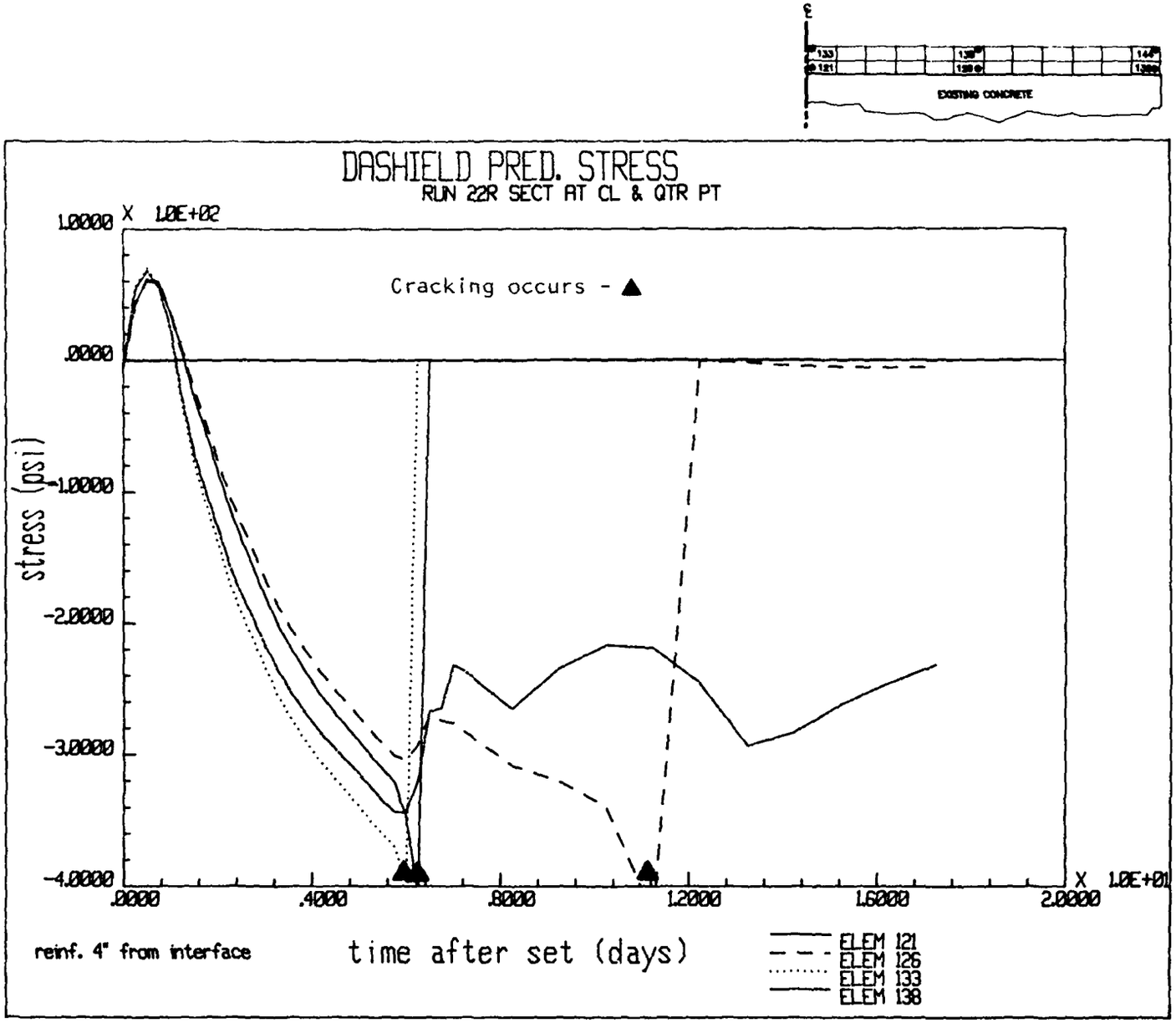

Figure 38. Predicted stresses, Run 22R, elements 121, 126, 133, and 138

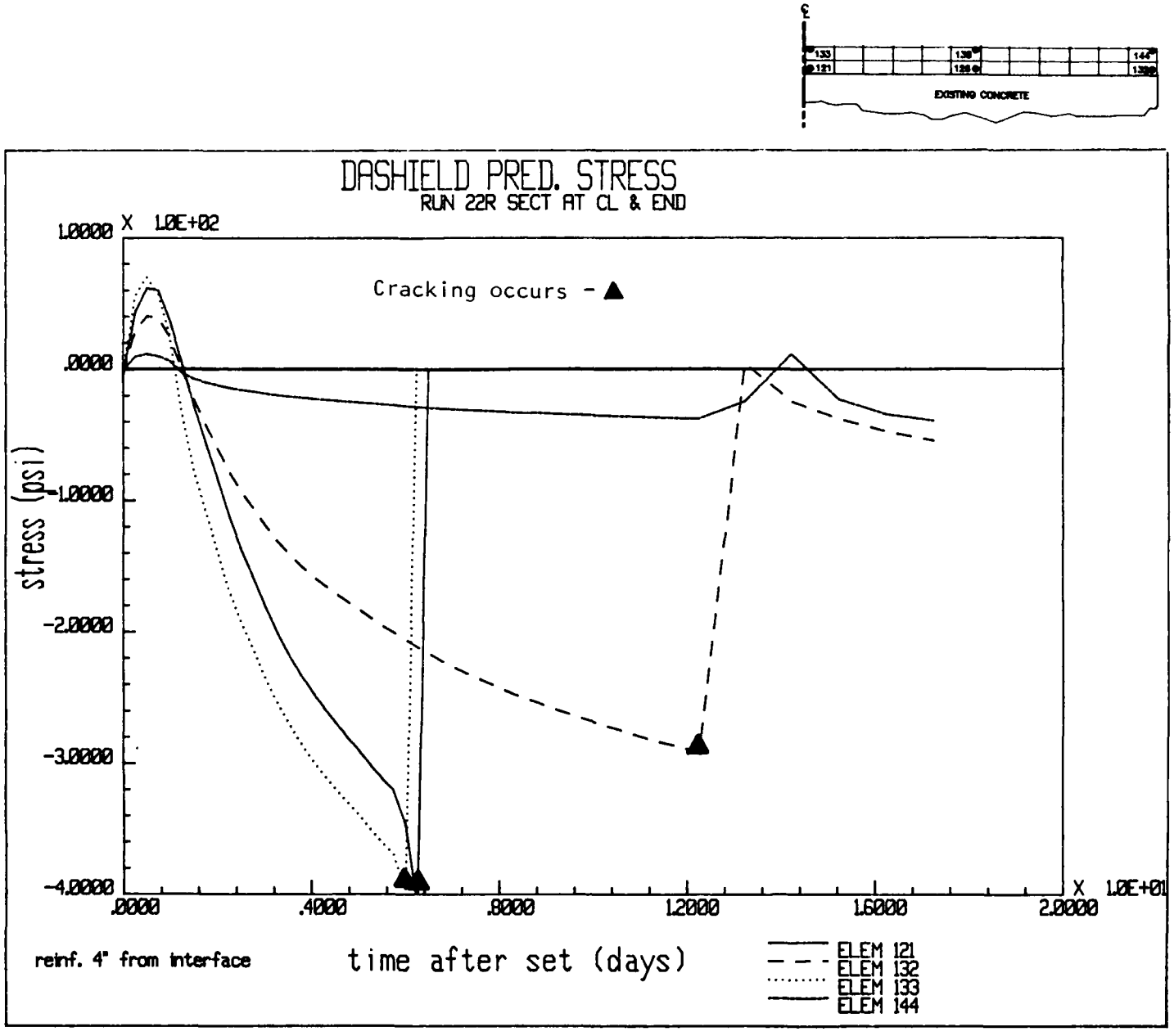

Figure 39. Predicted stresses, Run 22R, elements 121, 132, 133, and 144

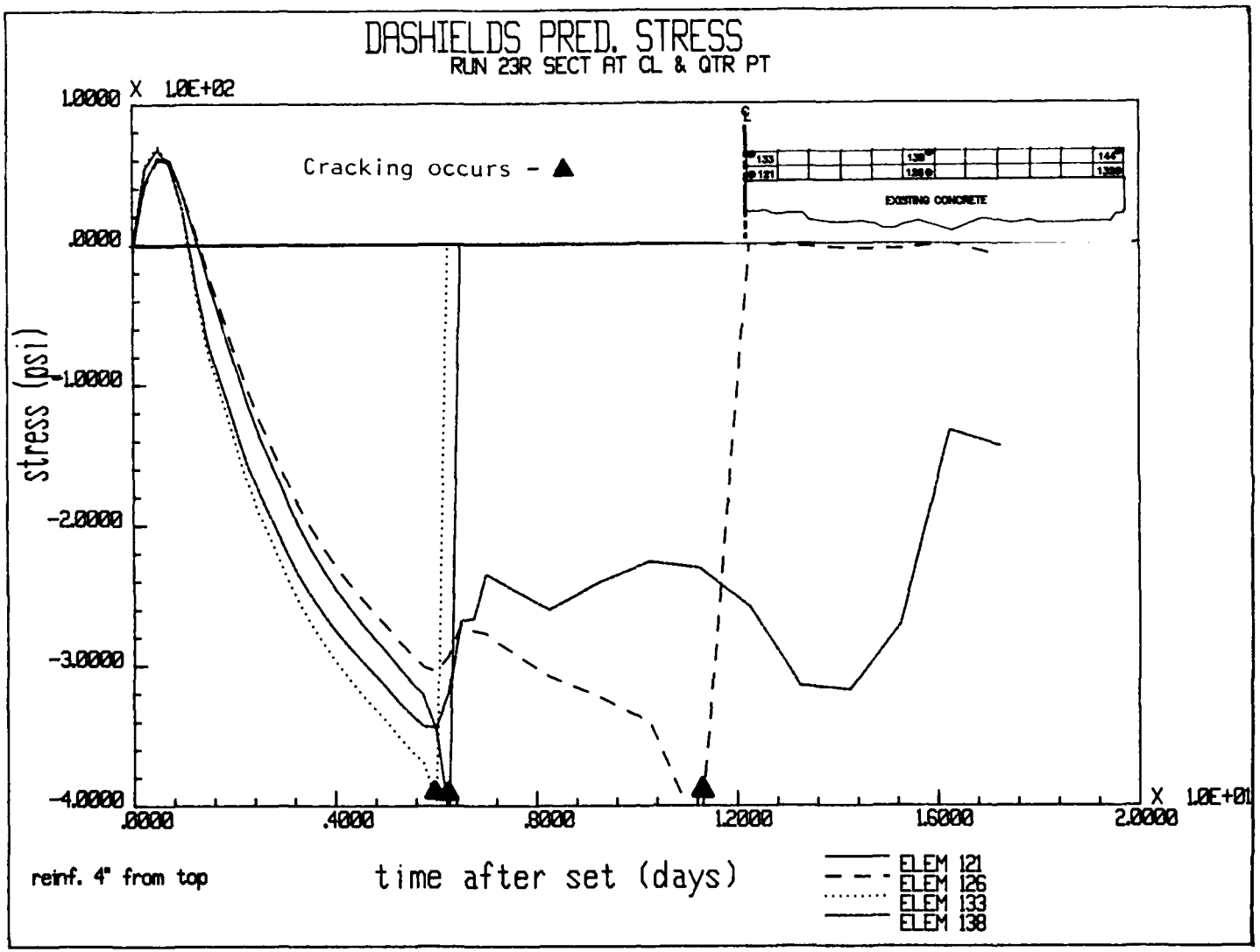

Figure 40. Predicted stresses, Run 23R, elements 121, 126, 133, and 138

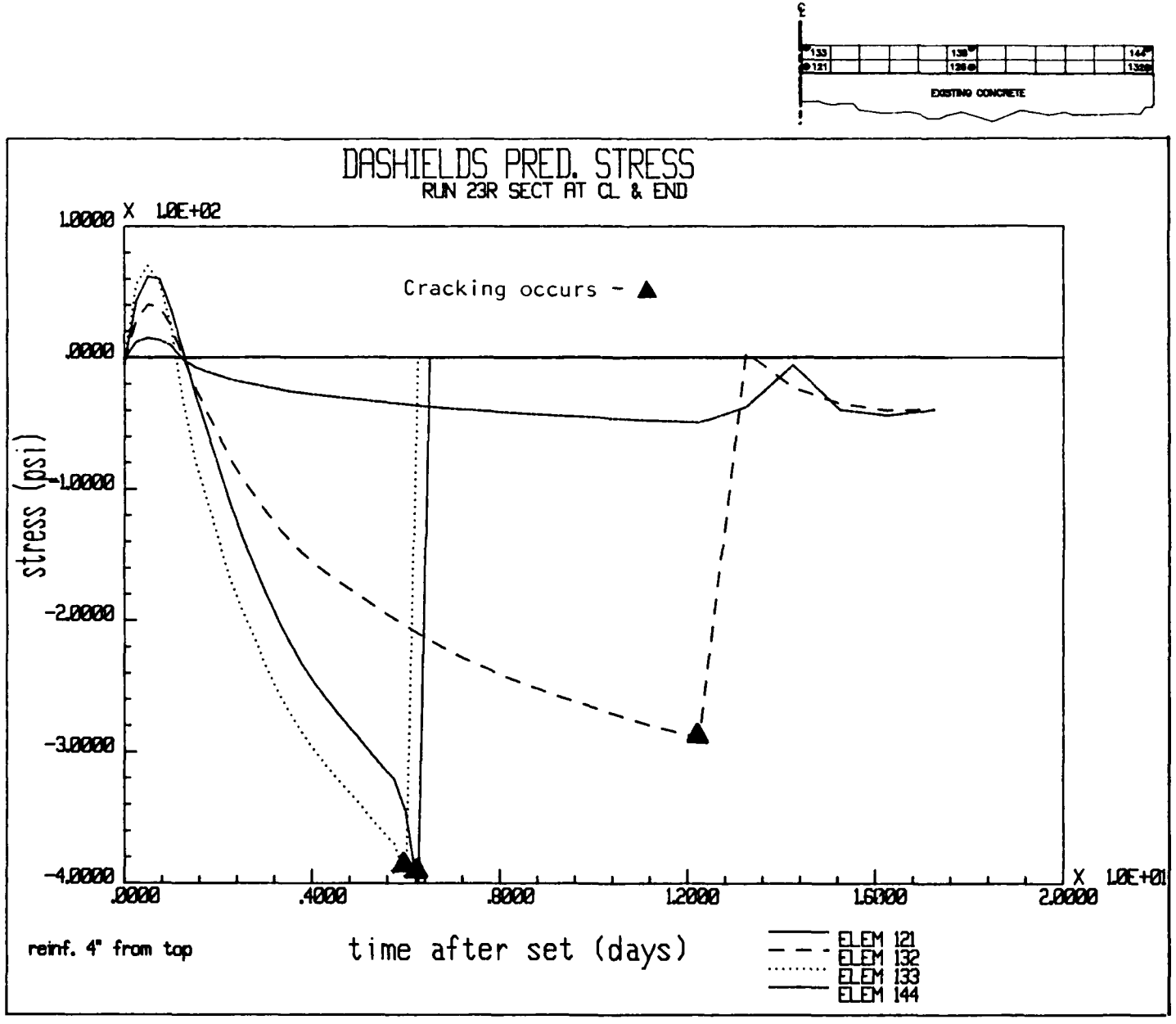

Figure 41. Predicted stresses, Run 23R, elements 121, 132, 133, and 144

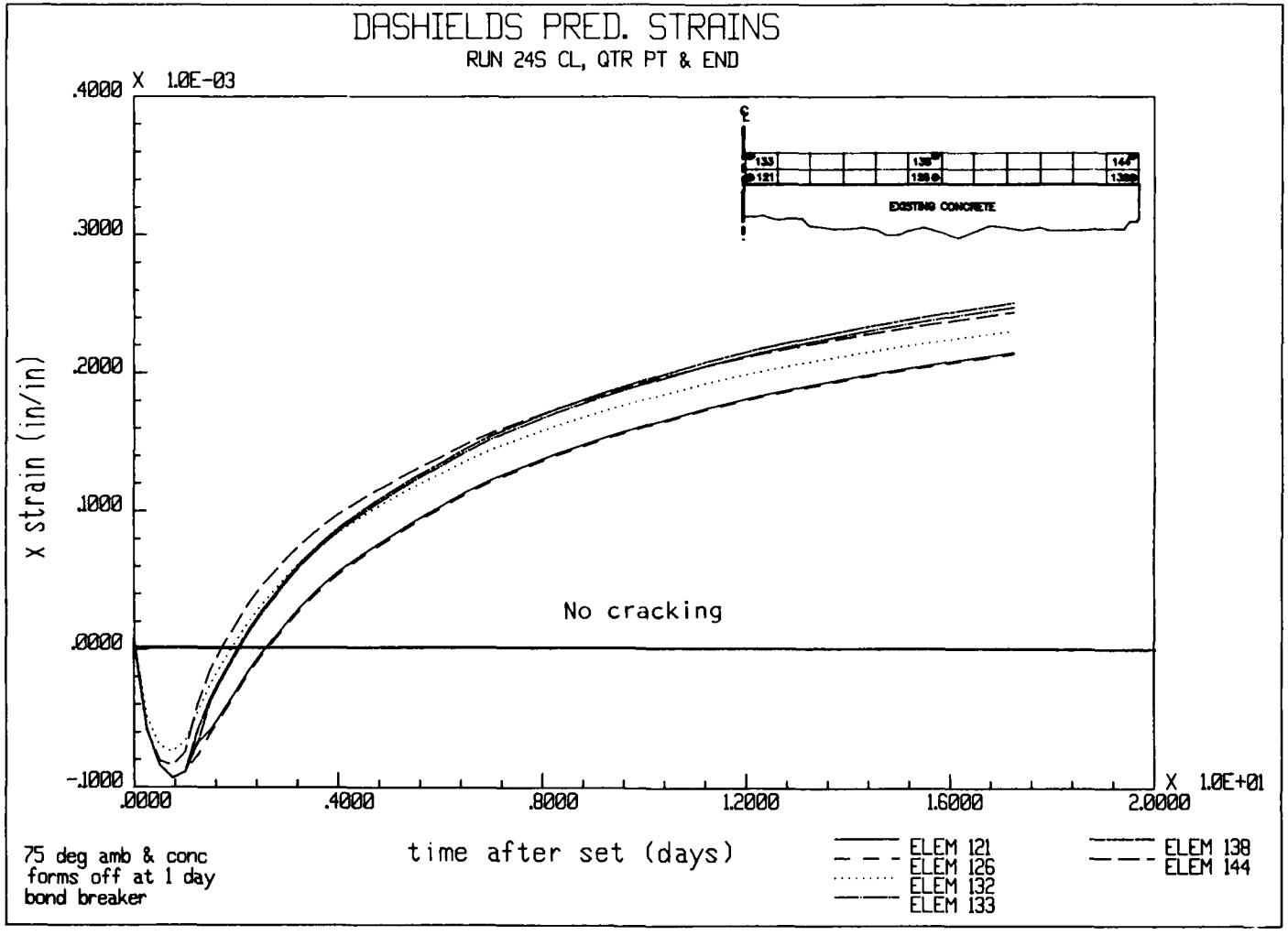

Figure 42. Predicted strains, Run 24S, elements 121, 126, 132, 133, 138, and 144

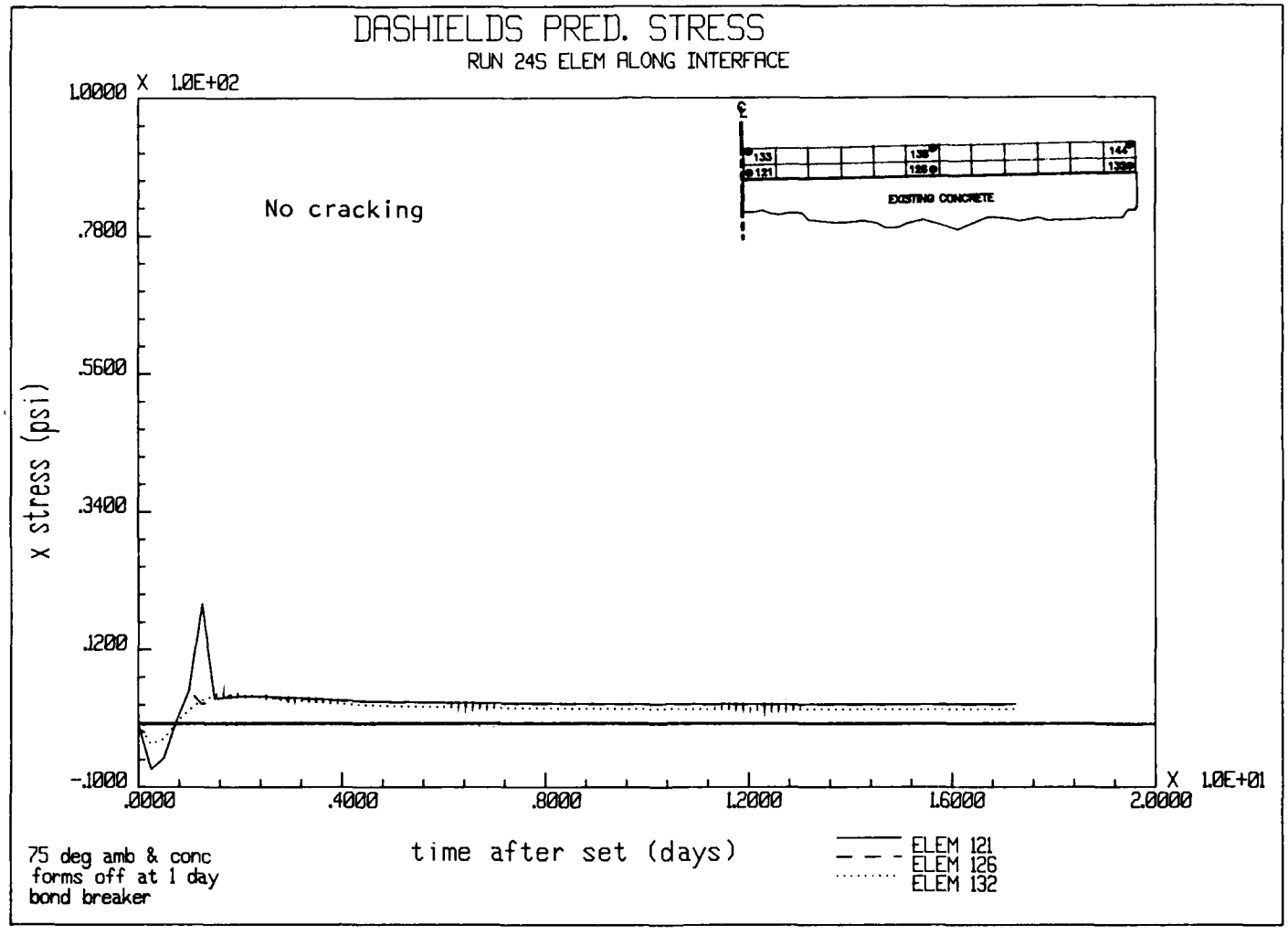

Figure 43. Predicted stresses, Run 24S, elements 121, 126, and 132

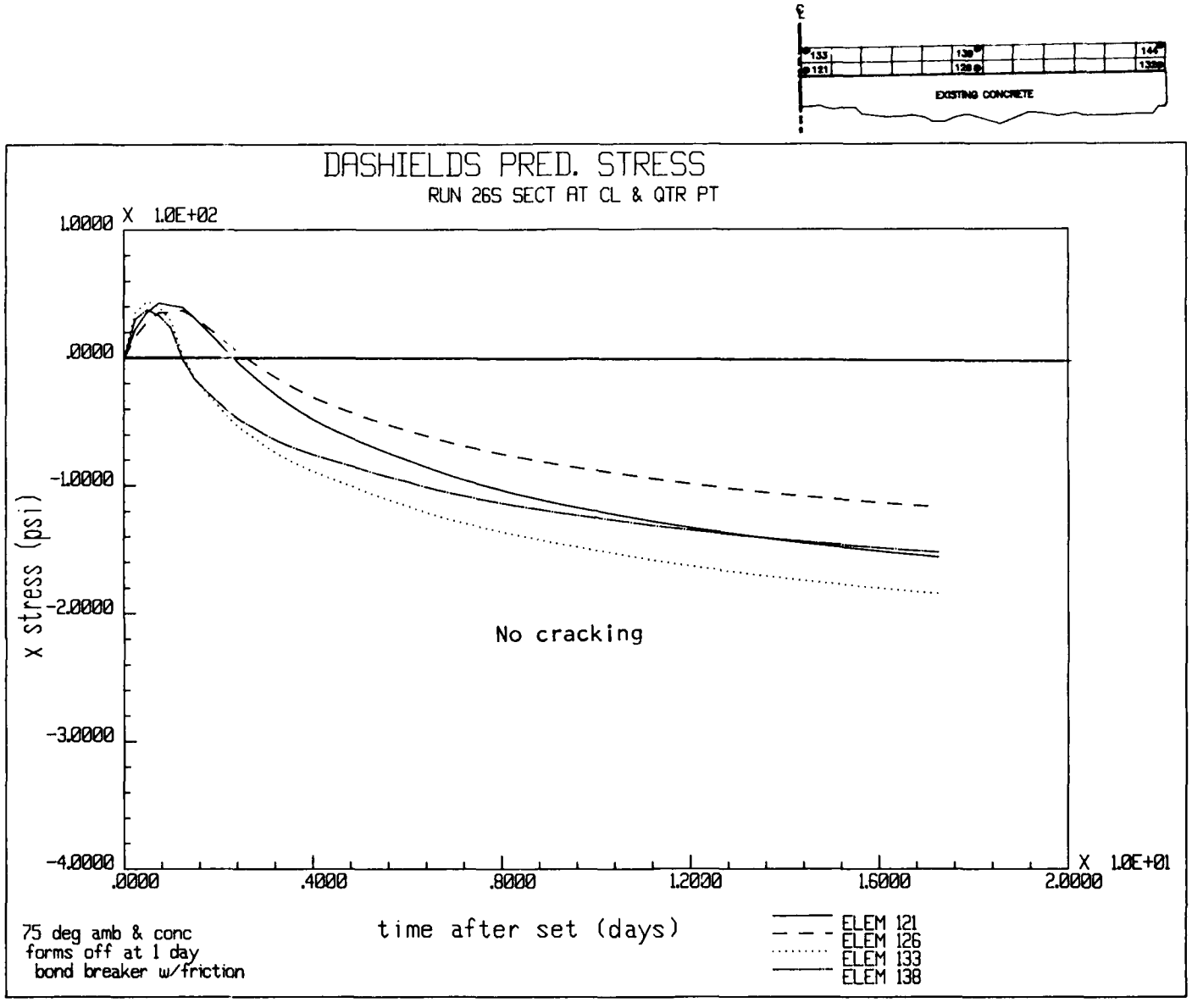

Figure 44. Predicted stresses, Run 26S, elements 121, 126, 133, and 138

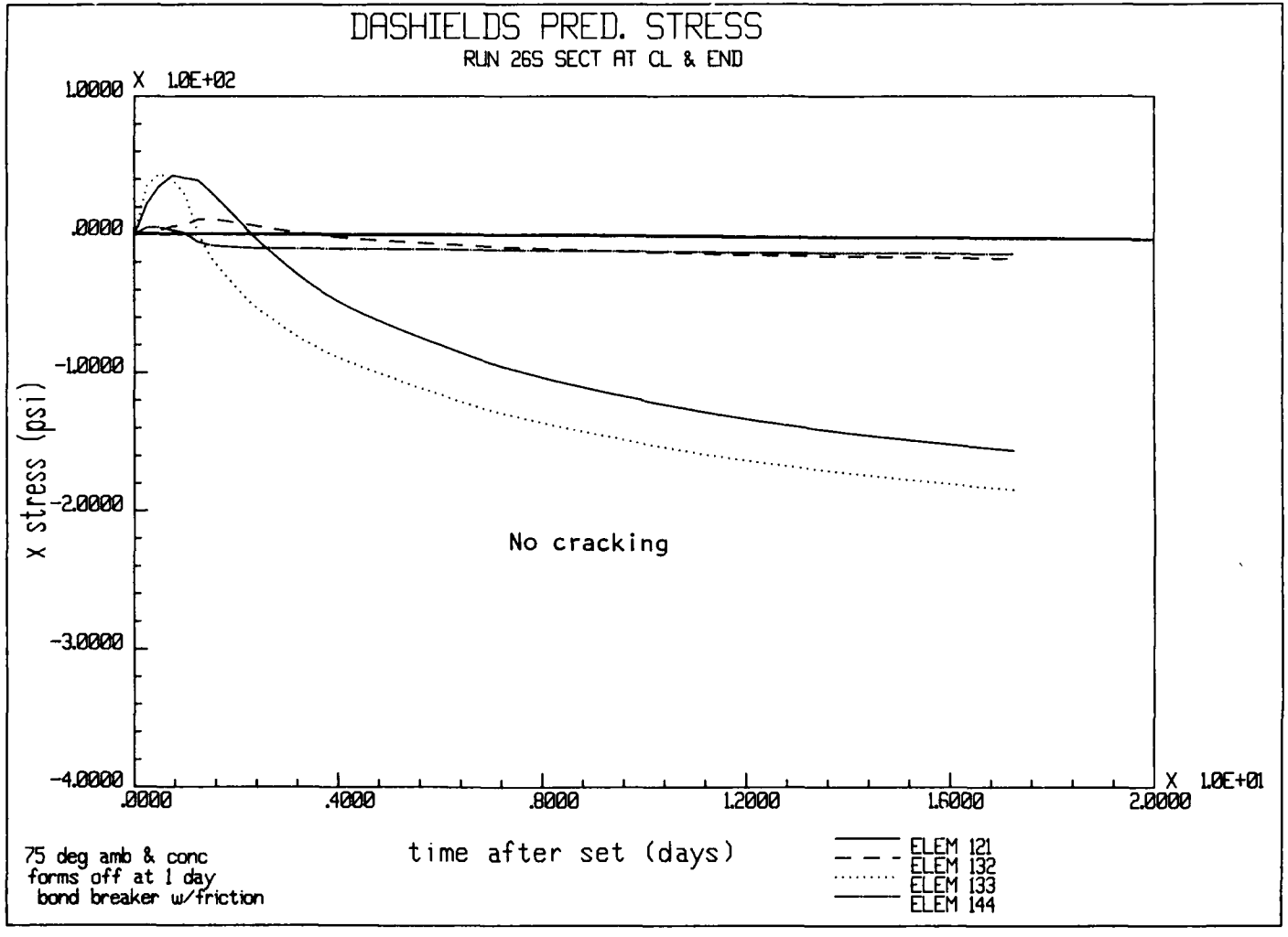

Figure 45. Predicted stresses, Run 26S, elements 121, 132, 133, and 144

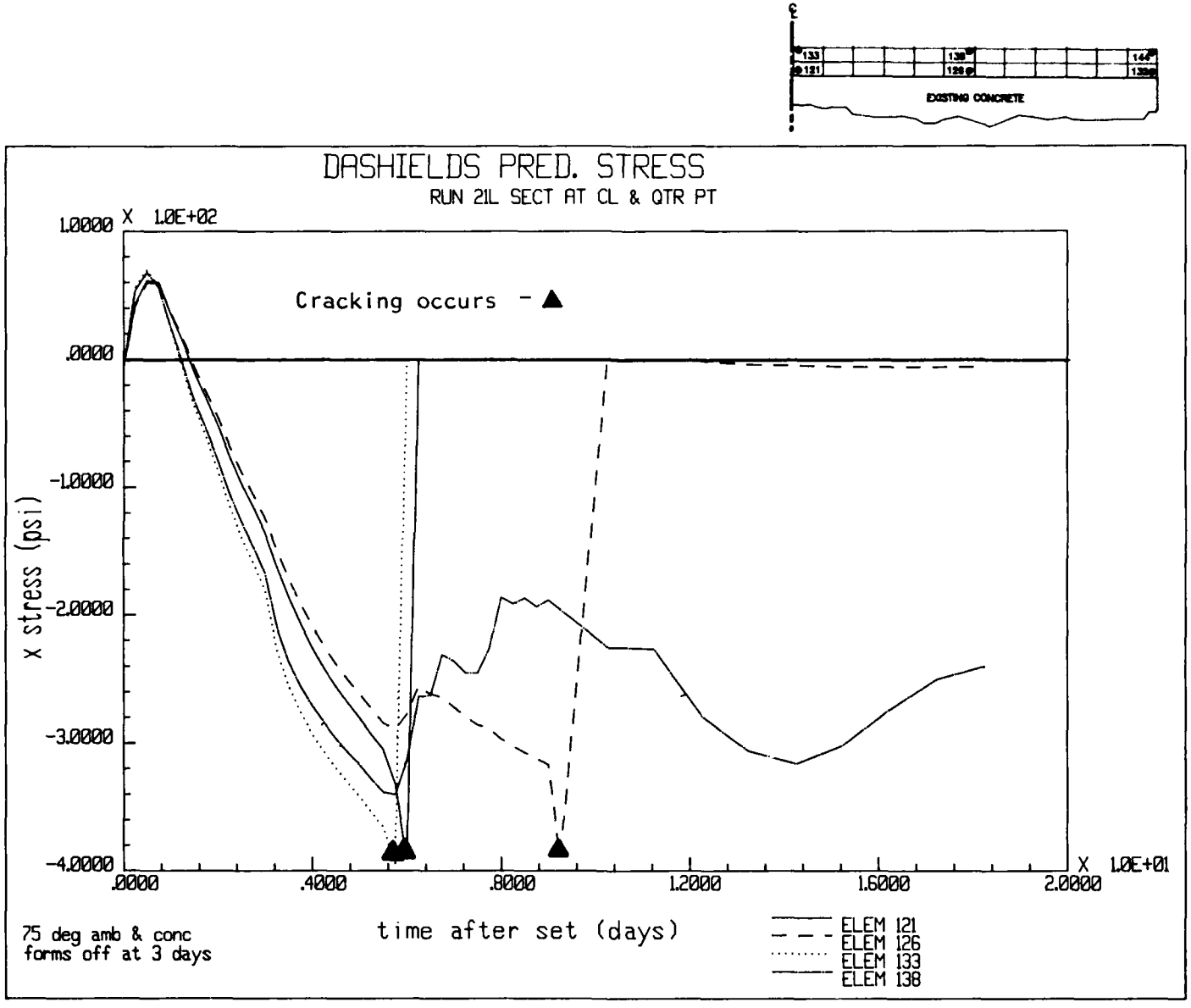

Figure 46. Predicted stresses, Run 21L, elements 121, 126, 133, and 138

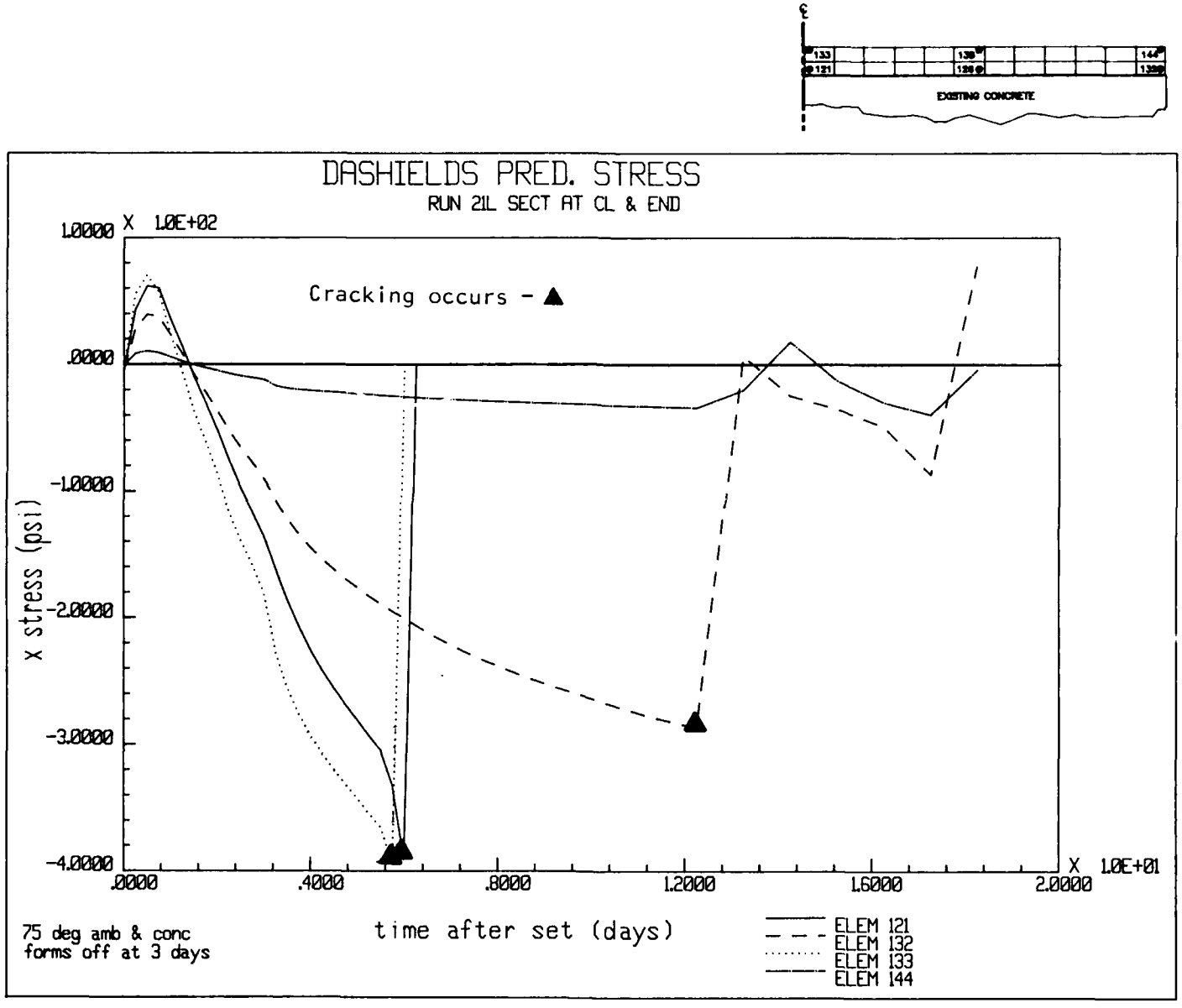

Figure 47. Predicted stresses, Run 21L, elements 121, 132, 133, and 144

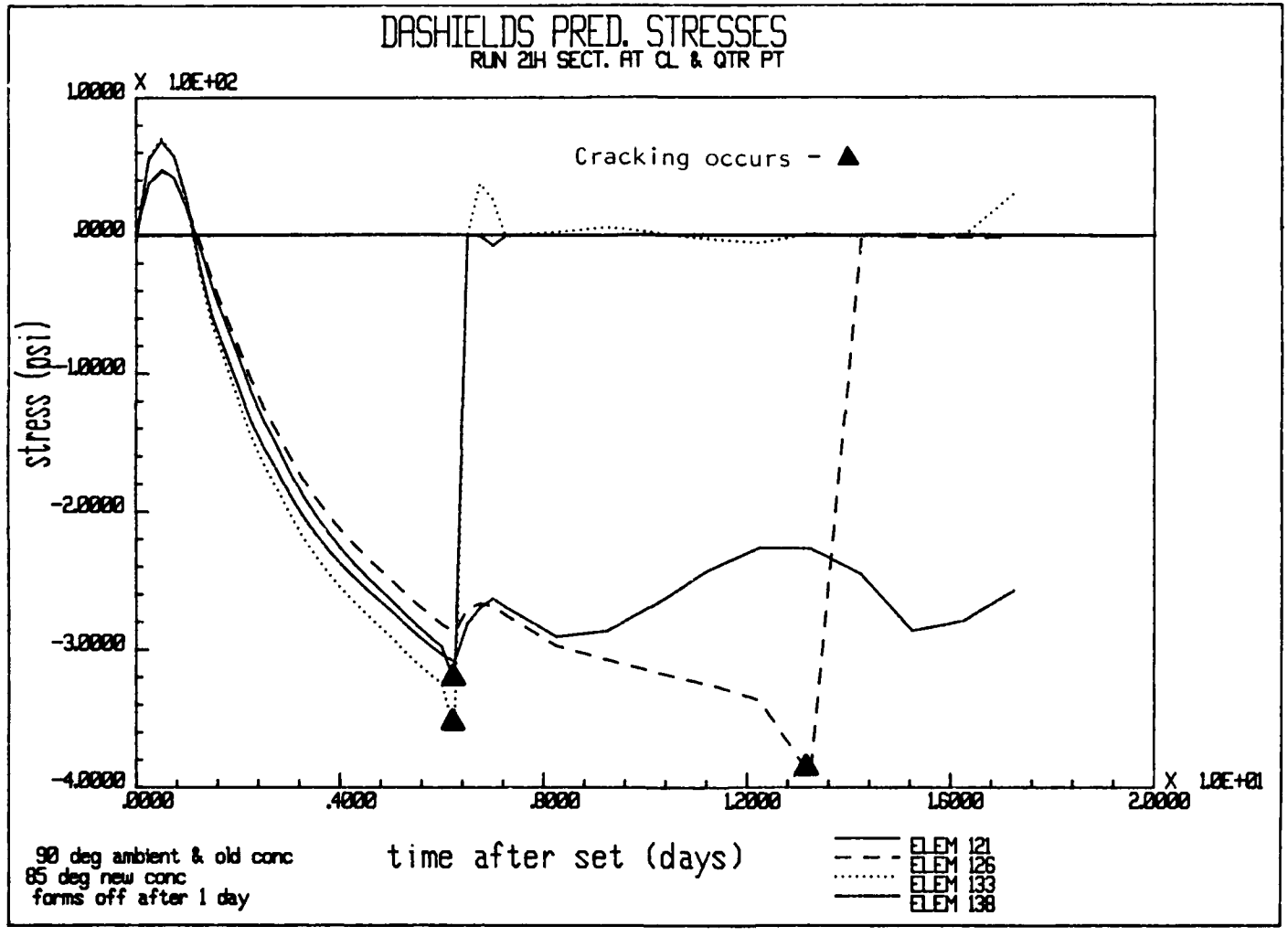

Figure 48. Predicted stresses, Run 21H, elements 121, 126, 133, and 138

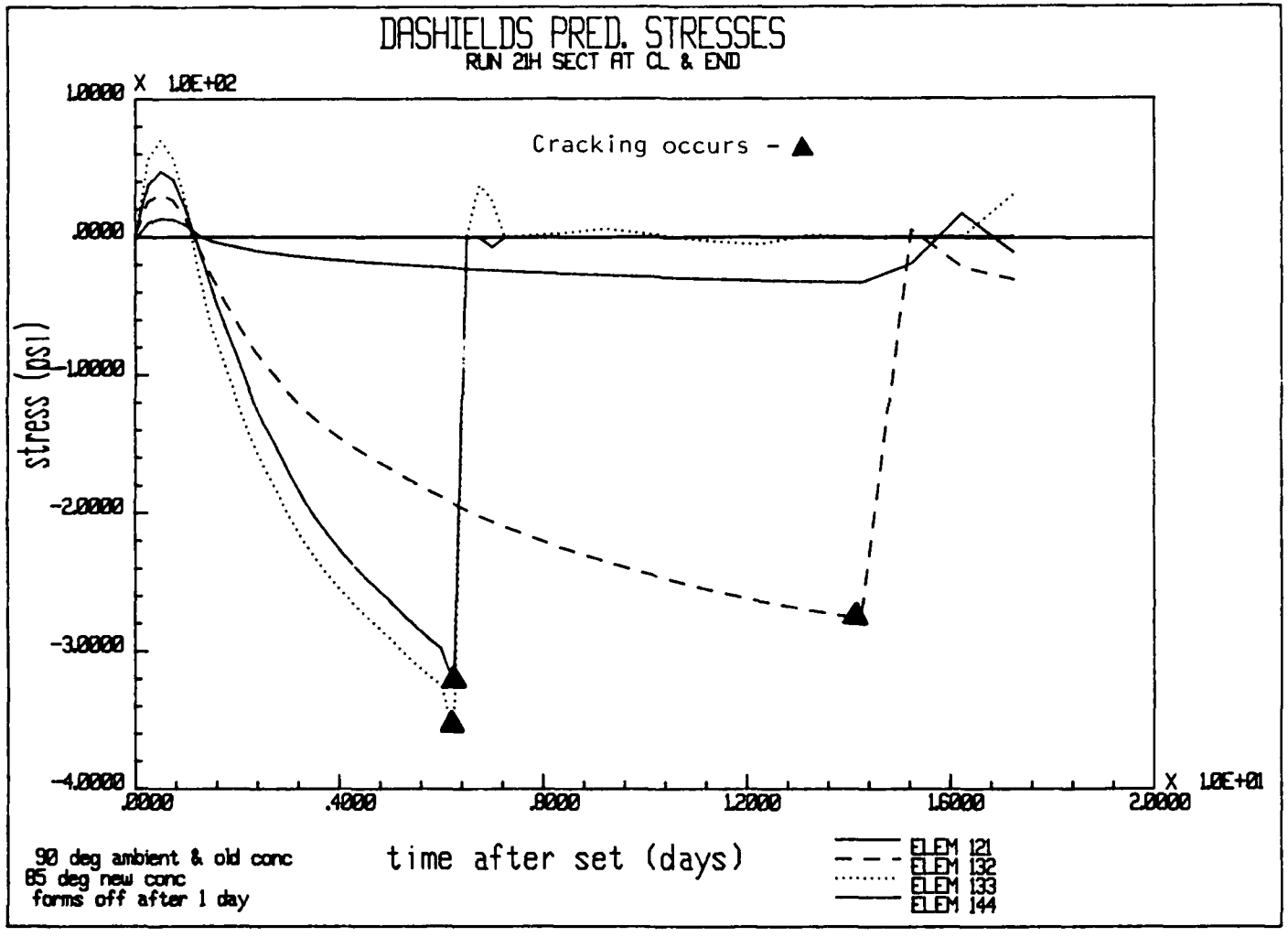

Figure 49. Predicted stresses, Run 21H, elements 121, 132, 133, and 134

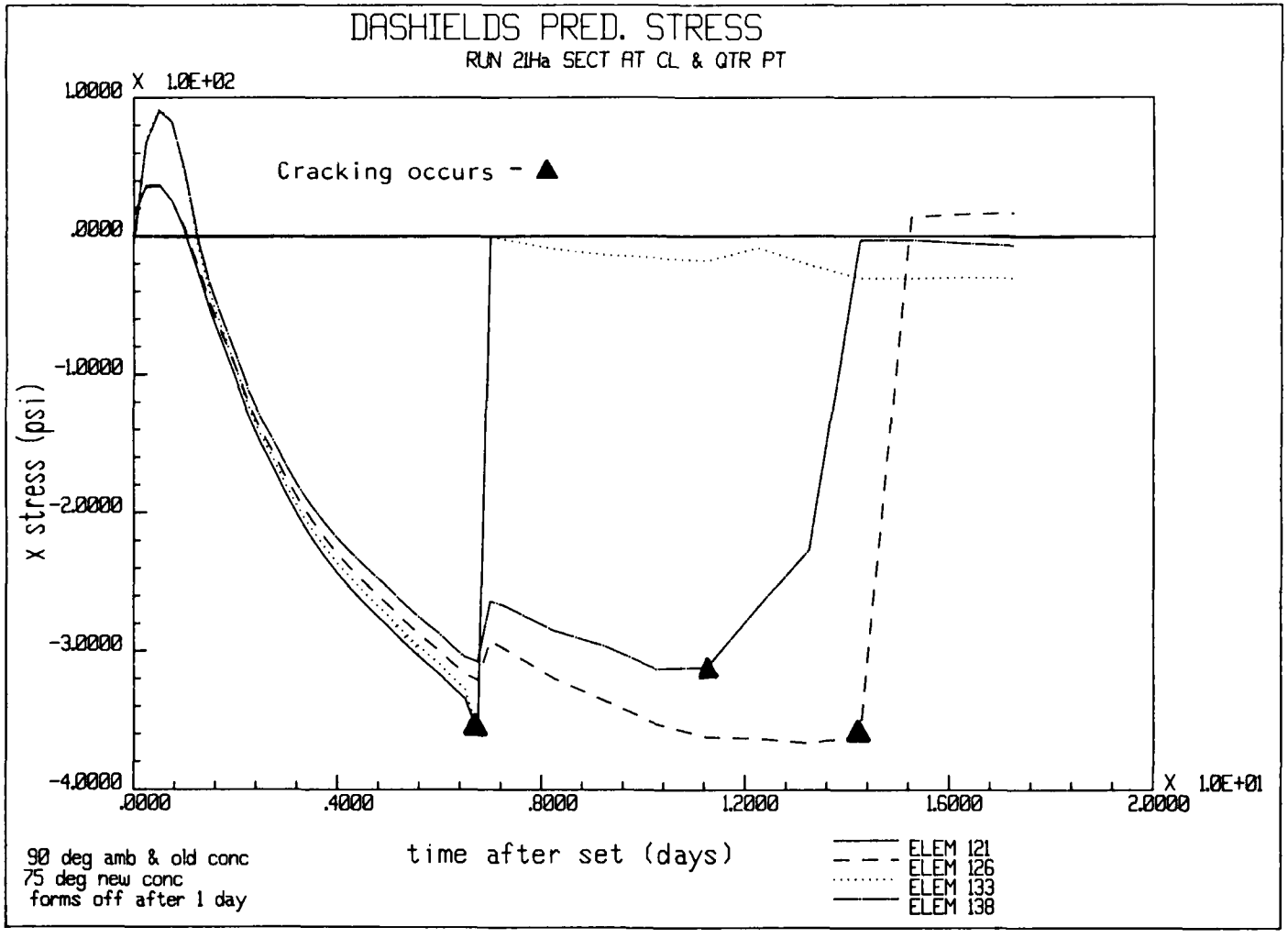

Figure 50. Predicted stresses, Run 21Ha, elements 121, 126, 133, and 138

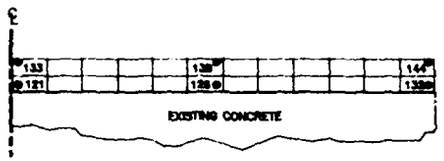

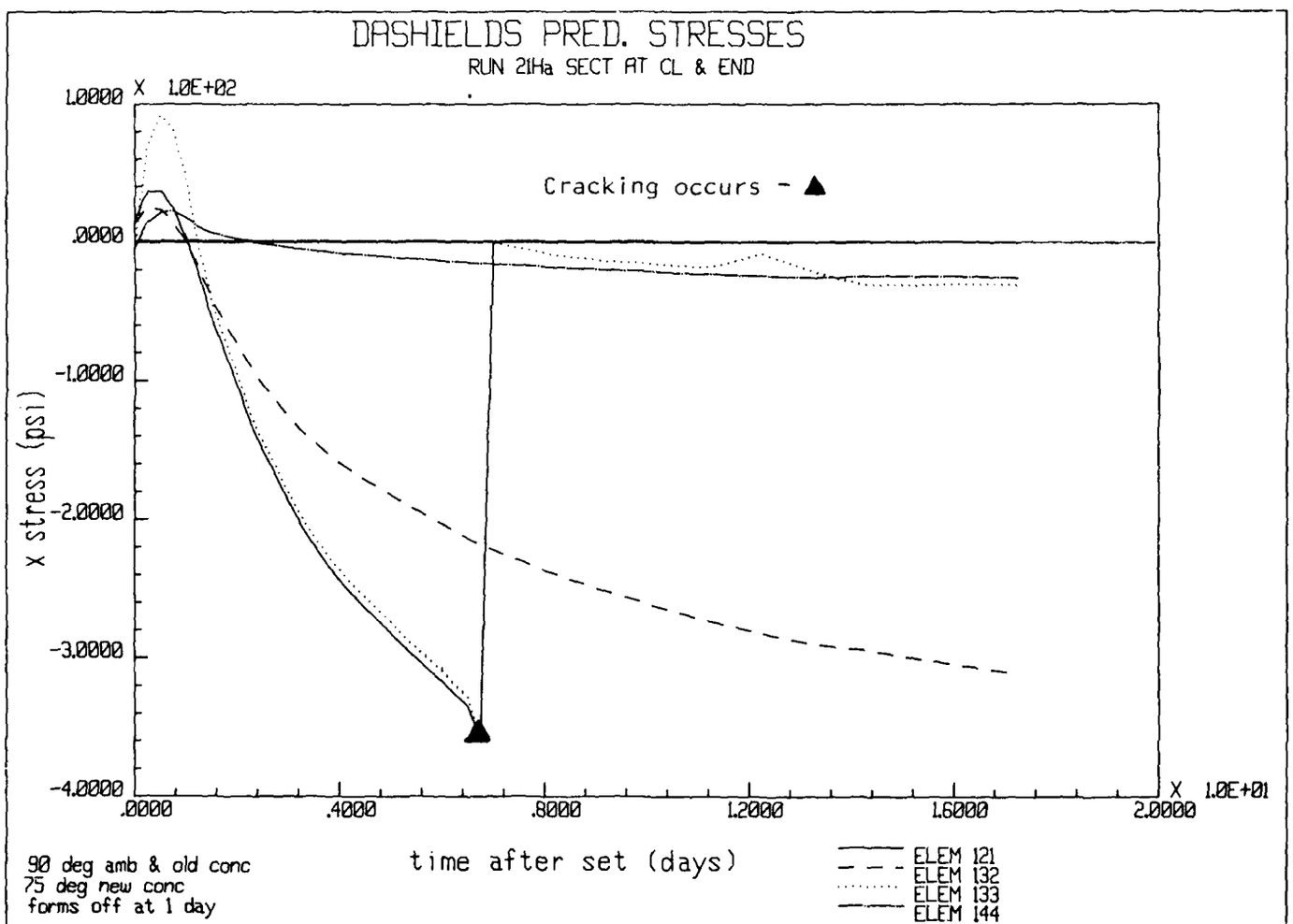

Figure 51. Predicted stresses, Run 21Ha, elements 121, 132, 133, and 144

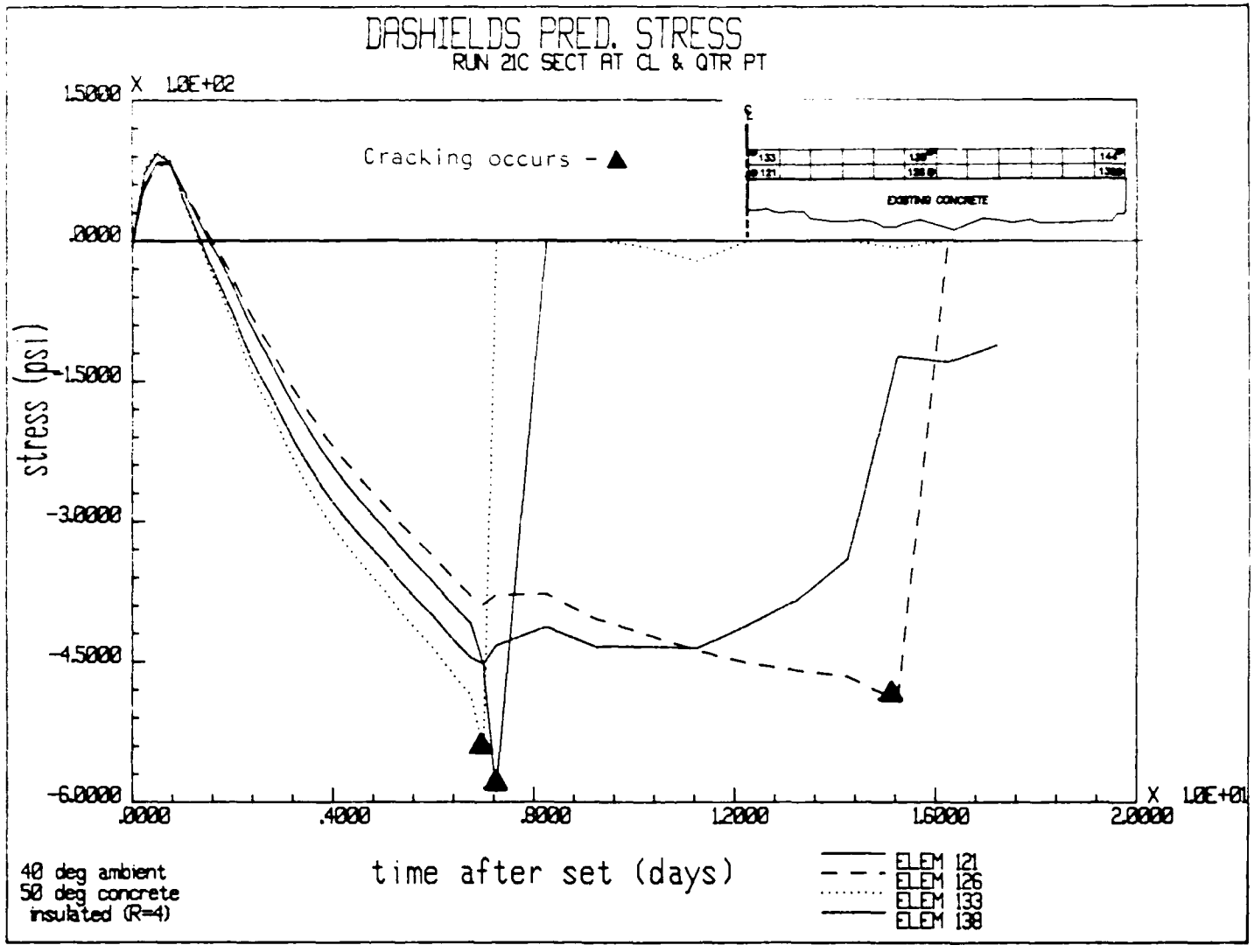

Figure 52. Predicted stresses, Run 21C, elements 121, 126, 133, and 138

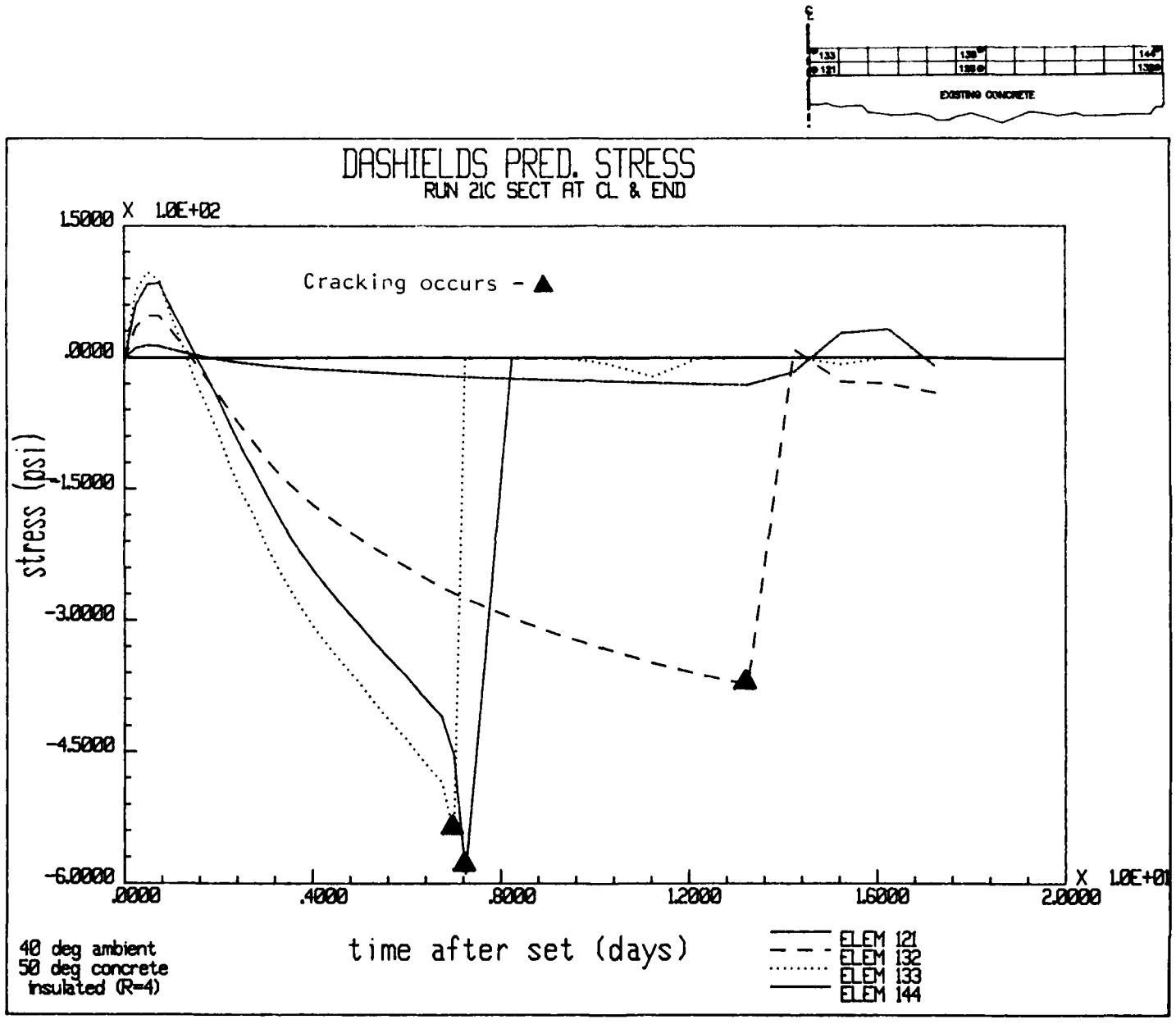

Figure 53. Predicted stresses, Run 21C, elements 121, 132, 133, and 144